DISSERTATION

OSCILLATING BEAM SMART ANTENNA SYSTEMS WITH JOINT TRANSMIT DIVERSITY/DIRECTIONALITY BENEFITS

Submitted by:

Seyed Alireza Zekavat

Department of Electrical and Computer Engineering

In Partial fulfillment of the requirements

For the Degree of Doctor of Philosophy

COLORADO STATE UNIVERSITY

Fort Collins, Colorado

Summer 2002

COLORADO STATE UNIVERSITY

April 18, 2002

WE HEREBY RECOMMEND THAT THE DISSERTATION PREPARED UNDER OUR SUPERVISION BY SEYED ALIREZA ZEKAVAT ENTITLED **OSCILLATING BEAM SMART ANTENNA SYSTEMS WITH JOINT TRANSMIT DIVERSITY/DIRECTIONALITY BENEFITS** BE ACCEPTED AS FULFILLING IN PART REQUIREMENTS FOR THE DEGREE OF DOCTOR OF PHILOSOPHY.

Committee on Graduate Work

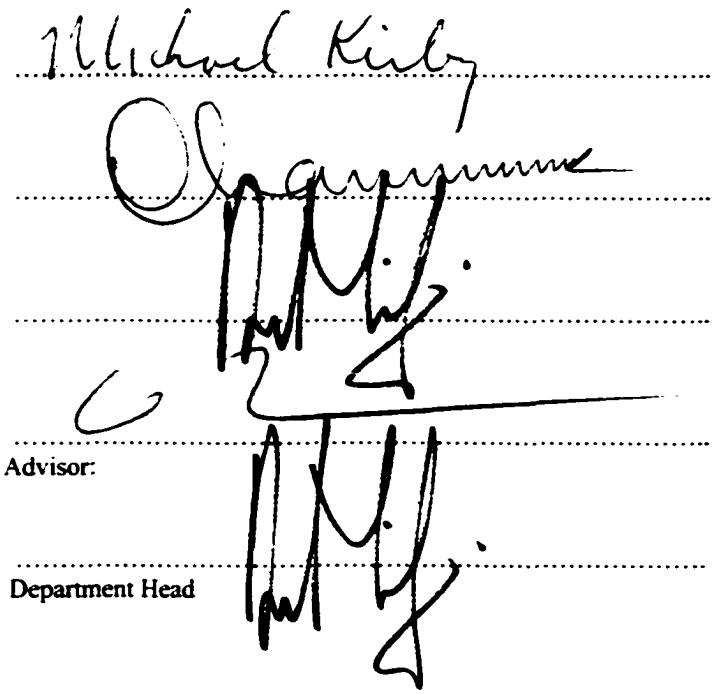

Advisor:

Department Head

Abstract of Dissertation

Oscillating Beam Smart Antenna Systems with Joint Transmit Diversity/Directionality Benefits

This dissertation proposes a novel transmit diversity technique: By applying carefully-selected time-varying delays to the array elements of a smart antenna located at the base station (BS), small oscillations are generated in the beam pattern. Assuming a rich scattering environment (e.g., an urban area), these small oscillations create a time-varying channel demonstrating intra-symbol time variation characterized by coherence time T_C. At a single-antenna mobile, the time-varying channel (with coherence time T_C) creates a time diversity which is exploited to enhance the mobile's performance. The mobile lies in the antenna pattern half power beam width (HPBW) at all times - in this way, directionality is supported to ensure high network capacity.

In addition, a novel merger of multi-carrier code division multiple access (MC-CDMA) and the proposed smart antenna array is introduced at the base station (BS). We also introduce the merger of direct sequence CDMA (DS-CDMA) and the proposed oscillating-antenna-pattern smart antenna arrays. In both the MC-CDMA and DS-CDMA mergers, we observe: 1) very high capacity via the combining of space division multiple access (SDMA) (directionality of antenna array) and code division multiple access (inherent in MC-CDMA and DS-CDMA); and 2) very high performance via the construction of receivers that exploit both transmit diversity and frequency diversity.

We establish both the probability of error performance and the network capacity (measured in terms of numbers of users) of wireless systems merging MC-CDMA and smart antennas with oscillating-beam-patterns.

Seyed Alireza Zekavat
ECE Department
Colorado State University
Fort Collins, CO, 80523-1373
Summer 2002

Acknowledgement

The work and research throughout my Ph.D. program has been supported and inspired by wonderful people. Here, I wish to share my deep appreciation for their encouragement.

Dr. Carl R. Nassar, my advisor, thanks for your invaluable support, advice and dedication to research. Your guidelines led to amazing research and its presentation to the academic community in a book and a considerable number of journal and conference papers.

Dr. D. Lile, my committee member and department head, I highly appreciate your support and advice. Your leadership has been created powerful academic support for the department. I enjoyed being a part of your department.

Dr. V. Chandrasekar, my committee member, thanks for your patience and your invaluable teaching. I was fortunate to sit in your Radar course and delighted by the information I received.

Dr. M. Kirby, my committee member, it is my pleasure having you in my committee. Thanks for your kindness and support.

RAWCOM lab colleagues, I enjoyed being with you all and delighted by your collaboration for the duration of my Ph.D. program.

Fatemeh and Maryam, my wife and daughter, you created an environment that supported me and helped me be successful in my research. Your help has made me who I am today.

My Family, my father, mother, grandmother and aunt, your love, advice and prayer, during my life, shaped me and guided me in the best possible directions, the directions of honesty and a love of science.

Seyed Alireza Zekavat

Table of Contents

List of Figures

Chapter 1

Chapter 2

Chapter 3

Chapter 4

Chapter 5

Chapter 6

Appendix 1

Appendix 3

Chapter 1

Introduction

The wireless industry is undergoing rapid growth as a direct result of the market for wireless devices capable of providing voice, data, and video services to the end user. Researchers have invested considerable effort to satisfy this simple (in terms of expression) yet difficult (in terms of creation) market. Work is ongoing to increase the network capacity (numbers of users and bit rates), increase quality of service (probability-of-error performance) and reduce cost. Smart antenna technology is one key method which may help meet the capacity, quality, and cost requirements of future generation wireless systems.

In this dissertation, we introduce advances to smart antenna technology that enhance both the network capacity and the receiver performance of wireless communication networks, while requiring only a minor change to present-day systems. The implementation cost of the proposed technique is very low.

In this chapter, we introduce the terms and techniques of importance throughout the dissertation as well as the contribution of our research. In Section 1.1, the cellular concept is introduced. Section 1.2 presents smart antenna arrays and explains how they enhance network capacity in cellular system via directionality. In Sections 1.3 and 1.4, we explain the concept of diversity and its ability to enhance performance followed by an explanation of the transmit diversity available via antenna arrays. In Section 1.5, we explain the contribution of our research, which combines the directionality and transmit diversity benefits of antenna arrays. Section 1.6 introduces the dissertation chapters.

1.1 Cellular Wireless Communications

The key to meeting the network capacity demands in a wireless environment is spatial reuse: Split the wireless communication channel coverage area (for example a city) into smaller areas called "*cells*"(see Fig. 1.1) [1]-[3]. The base station (BS) located at the center of cell transmits the signals to all the users located in its cell and receives the signals from all these users. Neighboring cells avoid interference with one another via either a frequency reuse [4]-[7] or code reuse [8][9] scheme (or possibly a combination of both). Moreover, this cellular concept increases power efficiency by reducing the amount of power that must be transmitted from BS to users and vise versa. This reduces the cost of the transmitters (power amplifiers) at both the BS and the mobile user.

Splitting each cell to smaller cells (see Fig. 1.1) is the simplest way of further enhancing the wireless communication network capacity. However, increasing the number of cells

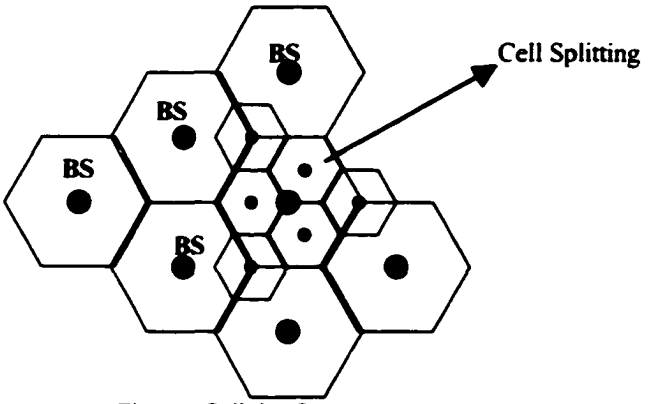

Fig. 1.1 Cellular Concept

involves increasing the number of base stations which, in turn, increases the cost and complexity of the wireless system.

Splitting each cell into sectors using directional (reflector) antennas (i.e., sectorizing the cell) is a more efficient way of enhancing system capacity (see Fig. 1.2). Mounting reflector antennas at base stations creates cell sectorization at a reasonable cost, yet it is

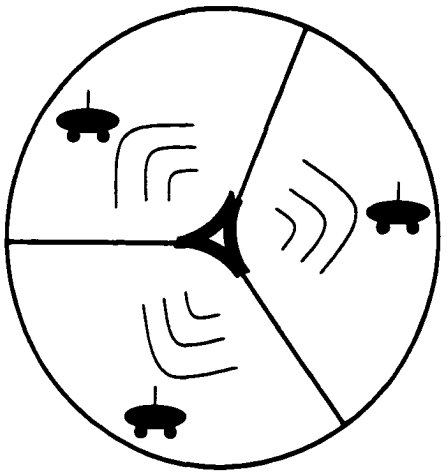

Fig. 1.2 Splitting a cell to sectors (sectorizing) enhances the communication system network capacity.

not the best technique. Reflector antennas are expensive and there is a limit to the possible number of sectors that can be created in each cell (e.g., three sectors per cell). The best substitute for the reflector antennas are the antenna arrays. Using antenna arrays we generate a large number of sectors at low cost.

1.2 Smart Antenna Arrays

Antenna arrays are literally an array of antenna elements (e.g., simple bipolar antennas). This may be a one-dimensional array, where antennas are separated by distance d (e.g., d is equal to half of the wavelength) (see Fig. 1.3) [10][11]. Theoretically, applying proper amplitudes and phase offsets to each antenna array element leads to the creation of a beam pattern directed toward the intended user. Using antenna arrays to generate highly

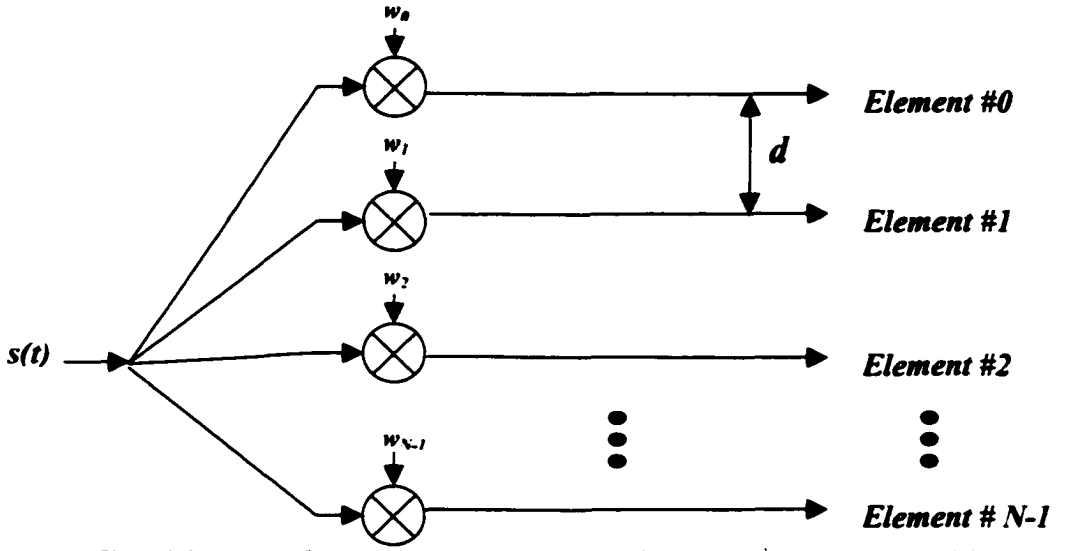

Fig. 1.3 Structure of an antenna array. Here, $w_i, i \in \{0,1,\ldots,N-1\}$ are complex variables.

directional patterns, we can split each cell to very small sectors create a high-capacity low-cost wireless network.

Smart antenna arrays are smart because they determine the location of the desired user and direct the antenna pattern toward that user. Smart antennas located at the base station (BS) represent an important technological innovation. These antennas are capable of increasing the network capacity by use of space division multiple access (SDMA) [12]-[16].

Two types of smart antennas are switched beam smart antennas and adaptive antennas. In switched beam smart antenna systems, we use fixed (predefined) antenna patterns, and a switch is used to select the best beam to communicate with the desired user (see Fig. 1.4(a)). In adaptive antennas we find the direction of the desired user using direction of arrival (DOA) techniques, and direct an antenna pattern toward the desired user(s) (see Fig. 1.4(b)).

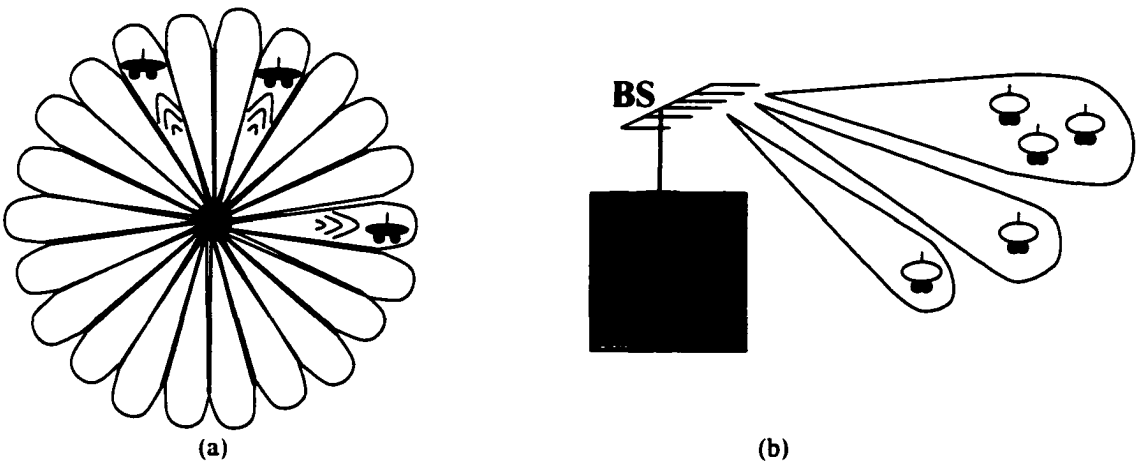

Fig. 1.4 (a) Switched beam smart antennas, and (b) adaptive antennas.

1.3 Diversity Techniques

Antenna arrays can alternatively be used to generate diversity gains at the mobile. This subsection introduces the concepts of diversity.

Diversity schemes present a solution to the fading effect that exists in wireless links. Fading is explained as follows: The signal transmitted from the transmitter (here, a BS transmitter) is scattered by various structures in the channel (e.g., buildings, vehicles, etc) (see Fig. 1.5). As a result, the signal input at the receiver (e.g., mobile) is the combining of different signals from all paths. These signals might combine constructively or destructively. If they add destructively, the amplitude of the received signal will be very small. In this case, we say that the signal is in a deep fade (see Fig. 1.6). The effect generated by the combining of multipath signals is called fading, and may create errors at the received signal. Diversity techniques are introduced to reduce these fading effects [1]-[3].

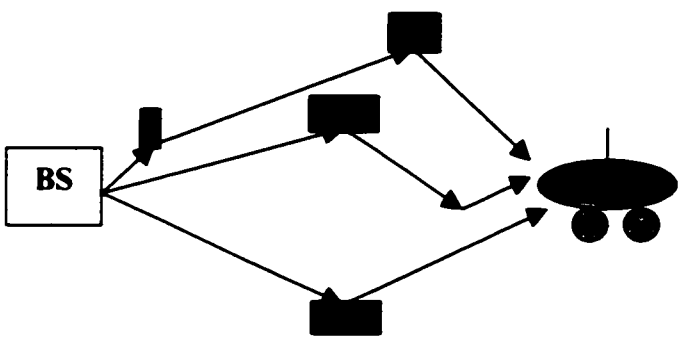

Fig. 1.5 Scattering the transmitted signal from the buildings, results in multipath fading.

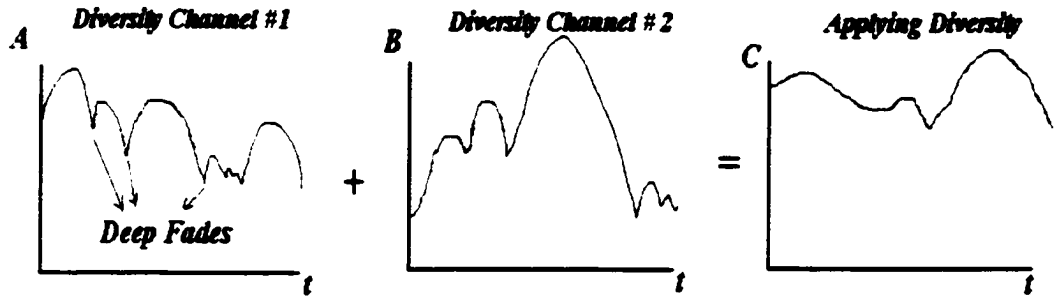

Fig. 1.6 Multipath fading effect, and diversity.

In general, diversity techniques refer to the transmission of a signal over L independent fading channels (e.g., over L different frequencies, at L different times, etc.), ensuring a low probability that all signal components fade simultaneously [1]-[3]. For example, in Fig. 1.6, assume signal A is received via diversity channel 1 and signal B is received via diversity channel 2. We observe a large number of deep fades in signals A and B. If we carefully combine these two signals (e.g., coherently combine them), signal C is generated. Comparing signal C with signals A and B, the number of deep fades in signal C is reduced; hence, the probability of error in signal C is far better than in signals A and B. This generates a receiver with higher probability-of-error performance.

Diversity techniques such as frequency, time and space diversity traditionally come at a considerable cost in system bandwidth (frequency diversity), bit rate (time diversity) and/or expense (spatial diversity) as well as costs in complexity of the receiver structure. The amount of diversity is traditionally chosen based on compromise between performance gain and system cost.

1.4 Transmit Diversity Techniques

Novel diversity techniques minimizing mobile receiver cost have been among recent antenna array applications. Of particular interest have been *transmit diversity* methods which achieve diversity benefits at the receiving mobile when the antenna array is located at the transmitting base station. Examples of diversity schemes are as follows.

In delay diversity [17]-[19], the transmitter sends N data bearing signals, one per array element, where each element has a unique delay chosen to create an artificially resolvable multipath at the receiver. In [17] and [19], however, the diversity gain comes at a considerable cost to receiver complexity, and, moreover, antenna directionality is no longer available.

In antenna hopping [20][21], another novel transmit diversity scheme, each signal is sent on each antenna in separate portions of time, providing diversity gains but eliminating the benefit of using the whole antenna array as a smart antenna. Moreover, in order to achieve path diversity on transmissions from each element, antenna element separation is very high, resulting in large antenna dimensions. In addition, antenna switching produces abrupt periodic phase changes in the received signal, thereby causing periodic errors [21].

Phase sweeping [22][23] is another form of transmit diversity where a two-branch phase sweeping array at the transmitter induces more rapid fades at the receiver. This improves the channel coding gain in a very slow multipath fading environment. However, by using

two antennas spatially separated by a large distance it fails to offer the benefits associated with smart antenna schemes.

In space-time trellis coding [24][25], another transmit diversity technique, data is encoded by a channel coder and the encoded data is split into N unique streams, simultaneously transmitted on N transmit antennas. At the receiver, the symbols are decoded using a maximum likelihood decoder. This scheme combines the benefit of forward error correction and diversity transmission to provide considerable performance gains. However, this technique involves additional receiver processing, which increases exponentially as a function of bandwidth efficiency (bits/sec/Hz) and the required diversity order; hence, it is not cost-effective for some applications [26]. Moreover, when antenna arrays are used in this fashion, directionality benefits are no longer available.

1.5 Research Contribution

In this dissertation, we introduce a novel antenna array system capable of providing *both* transmit diversity and directionality. As a direct result, this antenna array supports: (1) Excellent probability of error performance (via transmit diversity) and (2) large network capacity (via a directionality which in turn enables SDMA). Specifically, we demonstrate a BS antenna array that sweeps (scans) the beam pattern directed to the mobile such that:

1) At all times, the intended mobile lies within the 3dB beamwidth of the antenna pattern;
2) the beam pattern moves to create L independent fades within each symbol duration T_S; this leads to large performance benefits due to L-fold diversity gains;
3) after each T_S, the antenna beam returns to its initial position, and sweeps the same area of space over T_S (leading to an oscillating antenna pattern and easing parameter estimation);
4) the movement of the beam pattern, as a percentage of half power beam width (HPBW), is small, thereby allowing the beam pattern to maintain directionality.

Here, we apply a carefully chosen set of time-varying phases to array elements, generating the mainlobe at the position of the intended user *and* small oscillations in the beam pattern. This beam pattern oscillation can be understood as a significant enhancement to jitter diversity [27][28], where an antenna array beam pattern is jittered for the sole purpose of avoiding deep fades.

Unlike traditional transmit diversity methods presented in Section 1.4, this scheme allows wireless systems to benefit from: 1) directionality (SDMA), 2) L fold diversity, and 3) low receiver cost.

We present a channel model which characterizes the time-varying channel that results from beam pattern oscillation [29]-[32]. We then use our channel model to evaluate the coherence time, T_C, at the mobile. The channel model introduced corresponds to the so-called geometric-based stochastic channel model (GSCM) [33]-[39]. This geometric

approach allows us to stochastically model the parameters of the time-varying channel impulse response. Simulations based on the GSCM show that, e.g., 7-fold time diversity can be exploited at the mobile (when beam pattern movement is small), which significantly improves the mobile receiver probability-of-error performance [40]-[47]. Assuming binary phase shift keying (BPSK), we present the available performance gains of the novel antenna array (both theoretically and via simulations) [48][49].

In addition, we innovatively apply the proposed antenna arrays to MC-CDMA (multi-carrier code division multiple access) and DS-CDMA (direct sequence CDMA) systems [50]-[55]. Through a merger of our antenna array system and CDMA schemes, we achieve (1) excellent performance at the mobile via joint frequency-time diversity (the frequency diversity is inherent in MC-CDMA and DS-CDMA, and the time diversity arises via beam pattern movement); and (2) very high network capacity via joint space-code division multiple access [56]-[64].

1.6 Dissertation Chapters

Chapter 2 presents the principals underlying the proposed of smart antenna array. In this chapter we present the antenna array and the corresponding receiver structures assuming binary phase shift keying (BPSK), and we theoretically evaluate the probability-of-error of the proposed system, comparing it with simulation results.

In Chapter 3, we detail the time varying channel that results from the application of the proposed antenna array. Specifically, we determine the available time diversity at the receiver side achieved via beam pattern oscillation. To model the channel, we characterize the impulse response using a geometric-based stochastic channel modeling.

In chapters 4 and 5, we study the merger of the proposed smart antenna arrays and CI/MC-CDMA and CI/DS-CDMA systems, respectively. Chapter 6 investigates the capacity improvement achievable using the proposed smart antenna, and chapter 7 concludes the dissertation.

Chapter 2

Smart Antennas with Spatial Sweeping:

Achieving Directionality and Transmit Diversity

In this chapter, we introduce the novel antenna array system capable of both transmit diversity and directionality. Here, we propose a BS antenna array that sweeps the beam pattern directed to the mobile such that at all times, the intended mobile lies within the half power beam width (HPBW) of the antenna pattern; the beam pattern moves to create L independent fades within each symbol duration T_S; this leads to large performance benefits due to L-fold diversity gains; after each T_S, the antenna beam returns to its initial position, and sweeps the same area of space over T_S (leading to an oscillating antenna pattern and easing parameter estimation); the movement of the beam pattern, as a percentage of HPBW, is small, thereby allowing the beam pattern to maintain directionality.

Section 2.1 presents the antenna array structure that generates the desired movement. In Section 2.2, the receiver structures employing EGC and ML combining are proposed, and in Sections 2.3 and 2.4 theoretical and simulated probability-of-error performance results are presented, respectively. Section 2.5 concludes the chapter.

2.1 Proposed Antenna Array Structure

For ease in presentation, we will assume an M-element antenna array mounted horizontally at the BS (Fig. 2.1). In order to oscillate the antenna pattern, a time varying delay function $m\tau(t)$, $m \in \{0,1,....,M-1\}$ is applied to the m^{th} antenna array element (Fig. 2.1). The normalized array factor characterizing the resulting antenna pattern corresponds to

$$AF(t,\phi) = \frac{1}{M} \cdot \left[\frac{\sin\left(\frac{M}{2}\gamma(t,\phi)\right)}{\sin\left(\frac{1}{2}\gamma(t,\phi)\right)} \right]. \tag{2.1}$$

Here,

$$\gamma(t,\phi) = \frac{2\pi}{\lambda_o} d\cos\phi - \omega_o \tau(t), \tag{2.2}$$

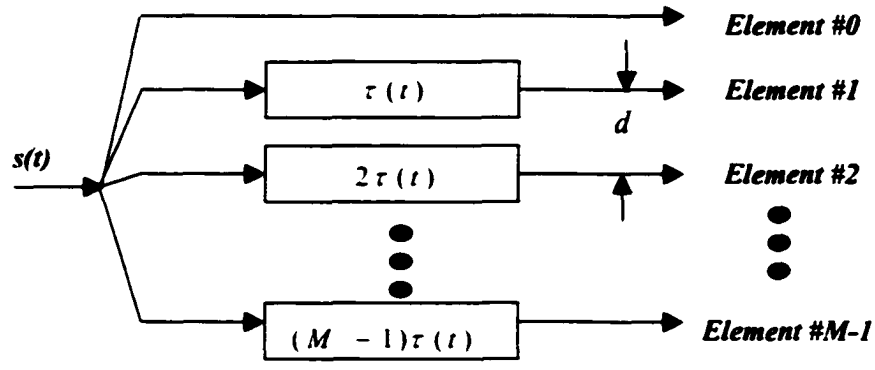

Fig. 2.1 Antenna array structure.

where λ_o is the wavelength (c/f_o), d is the distance between antenna elements, $\omega_o = 2\pi f_o$ where f_o is the frequency of the transmitted signal, and time t=0 refers to the first instant when the antenna array contacts a mobile user. For simplicity in presentation, it is assumed throughout that the mobile is located at angle $\phi_o \cong \pi/2$.

Through appropriate selection of $\tau(t)$, an oscillating antenna beam pattern is created at the BS. The beam pattern is *controlled* to ensure the following two criteria are satisfied: 1) large scale fading, i.e., the mean and variance of the Rayleigh fade, is constant over symbol time T_S; and 2) the BS beam pattern oscillates just enough to allow the signals received in L different partitions of symbol duration T_S to demonstrate independent fades. This creates an L-fold diversity gain at the mobile receiver. In other words, the BS antenna array sweeps the beam pattern directed at the mobile just enough to create constant large scale fading for the symbol duration T_S while ensuring L independent fades within each T_S (see Fig. 2.2).

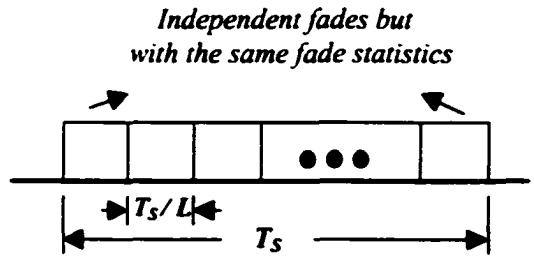

Fig. 2.2 Symbol time partitioned into L times, each with independent fades, and each fade with identical statistics.

A. Criterion 1: Constant Large Scale Fading

Our first criterion ensures constant large-scale fading within the symbol time duration T_S. This condition corresponds to:

$$\left| T_S \frac{d\phi}{dt} \right| = \kappa \cdot \beta, \quad \text{for all } t \tag{2.3}$$

where $d\phi/dt$ is the rate of antenna pattern movement and $T_S \cdot (d\phi/dt)$ is the amount of antenna pattern movement in symbol duration T_S. Additionally, β is the array half power beamwidth (HPBW), and κ is a parameter satisfying $0 < \kappa < 1$. This κ parameter ensures us that the received signal is within the 3dB-beamwidth of the antenna pattern for the entire symbol duration (providing the mobile of a strong signal). Equation (2.3) can be solved to create an equation for $\tau(t)$ (the antenna element delay in Fig. 2.1) as follows: from (2.2), letting $\gamma(t,\phi) = \gamma_o$,

$$\phi = \cos^{-1}\left[\frac{\lambda_o}{2\pi d} (\gamma_o + \omega_o \tau(t)) \right], \tag{2.4}$$

and, hence,

$$\left|\frac{d\phi}{dt}\right| = \frac{\lambda_o \omega_o}{2\pi d \cdot |\sin\phi|} \cdot \left|\frac{d\tau(t)}{dt}\right|. \tag{2.5}$$

By substituting (2.5) in (2.3)

$$\left|T_S \cdot \frac{d\phi}{dt}\right| = T_S \cdot \frac{\lambda_o \omega_o}{2\pi d \cdot |\sin\phi|} \cdot \left|\frac{d\tau(t)}{dt}\right| = \kappa \cdot \beta, \; 0 < \kappa < 1, \tag{2.6}$$

$$\frac{d\tau(t)}{dt} = \kappa \cdot \frac{2\pi d \cdot |\sin\phi|}{\lambda_o 2\pi f_o T_S} \cdot \beta, \tag{2.7}$$

which, solving for $\tau(t)$, reduces to:

$$\tau(t) = \kappa \cdot \frac{d \cdot |\sin\phi| \cdot \beta}{f_o \lambda_o T_S} \cdot \left(t - \frac{T_S}{2}\right), \tag{2.8}$$

where $T_S/2$ is introduced, when solving for $\tau(t)$, to maintain a symmetric movement of the beam pattern around its peak (over T_S). This suggests the selection of delay function $\tau(t)$ which is a linear function of t with slope $\kappa \cdot d \cdot |\sin\phi| \cdot \beta / f_o \lambda_o T_S$. In practice, we employ a $\tau(t)$ periodic over symbol time T_S (Fig. 2.3).

With this selection of $\tau(t)$, the antenna pattern returns to its initial position and sweeps the same area of space each T_S. That is, the antenna array delay $\tau(t)$ (Fig. 2.1) corresponds to the time function shown in Fig. 2.3, and leads to beam pattern movement shown in Fig. 2.4.

Here, the fades are identical in neigboring symbols (i.e., symbols, k, $k+1$, $k+2$, ...). This enables fading parameters, e.g., phases, in each segment of T_S to be tracked.

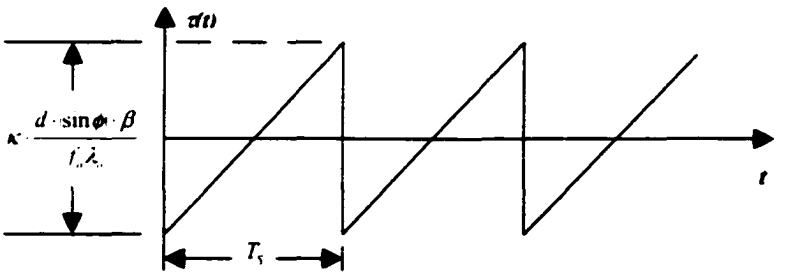

Fig. 2.3 Antenna element delay line function.

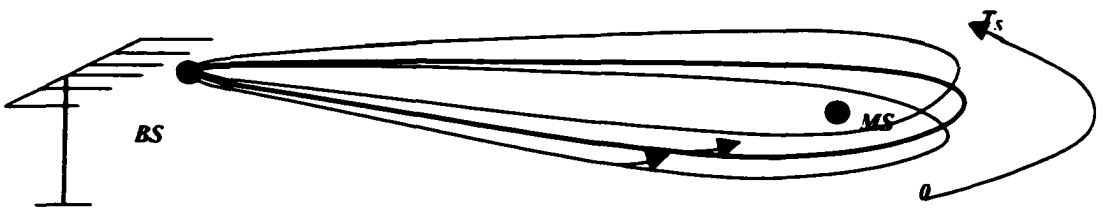

Fig. 2.4 Antenna beam pattern movement over each symbol duration T_S.

B. Criterion 2: Independent fades

Next, we want a controlled beam pattern movement ensuring L independent fades over each symbol duration T_S, i.e., assuring an independent fade at the receiver over each duration $[lT_S / L, (l+1)T_S / L]$. Our criteria corresponds to

$$\frac{T_S}{L} < T_C < 2\frac{T_S}{L}. \tag{2.9}$$

That is, we want the spatial movement due to time varying array elements to induce a coherence time, T_C, which allows for a constant fade over $[lT_S / L, (l+1)T_S / L]$ but independent fades between neighboring time intervals of duration T_S / L (Fig. 2.2).

With beam pattern movement based on (2.8) (Fig. 2.3), which contains a control parameter κ, we set κ to various values (in $0 < \kappa < 1$) and determine T_C / T_S via channel simulation (see Chapter 3). Ratios of T_C / T_S, combined with Equation (2.9), provided us with achievable values for L, the diversity gain, as a function of κ, the antenna array control parameter.

Assuming a medium-size city center, we found $(T_C / T_S) \approx 0.16$ whenever $\kappa \approx 0.05$ (see Chapter 3). Using $(T_C / T_S)_{min} = 0.16$ and (2.9), we determine $L \approx 7$, i.e., a diversity of 7-

fold is available. This corresponds to a very significant performance benefit at the receiver side.

2.2 Receiver Design for Smart Antenna with Spatial Sweeping

Assuming BPSK for ease in presentation, then, at the transmitter side, the k^{th} information bearing signal entering the transmit antenna array corresponds to

$$s(t) = \cos(\omega_o t + \theta_k), t \in [kT_S, (k+1)T_S], \tag{2.10}$$

where $\theta_k = 0$ *or* π and contains the information bit. The received signal corresponds to

$$r(t) = AF(t,\phi)\cdot\alpha(t)\cdot\cos\left(\omega_o t + \theta_k + \frac{M-1}{2}\left(\frac{2\pi}{\lambda_o}d\cos\phi - \omega_o\tau(t)\right) + \phi(t)\right) + n(t), \tag{2.11}$$

where $AF(t,\phi)$ is the array factor introduced in (2.1), $\alpha(t)$ and $\phi(t)$ are the gain and phase due to the channel time varying fade, and $n(t)$ is the additive white Gaussian noise (AWGN) with variance $N_o/2$. The received signal in our proposed system, considering (1) the fade $\alpha(t)$ is constant over each duration $[lT_S, (l+1)T_S]$, (2) the phase $\phi(t)$ is tracked and removed, and (3) the mobile is located at $\phi_o \cong \pi/2$ (i.e., $AF(t,\phi) \cong 1$) corresponds to

$$r_l(t) = \alpha_l \cdot \cos\left(\omega_o\left(t - \frac{M-1}{2}\cdot\tau(t)\right) + \theta_k\right) + n_l(t), l \in \{0,1,\ldots,L-1\} \quad (2.12)$$

where $r_l(t)$ refers to the received signal over interval $[lT_S/L,(l+1)T_S/L]$; $n_l(t)$, $l \in \{0,1,\ldots,L-1\}$ is an additive white Gaussian noise with variance $N_o/2L$; and α_l is a Rayleigh random variable. With $\tau(t)$ selected according to (2.5), $\kappa \le 0.05$, and assuming typical parameter values for mobile communication systems, it is easily shown that the frequency offset induced by $\tau(t)$ is less than 5% of a 1MHz bandwidth. Hence, frequency expansion due to time varying $\tau(t)$ can typically be neglected. Additionally, the proposed array structure ensures an independent α_l for different values of l.

Fig. 2.5(a) shows a typical BPSK receiver (assuming rectangular pulse shaping and no time diversity benefit is present, i.e., $\alpha(t) = \alpha$, $t \in [0,T_S]$). Fig. 2.5(b) demonstrates a BPSK receiver designed to process an L-fold time diversity benefit (conceptually), i.e., here, $\alpha(t)$($t \in [0,T_S]$) is well approximated by $\alpha(t) = \alpha_l$, $t \in [(l-1)T_S/L, lT_S/L]$. (Fig. 2.5(b) is better implemented by performing over sampling and considering each sampling phase as a separate branch signal.)

In Fig. 2.5(b) the parallel branches represent the integration over consecutive non-overlapping time instances $t \in [(l-1)T_S/L, lT_S/L]$. We can replace this receiver representation with Fig. 2.5(c). Here, the diversity components enter serially (in time) to the combiner, i.e., the matched filter of Fig. (2.5)(a) has been replaced with the matched filter of Fig. (2.5)(c) and a combiner.

In Fig. (2.5)(c), $v_{lo}(t)$ represents the local oscillator term:

$$v_{lo}(t) = \sqrt{\frac{T_S}{2}} \cos\left(\omega_o\left(t - \frac{M-1}{2} \cdot \tau(t)\right)\right). \tag{2.13}$$

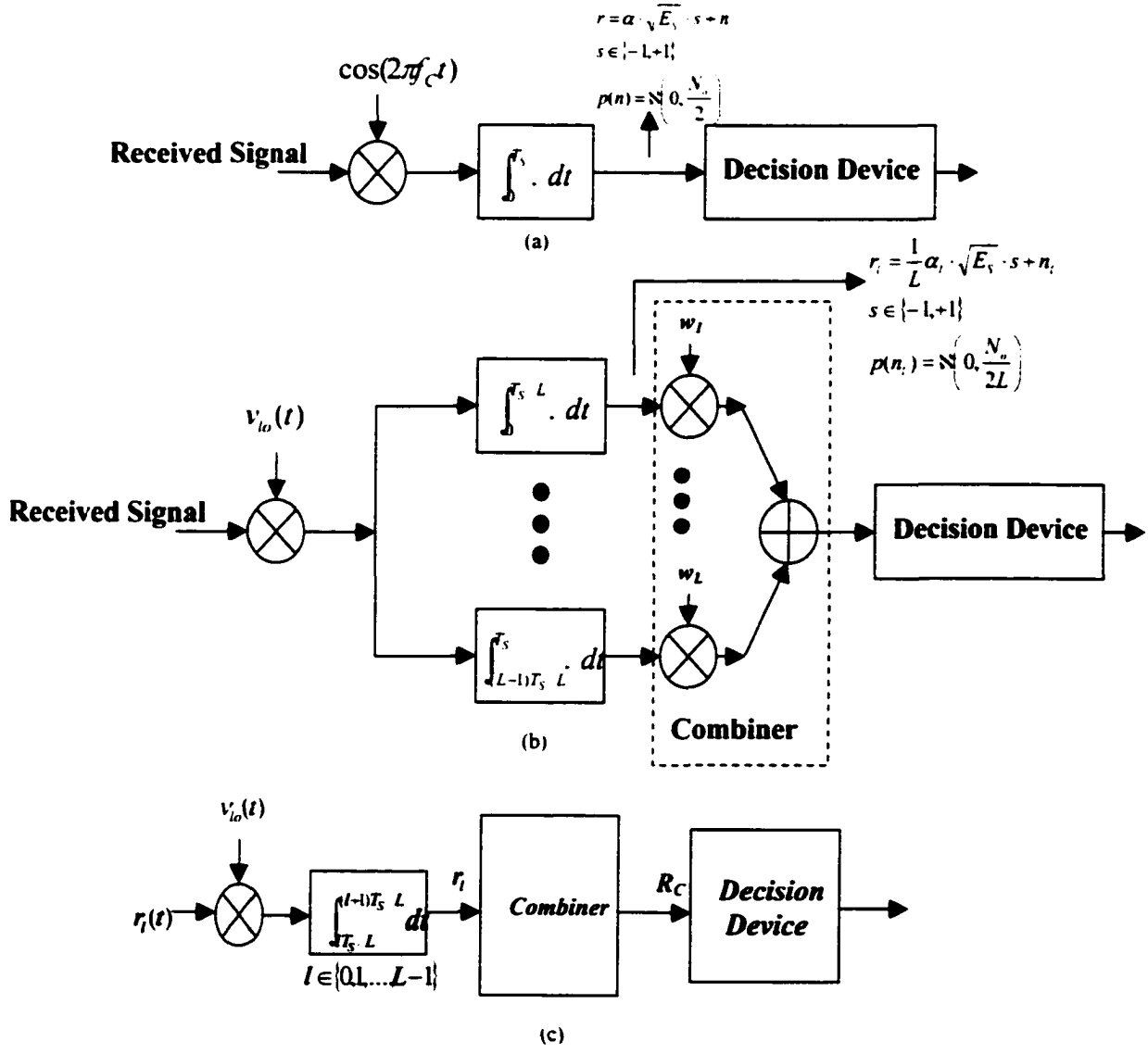

Fig. 2.5 (a) BPSK receiver (without diversity), (b) BPSK time diversity receiver, (c) simplified time diversity receiver.

Over each interval $[(kT_S + lT_S / L),(kT_S + (l+1)T_S / L)]$ the signal at the output of the integrator in Fig. 2.5(c) corresponds to

$$r_l = \alpha_l \frac{1}{L}\sqrt{\frac{T_S}{2}}\cos\theta_k + n_l,\ l \in \{0,1,\ldots,L-1\}, \tag{2.14}$$

where n_l is a zero mean Gaussian random variable with variance $N_o / 2L$; also, $s = \cos(\theta_k) \in \{-1,+1\}$; and $\sqrt{E_S} = \sqrt{T_S / 2}$. Following the creation of the L r_l values, the detector can be designed on the basis of equal gain combining (EGC) or maximal ratio combining (MRC). In EGC, the decision variable after combining is

$$R_{C,EGC} = \sum_{l=0}^{L-1} r_l \tag{2.15}$$

while in MRC detection, the decision variable after the combiner corresponds to

$$R_{C,ML} = \sum_{l=0}^{L-1} \alpha_l r_l\ . \tag{2.16}$$

2.3 Theoretical Performance

In this section we present the theoretical performance of the receiver for the two combining schemes of (2.15) and (2.16).

2.3.1 EGC probability of error

In EGC, the combining of (2.15) is employed, which leads to (using r_l in (2.14)):

$$R_{C,EGC} = \alpha\sqrt{E_S}\ s + n, \tag{2.17}$$

where:

$$\alpha = \frac{1}{L}\sum_{l=0}^{L-1}\alpha_l, \tag{2.18}$$

$$n = \sum_{l=0}^{L-1} n_l. \tag{2.19}$$

Assuming α_l is a Rayleigh random variable with the probability density function $f(\alpha_l) = \frac{\alpha_l}{\sigma_o^2} e^{-\alpha_l^2/2\sigma_o^2}$, then the mean of α (Equation (2.18)) corresponds to

$$\mu_\alpha = E(\alpha) = E(\alpha_l) = \sqrt{\frac{\pi}{2}\sigma_o^2} \tag{2.20}$$

and the variance of α is

$$\sigma_\alpha^2 = Var(\alpha) = \frac{1}{L}\cdot\left(\frac{4-\pi}{2}\right)\sigma_o^2. \tag{2.21}$$

Additionally for the noise term, n, in (2.19), the mean remains zero, and the variance corresponds to:

$$E(n^2) = L \cdot E(n_l^2) = \sigma_n^2 = N_o / 2L \ . \tag{2.22}$$

Now, assuming we design the proposed system with L sufficiently large, we can apply the central limit theorem: from (2.18), we can assume α is a Gaussian random variable with the mean and variance characterized by (2.20) and (2.21) respectively. Probability of error then corresponds to

$$P(\varepsilon) = \int_{\varepsilon}^{\infty} P(\varepsilon|\alpha) f(\alpha) d\alpha \ , \tag{2.23}$$

where:

$$P(\varepsilon|\alpha) = Q\left(\frac{\alpha\sqrt{E_S}}{\sigma_n}\right), \tag{2.24}$$

and

$$f(\alpha) = \frac{1}{\sqrt{2\pi\sigma_\alpha^2}} \exp\left(-\frac{(\alpha - \mu_\alpha)^2}{2\sigma_\alpha^2}\right). \tag{2.25}$$

After substituting (2.24) and (2.25) into (2.23), and performing mathematical manipulation:

$$P(\varepsilon)=Q\left(\sqrt{\frac{\pi}{4-\pi}}\cdot L\frac{\sqrt{\frac{4-\pi}{2}\cdot\frac{E_S}{N_o}\cdot E(\alpha_i^2)}}{\sqrt{L+\frac{4-\pi}{2}\cdot\frac{E_S}{N_o}\cdot E(\alpha_i^2)}}\right)-Q\left(\sqrt{\frac{\pi}{4-\pi}}\cdot L\right). \tag{2.26}$$

Here, $N_o = 2\sigma_n^2$ is the noise power. Letting $E(\alpha_i^2)=1$, then, as L increases, the second term in (2.26) will tend to zero, i.e.,

$$\lim_{L\to\infty} P(\varepsilon)=Q\left(\sqrt{\frac{\pi}{2}}\sqrt{\frac{E_S}{N_o}}\right), \tag{2.27}$$

which is close to the $P(\varepsilon)$ of BPSK in an AWGN channel.

2.3.2 Probability of error for MRC combining

Using the method presented in [65] for the computation of the probability of error in a diversity receiver employing MRC combining, and realizing that in our case each branch has signal energy $\sqrt{E_S}/L$ rather than $\sqrt{E_S}$, and each noise component has variance σ_n^2/L rather than σ_n^2 we determine:

$$P(\varepsilon)=\left[\frac{1}{2}(1-\mu)\right]^{L}\sum_{l=0}^{L-1}\binom{2L-1}{l}\left[\frac{1}{2}(1+\mu)\right]^{l}, \tag{2.28}$$

where

$$\mu=\sqrt{\frac{\gamma_C/L}{1+\gamma_C/L}},\ \gamma_C=E\left[\sum_{l=0}^{L-1}\alpha_l^2\right]\cdot\frac{E_s}{N_o}. \tag{2.29}$$

$$\binom{2L-1}{l}=\frac{(2L-1)!}{((2L-1)-l)!\cdot l!} \tag{2.30}$$

As $L\to\infty$, then $P(\varepsilon)$ tends toward that of an AWGN channel. The theoretical probability of error results for both EGC and MRC, with L = 7, are provided in Fig. 2.6(a). Probability of error of MRC combining is better than that of EGC, but MRC combining requires amplitude tracking which increases receiver complexity.

2.4 Simulated Performance

Simulation results are generated for the proposed antenna array with a spatial sweeping system, assuming L = 7 and BPSK transmission. To generate these results, we employed Monte Carlo simulation using the r_l of (2.14). Fig. 2.6(b) presents simulation performance results. These results confirm that the proposed system, with little change in receiver complexity, moves performance away from poor fading channel performance and toward more desired AWGN results. It is observed that the introduction of the beam

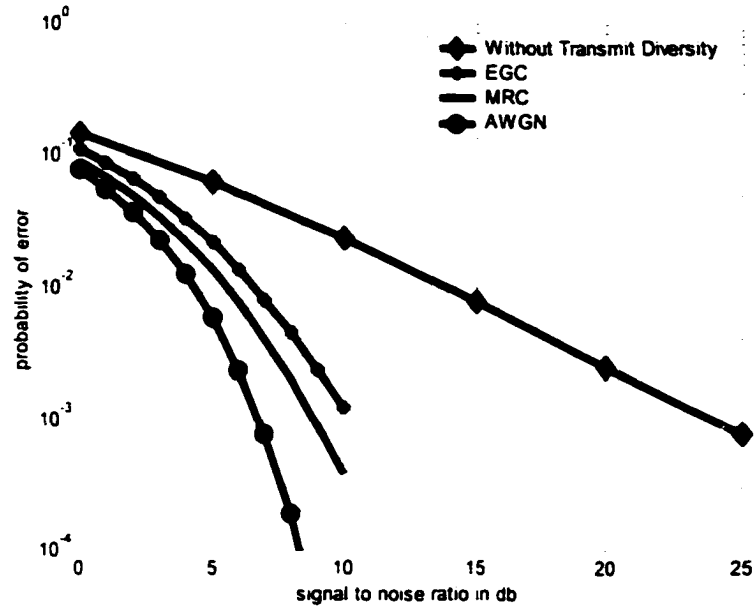

(a)

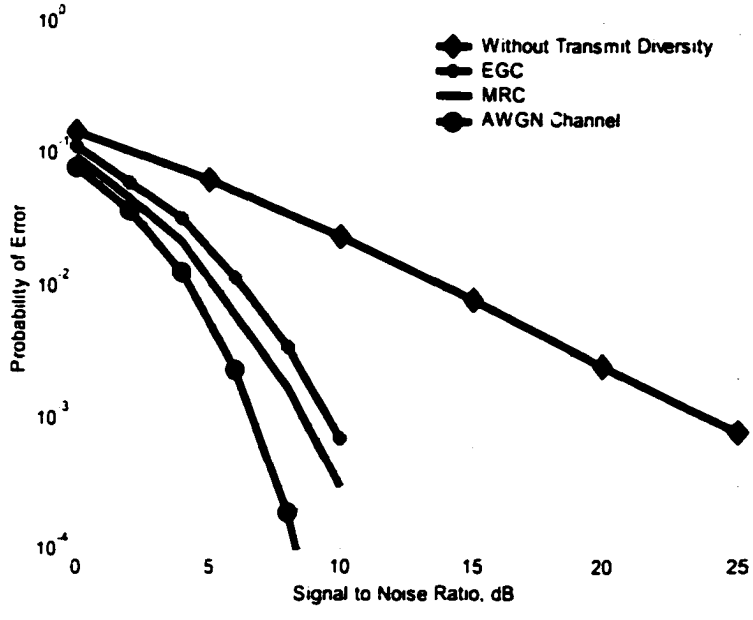

(b)

Fig. 2.6 (a) Analytical, and (b) simulation results

($P(\varepsilon)$ versus $\frac{E_S}{N_o} E\left(\sum_{l=0}^{L-1} \alpha_l^2\right)$ in dB) for EGC and ML taking L=7.

sweeping antenna arrays at the BS creates an improvement of more than 14 dB at a probability of error of 10^{-3} (at the mobile) compared to the "without transmit diversity" condition. The simulation results support the theoretical suppositions. It is important to note that these performance benefits are achieved while maintaining directionality, i.e., enabling network capacity gain via SDMA.

2.5 Conclusions

By carefully designing the delay elements of base station antenna arrays, we can not only achieve a directionality benefit, but, additionally, we induce time diversity at the mobile receiver, significantly increasing receiver performance.

We studied receivers employing EGC and ML combining. Theoretical results match simulated performance. A key feature in receiver design is that time separation between each diversity component allows for a low complexity receiver even in cases of larger degrees of diversity.

Chapter 3

Channel Modeling for Spatial Sweeping Smart Antennas: Establishing the Available Transmit Diversity

The modeling and characterization of mobile channels has been the subject of much research over the past three decades. This research has lead to detailed mobile channel models in the presence of vehicle movement; however to the best of our knowledge, there has been no work done on modeling channels in the presence of beam pattern movement. Beam pattern movement is quite different than movement of the mobile; for example, as the beam pattern moves some buildings fall out of the antenna pattern mainlobe, while others enter. This chapter is dedicated to the modeling of wireless channels in the presence of beam pattern movement. The net result is that a small beam pattern movement can lead to, e.g., 7-fold time diversity benefits.

Section 3.1 presents the assumptions made in our channel-modeling scheme (a geometric-based stochastic channel modeling). In Section 3.2, the channel impulse response is introduced and its parameters are characterized. Section 3.3 simplifies the channel impulse response model assuming a flat fading channel and Section 3.4 presents the channel simulation and coherence time results. Sections 3.5 and 3.6 consider a more comprehensive impulse response model and the related coherence time simulation results, respectively. Section 3.7 concludes this chapter.

3.1 Channel Model Assumptions

Assume the proposed antenna array (of chapter 2) is located at the base station (BS), and a single element omnidirectional antenna at the mobile. In addition, we assume the following for the channel:

1) Scatterers contributing to multipath are located in one of two possible coverage areas:
   A. a circle with the mobile at its center (Fig. 3.1(a)) (which is a suitable model when we assume the BS antenna has enough height to illuminate only an area approximated by the circle) [33][34]); or
   B. the semi-elliptic area in Fig. 3.1(b) (accurate when we assume the height of the BS antenna array is close to the height of the surronding buildings).
2) The movement generated by the antenna array oscillation is dominant, and hence we ignore the movement of the mobile as well as any other relative speed due to the movement of other objects in the environment.

3) Scatterers are assumed to have dimensions in accordance with a known PDF.

4) Scatterers in the environment surrounding the BS are uniformly distributed [35].

5) Scatterers are considered diffuse reflectors which reflect the incident radiation in all directions [36][37].

6) The signal received at the mobile is the sum of horizontally propagated plane waves interacting with just one scatterer [37].

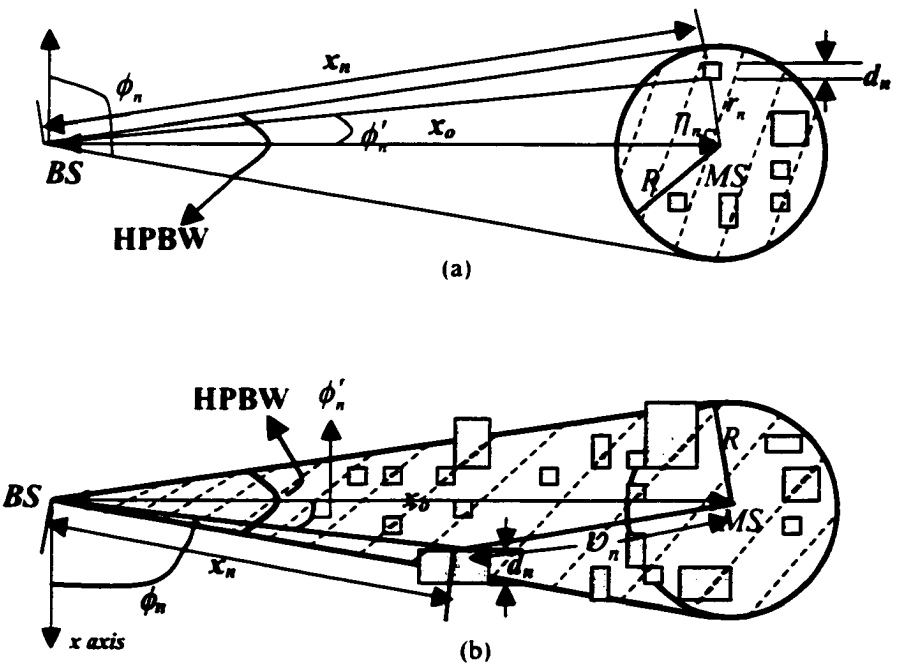

Fig 3.1(a,b) The two scenarios for the coverage area: a) circular scenario, b) semi-elliptic scenario.

3.2 Linear Time-Varying Channel Impulse Response Modeling

Under the assumptions of Section 3.1, we now characterize the channel in the presence of the proposed antenna array. A linear time-varying system best represents radio channels [29]-[31]. Specifically, the channel impulse response corresponds to

$$h(t,\tau)=\sum_{n=1}^{N(t)}\alpha_n(t)\cdot e^{j\theta_n(t)}\cdot\delta\left(\tau-\tau_n(t)\right). \tag{3.1}$$

Here, t is the observation time, τ is the response time of the impulse at each t, and $N(t)$, $\alpha_n(t)$, $\theta_n(t)$ and $\tau_n(t)$ are random, time-varying parameters corresponding to the number of multipath components, the multipath amplitude, the multipath phase and the multipath time of arrival, respectively. Additionally, $\delta(\cdot)$ represents the impulse function.

3.2.1 The amplitude of the multipaths, $\alpha_n(t)$

Antenna pattern ocsillation (Fig. 2.4) causes some scatterers to leave the coverage area (departing scatterers), while others arrive (arriving scatterers). Most remain in the coverage area. Thus, the term $\alpha_n(t)$ corresponds to

$$\alpha_n(t)=\begin{cases}\alpha_{1n} \text{ if the } n^{th} \text{ scatterer remains in the coverage area,}\\ \alpha_{2n}(t) \text{ if the } n^{th} \text{ scatterer departs,}\\ \alpha_{3n}(t) \text{ if the } n^{th} \text{ scatterer arrives.}\end{cases} \tag{3.2}$$

The term α_{1n} is a Rayleigh, Rician or Nakagami random variable (RV) [31]. The term $\alpha_{2n}(t)$ represents a decaying amplitude whose value diminishes as the effective radiated

cross section of the scatterer decreases. This time dependent amplitude decay is modeled as a linear function corresponding to

$$\alpha_{2n}(t) = \begin{cases} \alpha_{2n} & , t \in [0, \tau_{sn}) \\ \alpha_{2n} \cdot I_{(\tau_{sn}, \tau')}(t) \cdot \left(1 - \dfrac{t - \tau_{sn}}{T_{\tau_{sn}}}\right), & t \in [\tau_{sn}, T_S] \end{cases} \quad (3.3)$$

Here, (1) α_{2n} is a RV with statistics identical to α_{1n}, representing the amplitude of the n^{th} multipath when the scatterer is fully present in the antenna pattern coverage; (2) $\tau_{sn} \in [0, T_S]$ represents the time instant when the scatterer starts leaving the antenna pattern coverage area, a value determined by the modeling to be presented in Subsection 3.2.3; and (3) the function $I_{(\tau_{sn}, \tau')}(t)$ is the indicator function, unity over the values $t \in [\tau_{sn}, \tau']$ and zero otherwise. Here, $\tau' = \tau_{sn} + T_{\tau_{sn}}$ if $\tau_{sn} + T_{\tau_{sn}} \le T_S$, and $\tau' = T_S$ otherwise.

The time constant $T_{\tau_{sn}}$ represents the time it takes for the n^{th} scatterer to completely depart the HPBW, and corresponds to

$$T_{\tau_{sn}} = d_n \cdot (V_{rot}(x_n))^{-1}. \quad (3.4)$$

Here,

• d_n refers to the scatterer dimension (Fig. 3.1(a)).

• $V_{rot.}(x_n)$ is the speed of the beam pattern rotation at the scatterer position x_n.

• x_n, *for the circular scenario,* using Fig. 3.1(a) and simple geometry, is

$$x_n = \left(x_o^2 + r_n^2 - 2x_o r_n \cos(\eta_n)\right)^{\frac{1}{2}}, \tag{3.5}$$

where x_o is the BS-MS distance, r_n is the line connecting scatterer n to the mobile and is considered uniform over $[0, R]$ (R is the radius of the circle of Fig. 3.1(a)) and η_n is the angle between the line r_n and antenna pattern main axis, uniform over $[0, 2\pi)$ (a direct consequence of a uniform distribution of scatterers).

• x_n, *for the semi-elliptic scenario* (Fig. 3.1(b)) is considered uniform over $[0, x_{n,\max}]$ where $x_{n,\max}$ (using Fig. 3.7 and simple geometric arguments) corresponds to

$$x_{n,\max} = \left(x_o^2 + R^2 + 2x_o R\cos(\phi_n' + \varphi)\right)^{\frac{1}{2}}. \tag{3.6}$$

Here, x_o is the BS-MS distance, ϕ_n' is a random variable with the PDF introduced in Section 3.5, $\varphi = \sin^{-1}\left((x_o \sin\phi_n')/R\right)$, and R is the radius of the circle with the MS located at its center, i.e., $R = x_o \cdot \sin(\frac{1}{2}\beta)$.

The term $\alpha_{3_n}(t)$ is a linearly increasing function corresponding to

$$\alpha_{3n}(t) = \begin{cases} \alpha_{3n} \cdot I_{[\tau_{an},\tau_{an}+T_{\tau_{an}})}(t) \cdot \left(\dfrac{t-\tau_{an}}{T_{\tau_{an}}} \right), & t \in \left[0, \tau_{an} + T_{\tau_{an}}\right] \\ \alpha_{3n} & , t \in \left[\tau_{an} + T_{\tau_{an}}, T_S\right] \end{cases} \tag{3.7}$$

where (1) α_{3n} is a RV representing the amplitude of the multipath when the scatterer is fully present in the HPBW; (2) $\tau_{an} \in [0, T_S]$ is the arrival time of the scatterer; and (3) $T_{\tau_{an}}$ is the time constant representing the time it takes the scatterer to completely enter into the antenna pattern coverage area. The statistics of α_{3n}, τ_{an} and $T_{\tau_{an}}$ are the same as those of α_{2n}, τ_{sn} and $T_{\tau_{sn}}$, respectively.

3.2.2 The signal phase, $\theta_n(t)$ and the time of arrival, $\tau_n(t)$

The phase $\theta_n(t)$ is determined by: 1) the distance x'_n ($x'_n = x_n + r_n$ in Fig. 3.1(a) and $x'_n = x_n + \upsilon_n$ in Fig 3.1(b)), which leads to phase offset $2\pi x'_n / \lambda_o$, and 2) the phase due to other sources (e.g., reflection coefficient phase), ξ_n [1]. Typically, ξ_n is a RV uniform over $[0, 2\pi)$, independent of $2\pi x'_n / \lambda_o$. Hence, $\theta_n(t) = \theta_n$ is a uniform RV over $[0, 2\pi)$.

Regarding the time of arrival (TOA) of multipaths, $\tau_n(t)$, we assume a probability density function (PDF) corresponding to a Poisson process or its modified version, as shown in [32][66].

3.2.3 The Number of multipaths, $N(t)$

As the beam pattern moves, scatterers enter and depart the mainlobe. The total number of scatterers in the mainlobe, as a function of time, is denoted $N(t)$. Assuming the interval $[0, T_S]$ is sampled at times t_k . $k = 0,1,...., n_S - 1$, where n_S is sufficiently large, $N(t_k)$ can be represented according to

$$N(t_k) = \begin{cases} N(t_{k-1}) + 1 & \textit{if a scatterer arrives,} \\ N(t_{k-1}) - 1 & \textit{if a scatterer leaves,} \\ N(t_{k-1}) & \textit{otherwise.} \end{cases} \tag{3.8}$$

Here, we assume the time difference $\Delta t = t_k - t_{k-1}$ is so small that the probability of more than one arrival or departure is negligible. To generate $N(t_k)$, an initial guess $N(t)|_{t=t_0=0}$ is selected according to:

$$N(t)|_{t=t_0=0} = \rho_o A_{ap}, \tag{3.9}$$

where

- ρ_o is the scatterer density measured in terms of *scatterers/m*^{2}.
- A_{ap} is the antenna pattern coverage area

In the case of circular coverage (Fig. 3.1(a)):

$$A_{ap} = \pi \cdot R^2. \tag{3.10}$$

where the circle radius, R, is

$$R = x_o \cdot \sin(\tfrac{1}{2}\beta); \tag{3.11}$$

here, x_o is the distance between the BS and the mobile and β denotes the BS antenna HPBW (half power beam width). For small values of β, $\sin(\frac{1}{2}\beta)$ can be approximated by $\beta/2$.

Alternatively, in the case of a semi-elliptic coverage:

$$A_{ap} = x_o^2 \cdot \left(\sin(\beta/2)\cos(\beta/2) + \tfrac{1}{2}(\pi + \beta)\sin^2(\beta/2)\right) \tag{3.12}$$

The probability of one arrival or one departure, p, is directly proportional to the change in coverage area of the antenna pattern (ΔA_{ap}) (due to its movement in Δt). Specifically

$$p = \rho_o \cdot \Delta A_{ap}. \tag{3.13}$$

For the *circular coverage scenario* ΔA_{ap} is approximated, using geometric calculations shown in Fig. 3.2, by:

$$\Delta A_{ap} \cong 2(x_o \cdot \sin(\tfrac{1}{2}\beta)) \cdot (x_o \cdot \Delta\phi). \tag{3.14}$$

Here, $\Delta\phi$ is the azimuth angle variation within time Δt, and corresponds to (using (2.3))

$$\Delta\phi = \kappa \cdot \frac{\Delta t}{T_S} \cdot \beta. \tag{3.15}$$

Substituting (3.15) in (3.14) and (3.14) in (3.13), and approximating $\sin(\frac{1}{2}\beta)$ by $\beta/2$, p corresponds to (for the circular coverage scenario)

$$p \cong \kappa \rho_o x_o^2 \beta^2 \cdot \frac{\Delta t}{T_S}. \tag{3.16}$$

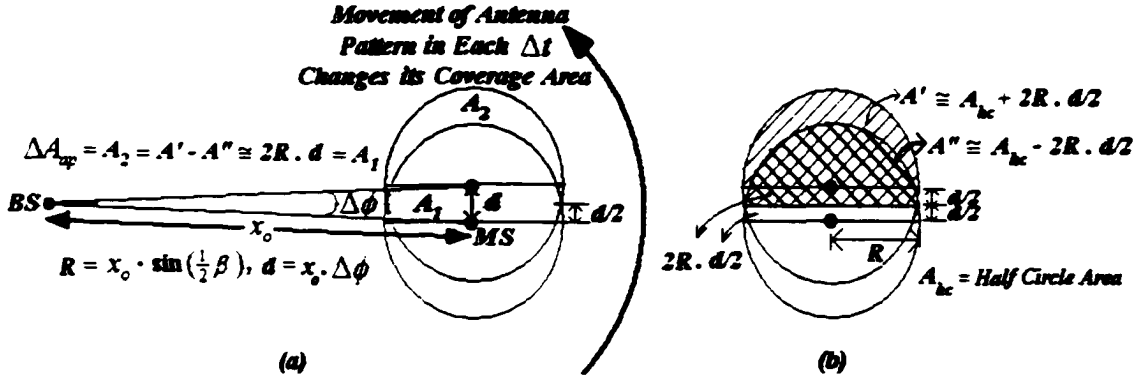

Fig. 3.2 Circular scenario: (a) Geometric calculation of $\Delta A_{ap} = A_2 = A' - A''$, (b) Calculation of A' and A''.

Meanwhile, for *semi-elliptic coverage*, we again have:

$$p = \rho_o \cdot \Delta A_{ap}, \tag{3.17}$$

where, now, ΔA_{ap} is approximated using the geometry of the coverage area (see Fig. 3.3), that corresponds to:

$$\Delta A_{ap} \cong \left(\tfrac{1}{2} x_o^2 \cdot \Delta\phi\right) \cdot \left(2\cos(\tfrac{1}{2}\beta) + \beta(\sin(\tfrac{1}{2}\beta) - \Delta\phi) + 2\sin(\tfrac{1}{2}\beta)\right) \tag{3.18}$$

Substituting (3.18) into (3.17), p corresponds to

$$p = 2\kappa \cdot A_R \cdot \frac{\Delta t}{T_S} \cdot N, \tag{3.19}$$

where $N = N(t)\big|_{t=t_0=0}$ and is presented in (3.9) and A_R is well approximated by

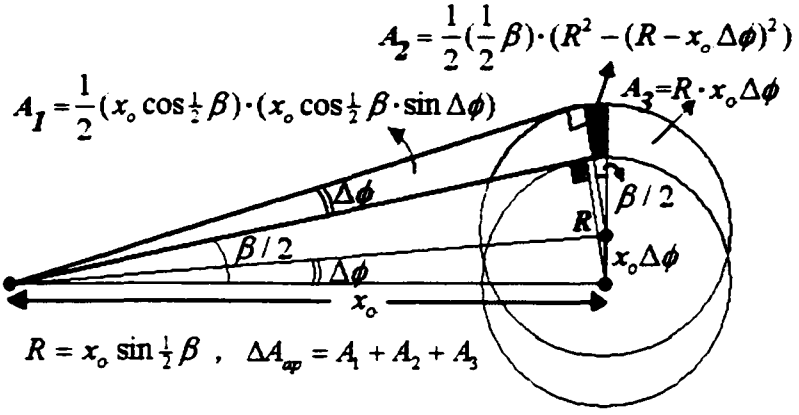

Fig. 3.3 Elliptic Scenario: Geometric calculation of ΔA_{ap}.

$$A_R = \frac{\beta}{\sin^2(\frac{1}{2}\beta)} \cdot \frac{\cos^2(\frac{1}{2}\beta) + \beta\sin(\frac{1}{2}\beta) + 2\sin(\frac{1}{2}\beta)}{2\cot(\frac{1}{2}\beta) + \pi + \beta}. \tag{3.20}$$

3.3 The Flat Fading Channel Approximation

If we assume the channel is flat, then the channel model of (3.1) simplifies to

$$h(t,\tau) = \left(\sum_{n=1}^{N(t)} \alpha_n(t) e^{j\theta_n(t)} \right) \cdot \delta(\tau - \tau_C) = \alpha(t) e^{j\theta(t)} \cdot \delta(\tau - \tau_C) \tag{3.21}$$

For both the circular and semi-elliptic coverage areas (Fig. 3.1), assuming a mobile to BS distance x_o=1000m, $\rho_o = 0.005 scatterer/m^2$ and HPBW=0.3 rad, the channel is well modeled as flat whenever $T_S \geq 1\mu\sec$.

3.4 Evaluation of Coherence Time

In this section, we use the channel model of Section 3.3 to determine the coherece time of the mobile channel in the presence of the proposed BS antenna array (Chapter 2). A medium-size city center is assumed [67][68]. That is, simulation parameters are selected as follows:

1. HPBW is in the range of 0.1 to 0.3 rad.

2. Simulations are performed for $x_o = 500$ and 1000m.

3. ρ_o is a value in the range of 0.001 to 0.005 *scatterers* / m^2.

4. The channel is assumed to be well modeled as flat (Equation (3.21)).

5. The control parameter κ (Equation (2.8)) is a value between 0.0005 to 0.05.

6. The scatterer dimension d_n is a normal RV with mean 20m and variance $(\frac{1}{4}20)^2 = 25$.

For simulation purposes, the interval $[0, T_S]$ is discretized into $n_s = 100$ sample times, $t_0, t_1, \ldots, t_{99}$, and for both the circular scenario and semi-elliptic scenario we performed the simulations as follows.

3.4.1 Simulations for circular scenario

As we mentioned, for simulation purposes, the interval $[0, T_S]$ is discretized into $n_s = 100$ sample times, $\{t_0 = 0, t_1, t_2, t_3, \ldots, t_{n_s-1} = T_S\}$. Initially, at time t_o, we establish a starting environment as follows. First, we assume the number of scatterers present corresponds to $N(t_o) = \rho_o A_{sp}$ (see (3.9)). Next, we determine the position of each of the $N(t_o)$ scatterers: (1) assuming a uniform distribution for η_n (the angle-of-arrival of scatterers at the mobile (Fig. 3.1(a))), we establish the angular position of each of the scatterers; and (2) the distance between scatterer and mobile (r_n in Fig. 3.1(a)) is established by sampling a uniform random variable between zero and R. (The distance between scatterer and BS (x_n in Fig. 3.1(a)) can now be determined by simple geometry.) Finally,

we determine the gain and phase (at the receiver) for each reflection from a scatterer via a sampling of RVs characterized in Section 3.2.

The amplitude of the received signal, $\alpha(t_k)$ (see Equation (3.21)) is calculated at each t_k based on the stochastic channel modeling. Specifically, at each t_k:

(1) determine if one scatterer arrival or departure process has begun, based on the probability of (3.16);
(2) if a scatterer arrives (or departs), its parameters are determined via, e.g., the amplitude of this scatterer is evaluated using (3.3) or (3.7); and
(3) the cumulative amplitude, $\alpha(t_k)$, is evaluated using (3.21). Note that the scatterer assumed to depart is always the scatterer nearest to the HPBW boundary point.

Typical $\alpha(t_k)$ versus t_k plots are shown in Fig. 3.4(a)-(c) for x_o = 1000m, ρ_o = 0.005 $scatterers/m^2$, κ = 0.05, and HPBW=0.5rad. These plots clearly demonstrate the varying nature of $\alpha(t)$ due to beam pattern movements. (It should be noted that an FFT of the gain (Fig. 3.4(a-2)-(c-2)), shows negligible bandwidth expansion.)

Now, the sampled autocorrelation function (ACF) for $\alpha(t)$ is computed over $[0, T_S]$ using [69]:

$$R(k) = \gamma(k)/\gamma(0), \tag{3.22}$$

where

$$\gamma(k) = \frac{1}{n_S} \cdot \sum_{i=0}^{n_S-k-1} (\alpha(t_{i+k}) - \bar{\alpha}) \cdot (\alpha(t_i) - \bar{\alpha}) \tag{3.23}$$

$$\bar{\alpha} = \frac{1}{n_S} \cdot \sum_{k=0}^{n_S-1} \alpha(t_k) \tag{3.24}$$

Next, coherence time T_C is determined by defining T_C as the time interval over which the ACF is greater than 0.5 [1]. The T_C / T_S mean that results from simulation is presented in Fig. 3.5(a-f).

Simulation results show coherence time decreases as: 1) the distance between BS and MS, x_o, increases; 2) the scatterer's density ρ_o increases; 3) HPBW increases; and 4) the parameter κ increases, i.e., T_C is inversely proportional to x_o, ρ_o, HPBW and κ. This is not surprising since, referring to (3.16), we observe that as x_o, ρ_o, HPBW and/or κ increase, the value p (the probability of scatterer arrival or departure in the interval Δt) increases. Hence, as x_o, ρ_o, HPBW and/or κ rise, the environment changes more rapidly, resulting in a reduced coherence time T_C. Moreover, referring to (2.8), which characterizes the time varying delay element $\tau(t)$, we observe that the rate of change (i.e., slope) of $\tau(t)$ increases as κ and β (HPBW) increases. Hence, we expect a decrease in the coherence time as these parameters rise. This matches the observed results.

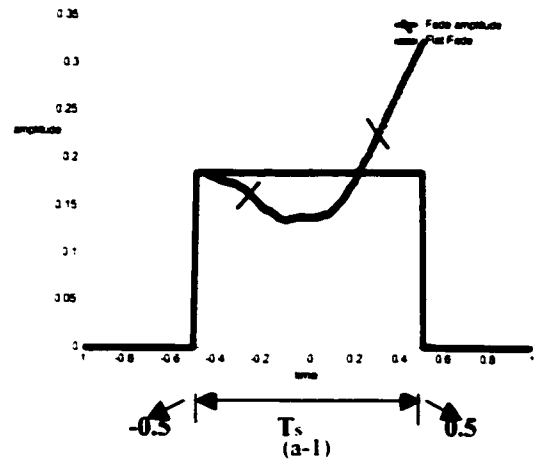

(a-1)

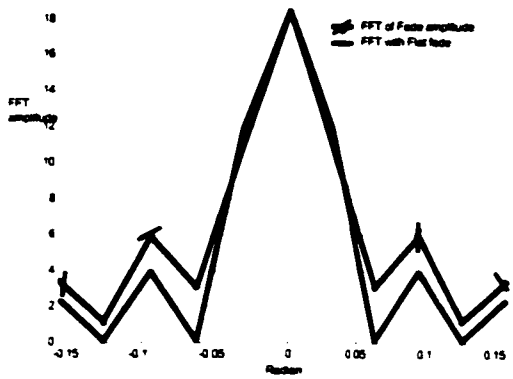

(a-2)

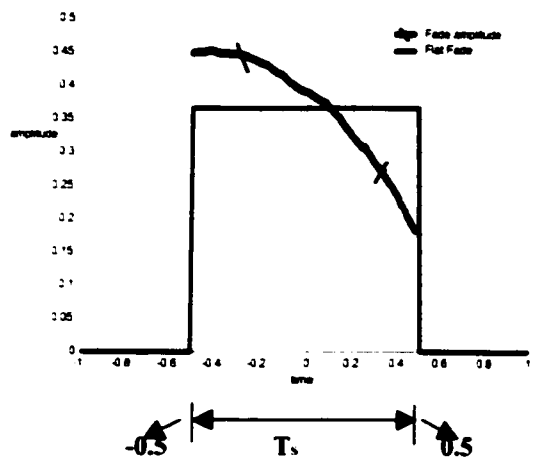

(b-1)

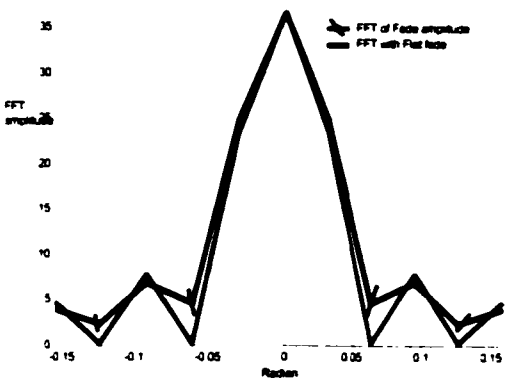

(b-2)

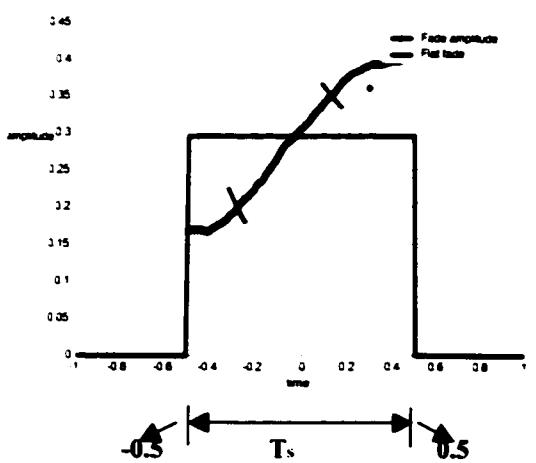

(c-1)

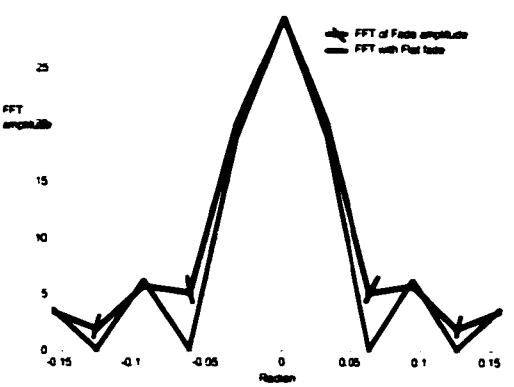

(c-2)

Fig. 3.4 (a-c) The time varying nature of $\alpha(t)$ and its spectrum

Also in Fig. 3.5, coherence times are observed as low as $T_C / T_S = 0.16$, a value achieved when antenna control pattern parameter κ = 0.05, i.e., when the beam pattern sweep corresponds to 5% of the HPBW. With time diversity gain L well modeled as $L = \frac{T_S}{T_C} = \frac{1}{T_C / T_S}$, the maximum diversity gain achieved via beam pattern oscillation with $\kappa \leq 0.05$ is $L \cong 7$. This $L \cong 7$ value does lead to large performance benefits in mobile receivers.

It is important to note that time diversity gain is limited to $L \leq 7$ only because κ is held to values $0 < \kappa \leq 0.05$. We keep κ in this small range of values to ensure that time varying delay $\tau(t)$ creates a minimal bandwidth expansion. For notably larger κ, i.e., bigger antenna array sweeps, diversity gain L can be further increased at the cost of bandwidth expansion.

3.4.2 Simulations for semi-elliptic scenario

Initially, at time t_o, we establish a starting environment as follows:

(1) we assume $N(t_o) = \rho_o A_{ap}$ scatterers are present in the coverage area where A_{ap} is determined by (3.18);

(2) generating ϕ_n, we determine (by sampling ϕ_n distribution function (see Section 3.5.1)) the angular position of each scatterer;

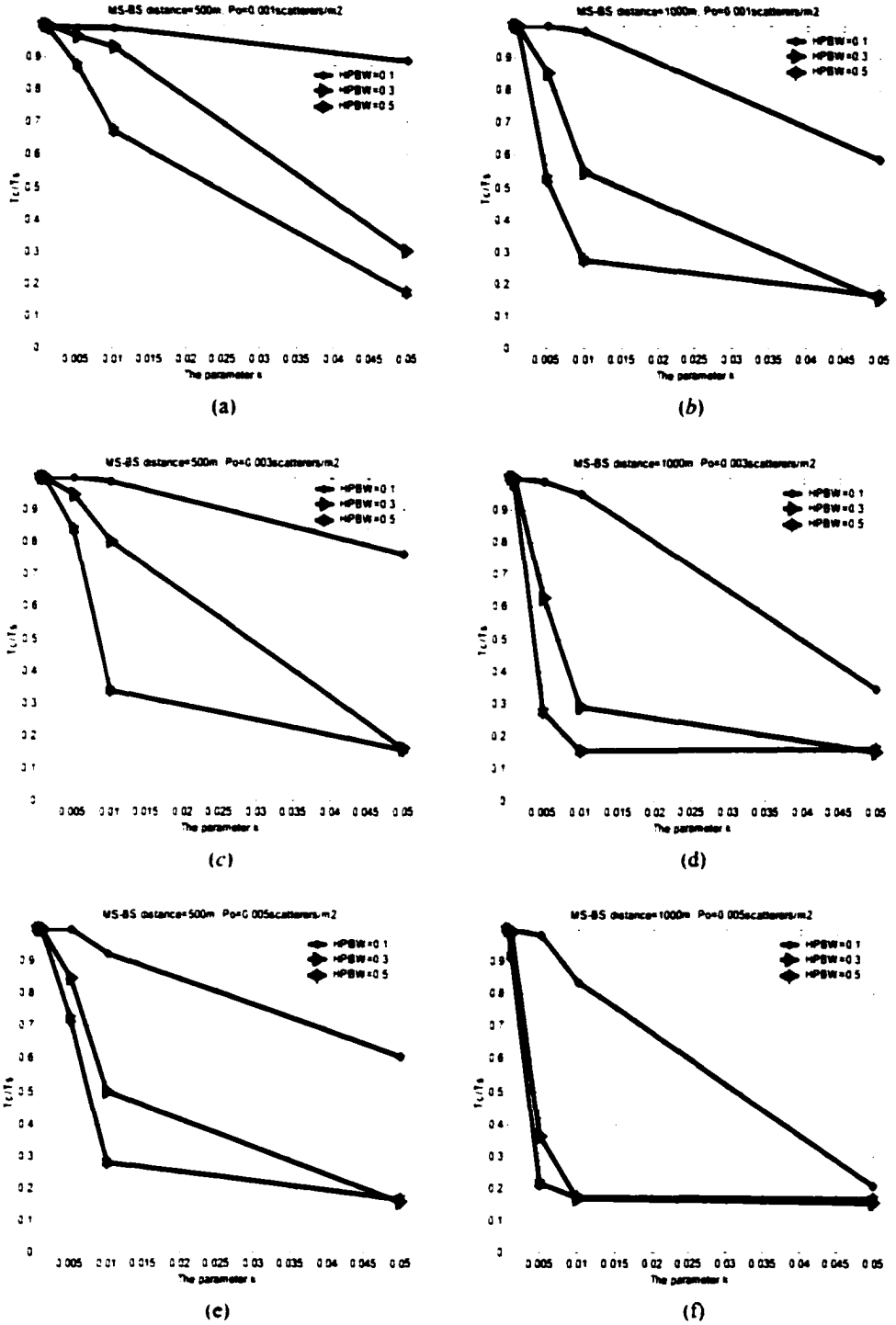

Fig. 3.5(a-f) The coherence time mean simulation results in terms of the parameter κ *(which is from 0.0005 to 0.05)* .
(a),(b) Scatterer density of 0.001 (at distances of 500m and 1000m, respectively).
(c),(d) Scatterer density of 0.003 (at distances of 500m and 1000m, respectively).
(e),(f) Scatterer density of 0.005 (at distances of 500m and 1000m, respectively).

(3) the distance between scatterer and BS is established next by sampling a uniform random variable between zero and $x_{n,\max}$ (see Fig. 3.7); and finally

(4) the gain for each scatterer is determined by sampling a Rayleigh pdf.

The amplitude of the received signal, $\alpha(t_k)$ (see (3.21)), is calculated at each t_k using the stochastic channel modeling described in Section 3.2. Specifically, at each t_k:

(1) determine if one scatterer arrival or departure process has begun, based on the probability of (3.19);

(2) if a scatterer arrives (or departs) its parameters are determined via, e.g., the amplitude of this scatterer is evaluated using (3.3) (or (3.7)); and

(3) the cumulative amplitude, $\alpha(t_k)$, is evaluated using (3.21). Note that the scatterer that departs is assumed to be the scatterer with an angle ϕ_n that puts it nearest to the HPBW boundry points.

The sample autocorrelation function (ACF) for $\alpha(t_k)$ is then determined over $[0, T_S]$ using well-known correlation methods (see (3.22)-(3.24)) and next, coherence time T_C is determined, again by defining T_C as the time interval over which the ACF is greater than 0.5. The T_C / T_S mean that results from simulation (averaged over 100 T_C / T_S values) is presented in Fig. 3.6(a-d). These figures plot the coherence time (T_C / T_S) as a function of κ, the parameter controlling the rate of beam pattern oscillation (see (2.8)). Three curves

are plotted per figure, each for a different scatterer density ($\rho_o = 0.001, \rho_o = 0.002, \rho_o = 0.003$ scatterers/m^2).

Similar to Fig. 3.5, from Fig. 3.6 coherence time decreases as: 1) control parameter κ increases; 2) the scatterer's density ρ_o increases; 3) the BS-MS distance x_o increases; and 4) HPBW increases.

Also in Fig. 3.6, coherence time is observed to be as low as $T_C / T_S \cong 0.17$, when the antenna pattern movement control parameter is $\kappa = 0.05$, i.e., when the beam pattern sweeps an angle corresponding to 5% of the HPBW. Because T_C / T_S characterizes the available time diversity, according to the well known relationship $L = (T_C / T_S)^{-1}$ (where L is the order of the available diversity gain), we observe $L = (T_C / T_S)^{-1} \cong 7$ fold time diversity benefit when oscillating the beam pattern by an amount corresponding to 5% of the HPBW.

It is very interesting to note that small values of κ, e.g., $\kappa = 0.05$, leads to $L = 7$ fold diversity. We believe this results because small changes in beam pattern movement impact a large number of scatterers in a dense urban environment (assuming MS-BS distance of, e.g., x_o = 500m or 1000m). This impact on large numbers of scatterers leads to the observed 7-fold diversity. Hence, when an antenna array with an oscillating beam pattern is mounted on a BS, 7-fold time diversity can be generated at the MS with small

antenna pattern movement. This corresponds to a very significant performance benefit at the receiver.

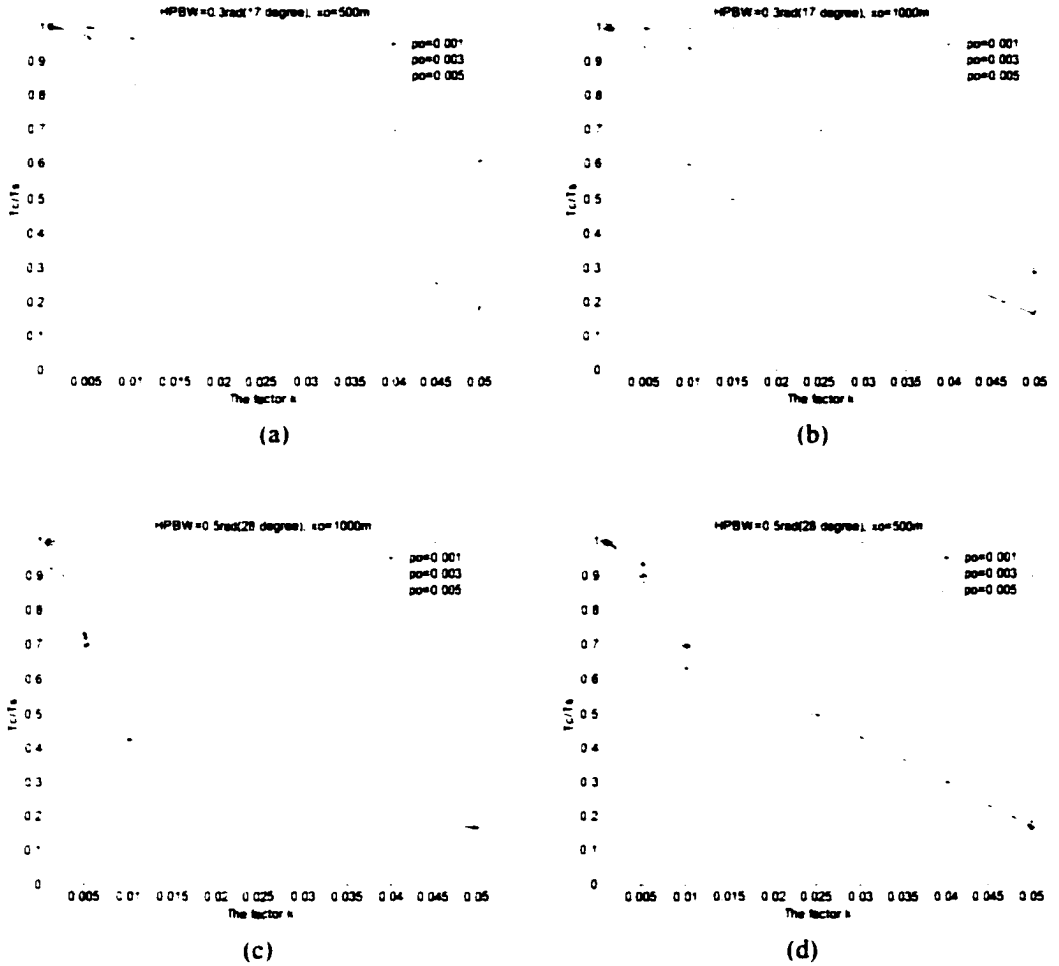

Fig. 3.6 T_C / T_S interms of control parameter κ for HPBW=0.3rad, and (a) $x_o = 500m$,(b) $x_o = 1000m$, and for HPBW=0.5rad, and (c) $x_o = 500m$,(d) $x_o = 1000m$.

3.5 Updates to the Channel Impulse Response: Antenna Array Factor and Phase

A linear time-varying impulse response model is the most widely accepted representation of the fading channel. However, in the model of (3.1), we have assumed that the array factor is 1 for all scatterers of interest, and we have ignored the phase effects introduced by the antenna array. Including these effects in the impulse response channel model leads to a more accurate impulse response model. Here, the impulse response of the channel corresponds to:

$$h(t,\tau) = \sum_{n=1}^{N(t)} AF(t,\phi_n) \cdot e^{j\omega(t,\phi_n)} \cdot \alpha_n(t) \cdot e^{j\theta_n(t)} \cdot \delta(\tau - \tau_n). \tag{3.25}$$

Here, ϕ_n represents the angular position of the n^{th} scatterer in the coverage area (Fig. 3.1); $AF(t,\phi_n)$ represents the gain due to the n^{th} scatterer's position in the antenna array mainlobe, and $\omega(t,\phi_n)$ is the corresponding phase offset. We simplify our notation by defining

$$\theta_n'(t,\phi_n) = \theta_n(t) + \omega(t,\phi_n). \tag{3.26}$$

The statistics of $N(t)$, $a_n(t)$ and τ_n are the same as those introduced in Section 3.2. Here, we introduce the statistics of ϕ_n and $\theta_n'(t,\phi_n)$ (Equations (3.25) and (3.26)).

3.5.1 Angular position of the scatterers ϕ_n

Case 1: The Circular Coverage Scenario

The angular position of the n^{th} scatterer, ϕ_n, is modeled as a random variable with PDF $f(\phi_n)$. To determine this PDF we turn our attention to Fig. 3.1(a). Here, it is apparent that ϕ_n is related to ϕ_n' (angle of arrival (AOA) at the BS) via

$$\phi_n = \pi/2 - \phi_n', \tag{3.27}$$

$$\phi_n' = \sin^{-1}\left(\left|\frac{r_n \sin(\eta_n)}{x_n}\right|\right), \tag{3.28}$$

where η_n, shown in Fig. 3.1(a), is uniform over $[0,2\pi)$; r_n, shown in Fig. 3.1(a), is uniform over $[0,R]$: and x_n, also shown in Fig. 3.1(a), corresponds to $x_n = \left(x_o^2 + r_n^2 - 2x_o r_n \cos(\eta_n)\right)^{1/2}$, where x_o is the MS-BS distance.

Case 2:The Semi-Elliptic Scenario

To determine the PDF of ϕ_n', assuming a uniform distribution of scatterers, we begin with the cumulative density function (CDF) of ϕ_n'. This corresponds to (Fig. 3.7)

$$F(\phi_n') = \frac{A(\phi_n')}{A_{ap}}. \tag{3.29}$$

where $A(\phi_n')$ is a portion of the coverage area contained within the angular spread of $2\phi_n'$, and corresponds to (see Appendix 1)

$$\begin{aligned} A(\phi_n') = {} & x_o^2 \cdot \sin(|\phi_n'|)\cos(|\phi_n'|) + \sin(|\phi_n'|)\cdot\sin(\beta/2)\sqrt{1-\left(\frac{\sin(|\phi_n'|)}{\sin(\beta/2)}\right)^2} \\ & + x_o^2 \cdot \left(\frac{\pi}{2} - \cos^{-1}\left(\frac{\sin(|\phi_n'|)}{\sin(\beta/2)}\right) + |\phi_n'|\right)\cdot\sin^2(\beta/2), \end{aligned} \tag{3.30}$$

and A_{ap} is the total antenna pattern coverage area, i.e.,

$$A_{ap} = x_o^2 \cdot \left(\sin(\beta/2)\cos(\beta/2) + \tfrac{1}{2}(\pi+\beta)\sin^2(\beta/2)\right). \tag{3.31}$$

Substituting (3.30) and (3.31) in (3.29) and differentiating, the PDF of ϕ_n' is

$$f(\phi_n') = \frac{1}{(\pi+\beta+2\cot(\beta/2))}\left[1+\frac{\cos(2|\phi_n'|)}{\sin^2(\beta/2)}+\frac{2\cos(|\phi_n'|)}{\sin(\beta/2)}\sqrt{1-\left(\frac{\sin(|\phi_n'|)}{\sin(\beta/2)}\right)^2}\right]. \tag{3.32}$$

This PDF is shown in Fig. 3.8 for two different values of HPBW (β). It is observed that as HPBW decreases, $f(\phi_n')$ tends to a uniform PDF.

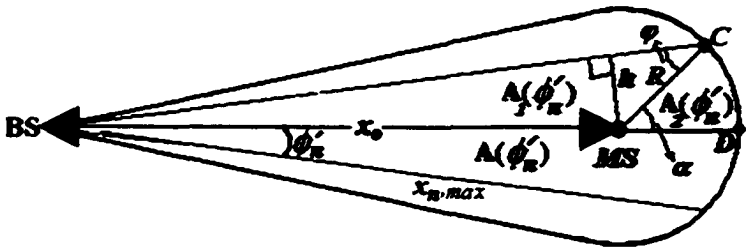

Fig. 3.7 Calculation of the CDF of AOA.

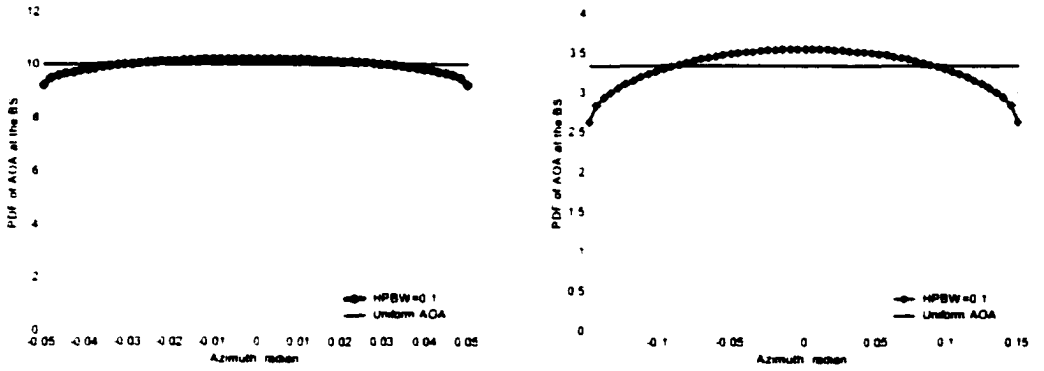

(*a*) (*b*)

Fig. 3.8 PDF of ϕ_n' (AOA at the BS) compared with uniform PDF for: a) HPBW=0.1, b) HPBW=0.3.

3.5.2. Phase offset, $\theta_n'(t,\phi_n)$

We now turn our attention to phase offset $\theta_n'(t,\phi_n) = \theta_n(t) + \omega(t,\phi_n)$. Here, the phase $\theta_n(t) = \theta_n$ is considered uniform over $[0,2\pi)$ (as shown in the previous subsection). Hence,

$$\theta_n'(t,\phi_n) = \theta_n + \omega(t,\phi_n). \tag{3.33}$$

where

$$\omega(t,\phi) = \frac{M-1}{2}\gamma(t,\phi). \tag{3.34}$$

Here, $\gamma(t,\phi)$ is introduced in (2.2). If we discretize the interval $[0,T_S]$ into n_s sample times, $t_0,t_1,....,t_k,.....t_{n_s-1}$, the phase offset $\theta_n'(t_k,\phi_n)$ can be determined using the value $\theta_n'(t_{k-1},\phi_n)$. This is achieved by calculating $\omega(t_k,\phi_n)$ and $\omega(t_{k-1},\phi_n)$ and noting that

$$\theta_n'(t_k,\phi_n) = \theta_n'(t_{k-1},\phi_n) + \left(\omega(t_k,\phi_n) - \omega(t_{k-1},\phi_n)\right). \tag{3.35}$$

To determine $\omega(t_k,\phi_n) - \omega(t_{k-1},\phi_n) = \psi_n(t_k)$, we apply (3.34) and (2.8) which leads to

$$\psi_n(t_k) = \frac{M-1}{2}\cdot\frac{2\pi d}{\lambda_o}\cdot\kappa\cdot\frac{\Delta t}{T_S}\left[(1-\beta)\sin(\phi_n) + \beta\cdot t_k\cdot\cos(\phi_n)\right]. \tag{3.36}$$

Here, M represents the number of antenna array elements, d is the distance between array elements and $\Delta t = t_k - t_{k-1}$. Finally, the initial value $\theta'(0,\phi_n)$ corresponds to

$$\theta_n'(0,\phi_n) = \theta_n + \frac{M-1}{2}\cdot\frac{2\pi d}{\lambda_o}\cdot\cos(\phi_n). \tag{3.37}$$

3.6 Coherence time and available diversity benefit for the updated impulse response

Next, we update the computation of coherence time when the impulse response $h(t,\tau)$ is changed from its representation in (3.1) to that of (3.25). To compute this cohernce time, we maintain all of the assumptions made in Section 3.1.

3.6.1 Circular coverage simulation results

Using simulation methods outlined in the previous subsection, the T_C / T_S mean that results is presented in Fig. 3.9(a) and Fig. 3.9(b). Fig. 3.9(a) plots the coherence time as a function of κ, the parameter controlling the rate of beam pattern oscillation (see (2.8)) assuming HPBW = 0.5rad. In this figure, three curves are plotted, each for different scatterer density, ($\rho_a = 0.001$, $\rho_a = 0.002$ and $\rho_a = 0.003$ scatterer/m^2). Fig. 3.9(b) represents the dependence of coherence time on HPBW for three different scatterer densities.

From Fig. 3.9(a,b), the coherence time decreases as control parameter κ increases (i.e., the sweeping rate increases), the scatterer density increases, the HPBW increases and the BS to mobile station distance increases. Moreover, coherence time is $T_C / T_S \cong 0.14$ when oscillating the beam pattern by an amount corresponding to 5% of the HPBW. That is, L

≅ 8 fold diversity is avalable over T_S. This is consistent with an earlier result where antenna array gain and phase were neglected in the beam pattern's mainlobe.

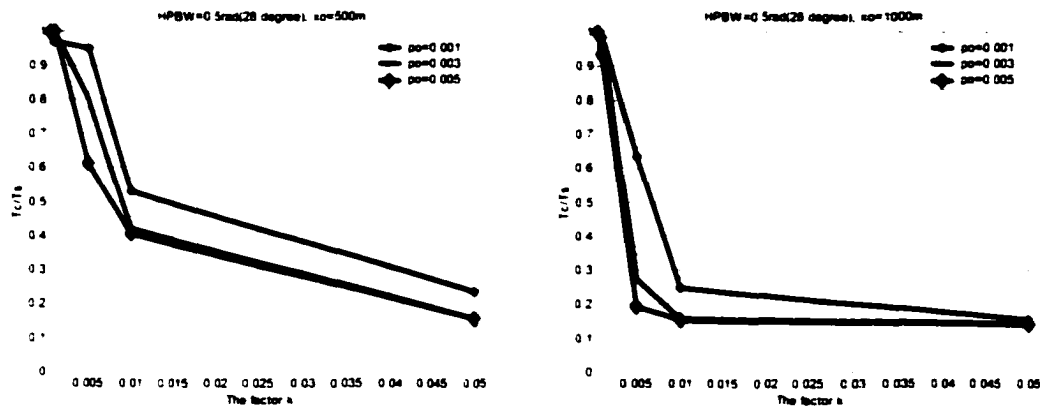

(a-1) (a-2)

Fig. 3.9(a) T_C / T_S interms of the control parameter κ for HPBW=0.5rad and (a-1) x_o=500m and (a-2) x_o=1000m (cicular scenario).

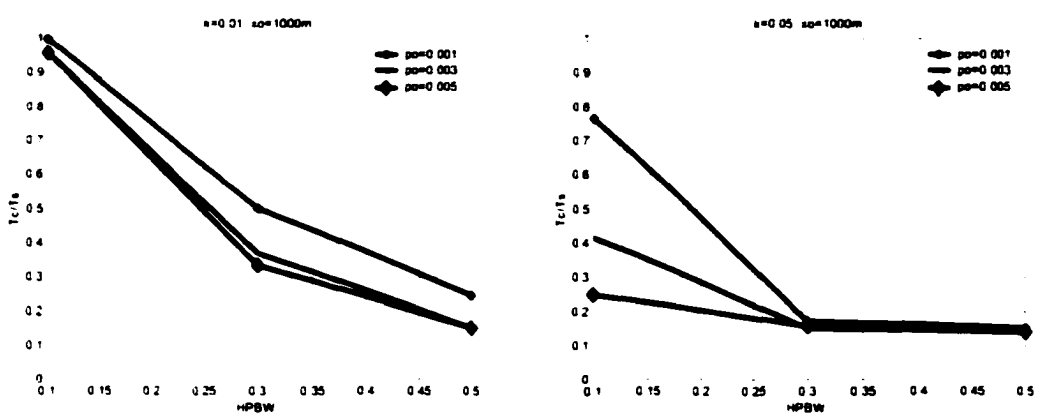

(b-1) (b-2)

Fig. 3.9(b) T_C / T_S in terms of HPBW for x_o=1000m, and (b-1) κ=0.01, (b-2) κ=0.05.

3.6.2 Semi-elliptical coverage simulation results

The T_C / T_S mean that results from our simulations is presented in Fig. 3.10(a) and Fig. 3.10(b). Fig. 3.10(a) plots the coherence time as a function of κ, the parameter controlling the rate of beam pattern oscillation (see (2.8)), assuming HPBW = 0.5rad. In this figure, three curves are plotted, each for a different scatterer density ($\rho_o = 0.001$, $\rho_o = 0.002$ and $\rho_o = 0.003$ scatterer/m^2). Fig. 3.10(b) represents the dependence of coherence time on HPBW for three different scatterer densities.

From Fig. 3.10(a) and (b) coherence time decreases as: 1) control parameter κ increases (i.e., sweeping rate increases); 2) the scatterer's density ρ_o increases; 3) BS-MS distance, x_o, increases; and 4) HPBW increases. Here, coherence time is $T_C / T_S \cong 0.17$, i.e., $L \cong 7$ fold diversity over T_S for a beam pattern movement corresponding to 5% of HPBW.

3.7 Conclusions

In this chapter, we considered a BS smart antenna array with an oscillating beam pattern, generating a controllable coherence time. The coherence time created by the oscillating beam pattern was determined by using a comprehensive geometric-based stochastic channel model with a semi-elliptic coverage. Simulation results show that a coherence time can be established by beam pattern oscillation which leads to L = 7 fold time

diversity at the MS (when small beam pattern movement is present). Hence, beam pattern motion can create a very significant increase in performance at the MS.

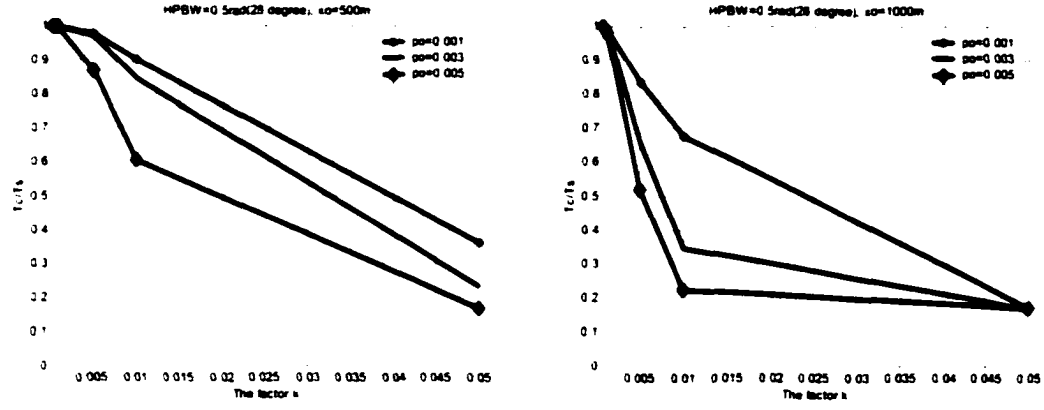

(a-1) (a-2)

Fig. 3.10(a) T_C / T_S for in terms of the control parameter κ and HPBW=0.5rad, and (a-1) x_o=500m and (a-2) x_o=1000m (semi-elliptic Scenario).

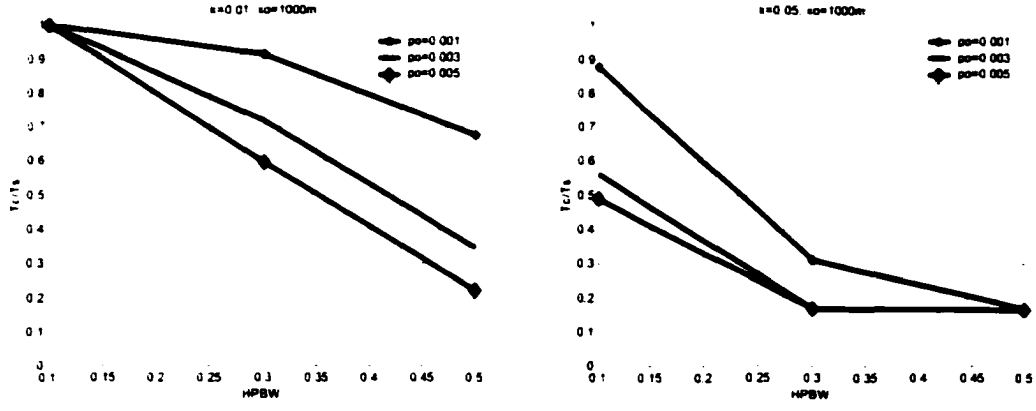

(b-1) (b-2)

Fig. 3.10(b) T_C / T_S in terms of HPBW for x_o=1000m, and (b-1) κ=0.01, (b-2) κ=0.05 .

Chapter 4

A Merger of Oscillating-Beam Smart Antenna Arrays and Multi-Carrier Systems:

Achieving Transmit Diversity, Frequency Diversity and Directionality

Multi-carrier code division multiple access (MC-CDMA) [50]-[53] is emerging as a powerful multiple access protocol. In MC-CDMA, each users' information symbol is transmitted over N carriers simultaneously. To ensure separablity of users' data streams at the receiver, each user assigns a unique spreading sequence to the N carriers, typically a set of values each either +1 or –1.

Recently, Carrier Interferometry (CI) codes (complex codes) were introduced to MC-CDMA [70]-[72], and these codes achieved: 1) high capacity by allowing N orthogonal users to occupy the channel simultaneously, and, if further users are to be supported, an additional N users can be added with minimal interference; and 2) high performance via low correlation between all $2N$ codes. We intend to innovatively apply the oscillating

beam antenna arrays to MC-CDMA systems using CI codes (referred to as CI/MC-CDMA in this chapter). This enables: 1) very high capacity via the merger of space division multiple access (SDMA) (directionality of antenna array) and code division multiple access inherent in CI/MC-CDMA; and 2) very high performance via the construction of receivers that exploit both transmit diversity and frequency diversity. In this chapter, we emphasize the performance benefits of the proposed merger.

The benchmark for comparison in this chapter is an MC-CDMA system employed in conjunction with a conventional smart antenna array. Here, the smart antenna array creates an adaptive beam pattern directed toward the intended user, leading to increased capacity via SDMA. However, unlike the proposed scheme, no improvements to performance are provided to the MC-CDMA system via application of the smart antenna array. This chapter highlights the performance benefits that can be achieved by small oscillations of the beam pattern.

Moreover, in this chapter, we consider a generalized scenario: at the BS, each set of Q ($Q \leq N$) carriers in the CI/MC-CDMA N-carrier system is fed into a unique M-element smart antenna array. By selecting $Q=N$, we return to the conventional scenario of one base station antenna array. In today's cellular 2G and 3G markets, where transmit bandwidths are small relative to carrier frequencies (e.g., 5MHz bandwidth versus 2GHz carrier frequency), all $Q = N$ carriers demonstrate a similar beam pattern when transmitted over a single antenna array. However, with an eye toward the future, where 4G cellular systems will require very large bandwidth to support anticipated 60Mb/s data rates (see,

e.g., [73]), it will not be possible to support all carriers in a single antenna array (due to the different beam patterns that would result from the different carriers). In this scenario, it becomes necessary to divide the N carriers into P groups of $Q \leq N$ neighboring carriers each.

With this in mind, we consider two generalized scenarios. In the first scenario, P smart antennas are separated by a distance that ensures independent fades between each set of Q carriers (at the receiver). By carefully designing the set of phase shifts applied to the elements of each antenna array, and by properly setting the distance between antenna elements, the resulting beam pattern created by the BS corresponds to an oscillating beam pattern. This creates a time-varying channel with a controllable coherence time.

In the second scenario, the smart antennas are located in close proximity to one another (at the BS), which is the case when, due to space limitation, we can not separate the antenna arrays by a large distance. Here, again, by carefully designing the phase shifts applied to each antenna array element, and by properly setting the distances between antenna elements, the resulting beam-pattern corresponds to an oscillating beam pattern

Receivers are designed to exploit both the transmit diversity, which corresponds to an induced time diversity, as well as the frequency diversity of the CI/MC-CDMA systems. Different receiver structures are examined, including EGC/MRC/MMSEC (Equal Gain Combining / Maximal Ratio Combining / Minimum Mean Square Error Combining) performed in the frequency domain followed by a corresponding time diversity combining (and vise-versa).

Section 4.1 introduces the CI/MC-CDMA structure and Section 4.2 presents the beam-sweeping antenna array structure. Section 4.3 presents receiver structures employing EGC in the frequency domain followed by EGC, MRC or MMSEC in the time domain (and vice versa). Section 4.4 presents simulated performance results, and Section 4.5 concludes the chapter.

4.1 A Brief Introduction to the CI/MC-CDMA System.

In MC-CDMA, each user's bit is transmitted simultaneously over N narrowband subcarriers. Subcarriers are equally spaced in frequency by Δf. To ensure separability of users at the receiver side, each user applies a unique spreading code to the carriers. Hence, the k^{th} user's i^{th} data bit, $b_k[i]$, is sent as:

$$s_k(t) = \mathrm{Re}\left\{b_k[i]e^{j2\pi f_o t}C_k(t)\right\}, \tag{4.1}$$

where $b_k[i]$ is assumed +1 and −1 for ease in presentation, f_o is the carrier frequency, and $C_k(t)$ is user k's spreading code, corresponding to

$$C_k(t) = \left(\sum_{n=0}^{N-1} e^{j2\pi n\Delta f t}\cdot e^{j\beta_k^n}\right)\cdot g(t). \tag{4.2}$$

Here, $\Delta f \geq 1/T_S$ is employed to maintain carrier orthogonality, and $g(t)$ is a rectangular waveform of unity height over 0 to T_S. Finally, $e^{j\beta_k^n}$ refers to the n^{th} element of the spreading sequence, where traditionally $\beta_k^n \in \{0,\pi\}$ (i.e., $e^{j\beta_k^n} \in \{-1,+1\}$). However, when CI codes are employed,

$$\beta_k^n = \frac{2\pi}{N} \cdot n \cdot k, \tag{4.3}$$

for users *0, 1, ..., N-1,* (i.e., $k \in \{0,1,....,N\text{-}1\}$). In this way, N orthogonal users are supported (similar to case of Hadamard-Walsh codes); moreover, if additional users are to be supported, an additional N users can be introduced pseudo-orthogonally by adding users with spreading codes characterized by:

$$\beta_k^n = \frac{2\pi}{N} \cdot n \cdot k + \frac{\pi}{N} \cdot n, \tag{4.4}$$

for users *N, N+1, ... 2N-1* (i.e., $k \in \{N, N+1,...,2N-1\}$).

4.2 Proposed Antenna Array Structure

Assuming a CI/MC-CDMA system with N subcarriers, we divide the subcarriers into P sets, each with Q neighboring subcarriers ($P \cdot Q = N$). We apply each set of Q subcarriers to one of P M-element antenna arrays. Fig. 4.1(a) shows the p^{th} set

($p \in \{0,1,...,P-1\}$), of Q subcarriers (with frequencies $f_{p,q} = f_o + (Q \cdot p + q) \cdot \Delta f$, $q \in \{0,1,...,Q-1\}$, and with a phase offsets $\beta_k^{Q \cdot p+q}$) entering the p^{th} smart antenna at the BS. The m^{th} array element of the p^{th} smart antenna applies the time-varying phase shift $m\theta(t,p)$, $m \in \{0,1,...,M-1\}$, and a correctional phase shift $m\psi_p$. (Note that in this section we replace antenna element delay $\tau(t)$ of Chapters 2 and 3 with phase shift $\theta(t)$, where $\theta(t) = 2\pi f_o \tau(t)$.) Fig. 4.1(b) shows the configuration of all P antenna arrays, one for each set of Q carriers, where we observe the spacing between identical elements on adjacent antenna arrays is D_p. It is assumed throughout that these arrays are spaced in an equidistant manner (as shown in Fig. 4.1(b)) along the x-axis, with the mobile located on the x-y plane.

All the P smart antenna arrays are designed to generate beam patterns satisfying: 1) the peak in the antenna patterns occurs at the same location in space; and 2) the beam pattern shape of all the smart antennas are identical.

It is important to note that in today's cellular systems, where transmit bandwidth is much less than carrier frequency (e.g., 5MHz bandwidth, 2GHz carrier frequency), all carriers can be placed on a single antenna array (i.e., $Q = N$, $P = 1$), and identical beam patterns will result for all carriers. However, in future generation cellular, or even in upcoming WLAN (Wireless Local Area Networks) standards (e.g., see [74]), where transmit bandwidths are no more than two orders of magnitude smaller than carrier frequency (e.g., 83MHz bandwidth, 2.46GHz carrier frequency), the requirements of "identical" *beam patterns can only be satisfied with* $P > 1$. Moreover, in future generation systems

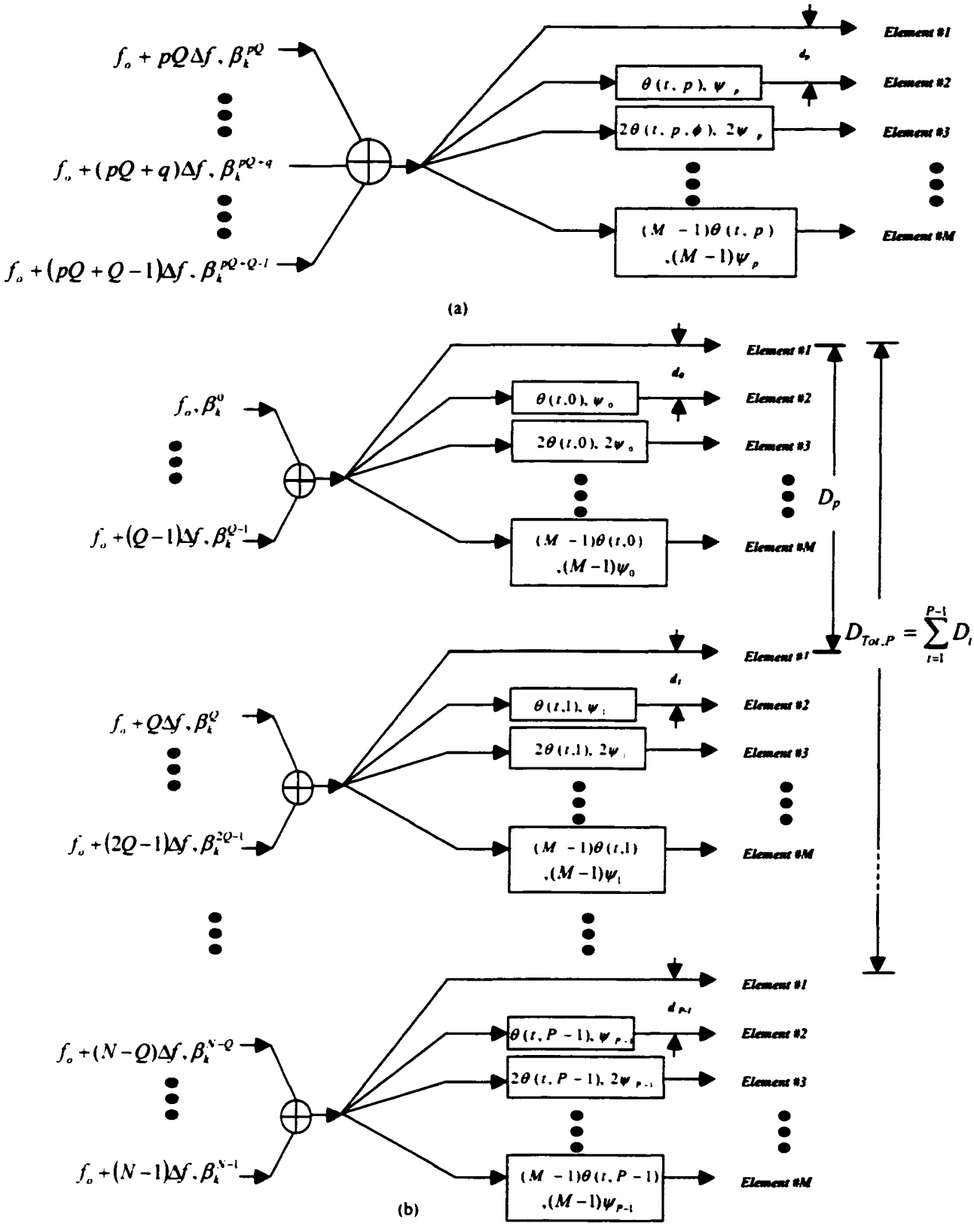

Fig. 4.1 (a) The p^{th} smart antenna array over which the p^{th} group of CI/MC-CDMA signal frequency components are sent, (b) the entire set of P antenna arrays.

that will operate over non-contiguous frequency bands (e.g., see [73]) and those that will support ultrawideband (UWB) communications, a constant beam pattern over the range of transmit frequencies can only be achieved with $P > 1$.

The reason we require identical beam patterns for all carriers can be easily understood by considering the scenario where the antenna array achieves directionality via a sectorization strategy. Here, if different carriers create different HPBWs (half power beam widths), there exist very undesirable scenarios. Referring to Fig. 4.2, a user is seen travelling in the area where he experiences an antenna array pattern from two sectors (due to unequal HPBWs). Here, the user experiences (1) large interference from the beam pattern of the unintended sector and (2) a reduction in power in the desired signal in the beam pattern from the desired sector.

Moreover, in the case of an adaptive (non-sectorizing) antenna array, the variability in beam pattern (including the variability in HPBW) makes it impossible to effectively null or minimize the beam pattern at unintended users, notably reducing the network capacity gains achievable in such a scenario.

Now, we consider two scenarios: (1) P antenna arrays located far apart from one another, and (2) P antenna arrays located in close proximity.

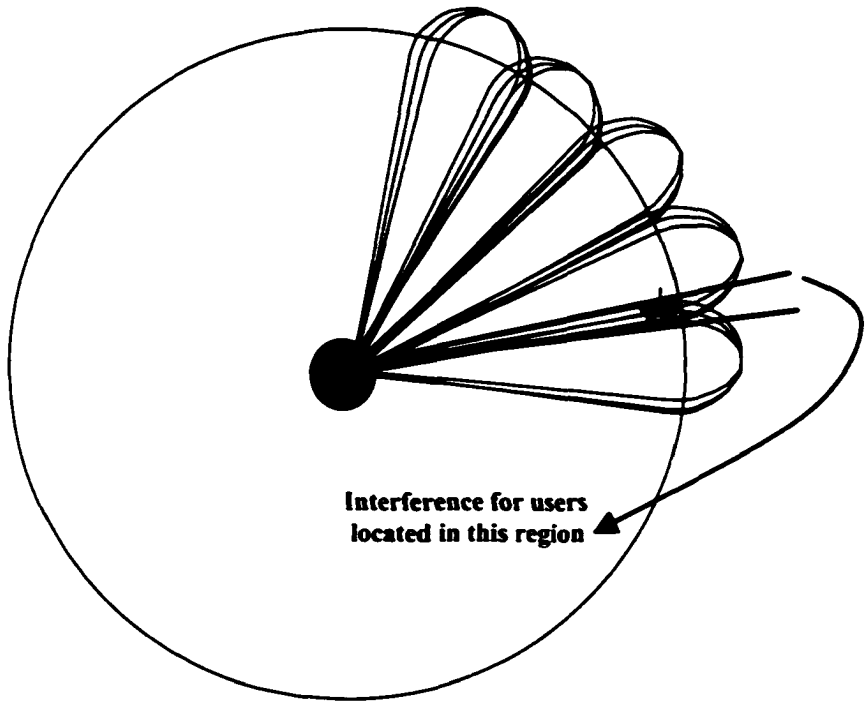

(a)

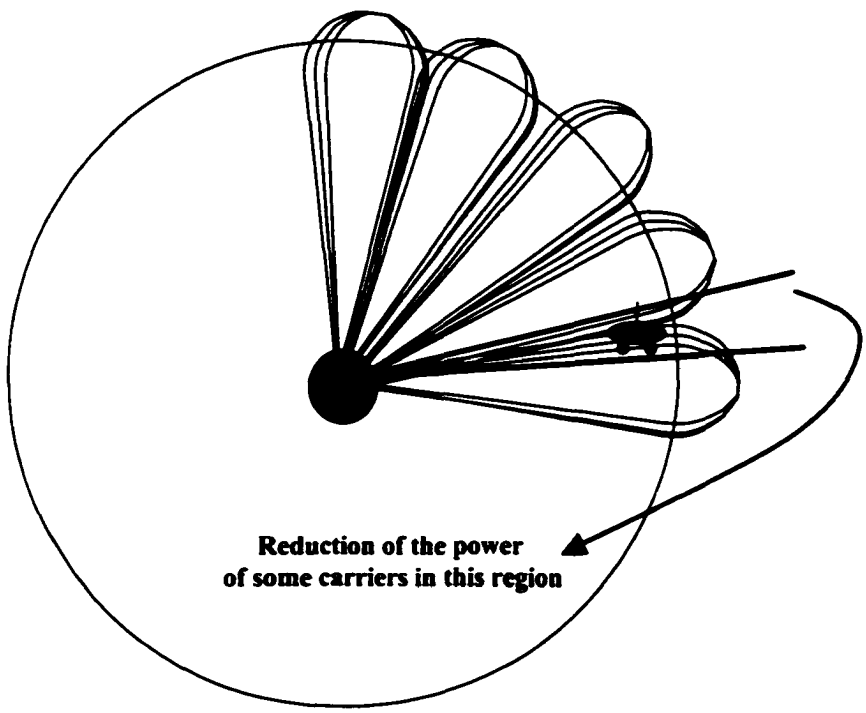

(b)

Fig. 4.2 (a) Interference in the overlapping area, if the patterns are positioned based on the smallest HPBW; (b) Reduction in some carriers' received signal, if the patterns are positioned based on the largest HPBW.

4.2.1 *P* antenna arrays located at a distance $D_p > 10\lambda$

Here, we assume it is physically posible to locate antenna arrays far apart from one another at a low cost (at the BS). In this case, in addition to requiring peaks at identical locations and matching beam patterns shapes across carriers: To enhance the mobile receiver performance, we will require that independent fades be generated at the receiver side from each smart antenna, meaning that the spacing between two adjacent smart arrays ($D_p = D$) must be larger than the wavelength of the transmitted signal (λ) (e.g., $D \geq 10\lambda$).

Criterion 1: Identical Peaks Across Antenna Arrays

To ensure the *P* antenna patterns peak at the same location, a phase shift $m \cdot \psi_p$ is applied to the m^{th} smart antenna element in the p^{th} antenna array (in addition to $m\theta(t, p)$). This compensates for the distance between adjacent smart antennas (D) and corresponds to

$$\psi_p \cong 2\pi(d_p / \lambda_p) \cdot \sin\phi_p,\ p \in \{0.1,.....P\text{-}1\}. \tag{4.5}$$

where d_p is the distance between the adjacent antenna elements as shown in Fig. 4.1, λ_p is the average wavelength of the carriers applied to the p^{th} antenna array, and

$$\phi_p = \tan^{-1}(pD / x_o). \tag{4.6}$$

Here, x_o is the BS-mobile distance, e.g., 500m, and $D_{Tot,p} = \sum_{i=1}^{p-1} D_i = (p-1)D$ represents the total distance between the first and p^{th} antenna array. At most, p=P-1 and hence $(p-1)D \le (P-2)D \cong (P-2)\cdot 10\lambda$. For typical values of x_o,

$$(P-2)\cdot 10\lambda << x_o, \tag{4.7}$$

and, in this case, from (4.6), $\phi_p \cong 0$. Applying this result to (4.5), we see that for typical values of x_o (BS-mobile distance), it is reasonable to assume $\psi_p \cong 0$. That is, in almost all cases of practical interest, it is not necessary to introduce a phase offset to array elements of different antenna arrays to compensate for the distance between these antenna arrays (and thereby ensure peaks in antenna patterns occur at the same spatial location).

Criterion 2: Identical Beam Patterns Across Antenna Arrays

To ensure the satisfaction of the identical beam pattern criteria, we consider the well-known array factor equation for a linear array structure:

$$AF_p = \frac{1}{M}\cdot\left[\frac{\sin\left(\frac{M}{2}\cdot\frac{2\pi d_p}{\lambda_p}\cos\phi\right)}{\sin\left(\frac{1}{2}\cdot\frac{2\pi d_p}{\lambda_p}\cos\phi\right)}\right] \tag{4.8}$$

where ϕ is the azimuth angle. As a starting point to identical beam pattern shapes across antenna arrays, we require

$$d_p / \lambda_p = d_o / \lambda_o \tag{4.9}$$

Now, using $\lambda_p = \lambda_o /(1 + pQ\Delta f / f_o)$, d_p is selected according to

$$d_p = d_o /(1 + pQ\Delta f / f_o). \tag{4.10}$$

Equation (4.10) ensures identical array-pattern shapes from one antenna array to the next, but we also require that a single array pattern emerge from each of the P antenna arrays. That is, referring to (4.8), it is evident that array factor, AF_p, and hence, the resulting beam pattern for the p^{th} array, is a function of frequency f_p. Moreover, we place Q subcarriers, with frequencies ranging from $f_o + pQ\Delta f$ to $f_o + (pQ + Q - 1)\Delta f$ within the p^{th} antenna array. We must ensure the size of Q is small enough that all frequencies placed in the p^{th} array generate identical patterns.

We start by assuming that whenever the null-to-null beamwidths of the beam patterns in antenna array $p \in \{0,1,\ldots,P-1\}$ are within 10% of one another beam patterns are "identical". Emulations based on Equation (4.8) (assuming $M \leq 12$ elements per array), are

then used to determine the range of frequencies for which "identical" beam patterns result. It is determined that whenever f_{min} and f_{max} enter an antenna array and satisfy

$$\frac{f_{max} - f_{min}}{f_o} < 0.01 \tag{4.11}$$

identical beam patterns are observed. Using this criteria, and considering our case of interest (with Q frequencies spaced by Δf entering the p^{th} antenna array), we require

$$Q \cdot \Delta f / f_o < 0.01 \tag{4.12}$$

For example, in a 3G-like system, 128 carriers spaced by 40kHz may be employed for a total bandwidth of approximately 5MHz. Assuming carrier frequency $f_o = 2GHz$, we find that the ratio of frequency separation to carrier frequency is always less than 0.0025. Hence, in this scenario, all subcarriers may be placed on a single antenna array. However, in either an ultrawideband system, a system operating over noncontiguous frequency bands, or a future generation (4G) cellular system, this need not be the case. For example, if we imagine a future generation system with a 100MHz bandwidth to support the anticipated 60Mb/s data rate (per user) of 4G (see, e.g., [73]), and we assume transmission at, e.g., 4GHz, then maximum frequency separation is 0.025 of the carrier frequency, and we require three unique antenna arrays to create identical beam patterns on each antenna array.

Additional Criteria

We must also consider criteria pertaining to beam pattern oscillation. This oscillation is created by careful control of the antenna element's phase offset, $\theta(t,p)$ (see Fig. 4.1). The p^{th} antenna array's beam-pattern-movement should ensure: 1) constant large scale fading, i.e., the mean of the Rayleigh fading is constant over the symbol duration T_S; and 2) L independent fades are generated within each partition T_S. In other words, the p^{th} antenna array's beam-pattern is swept in a manner which ensures constant large scale fading over symbol duration T_S while ensuring L independent fades within each T_S.

Criterion 3: Constant large scale fading.

Making reference to chapter 2, in order to ensure constant large-scale fading over each symbol time duration T_S, the mobile user must remain in the antenna array half power beamwidth (HPBW). That is

$$\left| T_S \cdot \frac{d\phi}{dt} \right| = \kappa \cdot \beta, \; 0 < \kappa < 1, \tag{4.13}$$

Using a derivation analogues to that in chapter 2, Equation (4.13) corresponds to selecting the phase offset applied to the p^{th} element according to:

$$\theta(t,p)=\kappa\cdot\frac{2\pi d_p\cdot\left|\sin(\phi-\phi_p)\right|\cdot\beta}{\lambda_p T_S}\cdot\left(t-\frac{T_S}{2}\right),t\in[0,T_S]\,, \tag{4.14}$$

where ϕ_p is the value introduced in (4.6). After each T_S, $\theta(t,p)$ returns to its $t=0$ value (returning the beam pattern to its original position) and $\theta(t,p)$ then recreates an identical spatial movement over the next T_S duration. Assuming the condition in Equation (4.7) holds true, and assuming a small HPBW, (4.14) can be simplified (using (4.9)) to

$$\theta(t,p)=\theta(t)\cong\kappa\cdot\frac{2\pi d_o\cdot\beta}{\lambda_o T_S}\cdot\left(t-\frac{T_S}{2}\right),\mathrm{t}\in[0,\mathrm{T_S}] \tag{4.15}$$

Criterion 4: L independent fades.

Movement of the antenna array beam pattern based on the time-varying antenna array phases in (4.14) or (4.15) results in a time varying channel, and rate of variation of the channel is measured by coherence time. Coherence time, in turn, determines L, the number of independent fades over duration T_S. Computation of the coherence time requires modeling a channel in the presence of a moving beam pattern. In Chapter 3, a linear time-varying impulse response model is introduced to characterize the channel with a beam pattern oscillation based on (4.15). The channel statistics were characterized using the so-called Geometric-based Stochastic Channel Model (GSCM). Simulation results assuming a city center, with $0.0005<\kappa<0.05$, demonstrated that the channel coherence time due to beam pattern movement leads to an available diversity gain as high as $L\approx 7$ for $\kappa<0.05$.

4.2.2 *P* Antenna arrays located in close proximity

One limitation in mobile communications systems is the availability of space at the BS. In some cases it may not be possible to locate the antenna arrays at a large distance from each other. In this subsection, considering p antenna arrays in a close proximity, we define new antenna array criteria.

Criterion 1: Identical Peaks Across Antenna Arrays

Since the antenna arrays are located in close proximity, $D_{Tot,p} = \sum_{i=1}^{p} D_i << x_o$, and as a direct consequence, the P antenna arrays will peak at identical locations (discussed in the previous subsection).

Criterion 2: Identical HPBW Across Antenna Arrays

Similar to the Subsection 4.2.1, to ensure identical HPBW across antenna arrays, we require:

$$d_p / \lambda_p = d_o / \lambda_o, \tag{4.16}$$

where $\lambda_p = \lambda_o/(1+pQ\Delta f/f_o)$ is the average wavelength of the carriers applied to the p^{th} antenna array. In addition to (4.16), we introduce a condition which ensures small antenna array spacing, namely

$$D_1 = Q \cdot d_o, \tag{4.17}$$

where $D_1 = Q \cdot d_o$ implies that the first and second antenna arrays are separated by distance d_o, p refers to the p^{th} antenna array and $D_{Tot,p} = \sum_{i=1}^{p} D_i$ represents the cumulative distance between the p^{th} antenna array and the first one. To satisfy (4.16), d_p is chosen according to

$$d_p = d_o/(1+pQ\Delta f/f_o). \tag{4.18}$$

Now, if we consider

$$D_{Tot,p}/\lambda_p = p \cdot (D_1/\lambda_1) \tag{4.19}$$

The distance D_p corresponds to

$$D_p = \frac{D_1 \cdot (1+Q\Delta f/f_o)}{((1+pQ\Delta f/f_o)\cdot(1+(p-1)Q\Delta f/f_o))}, \tag{4.20}$$

and, using (4.18) and (4.20), we achieve an elegant expression for the normalized antenna array factor (considering all antenna arrays)

$$AF_{Total}(t,\phi) = \left(\frac{1}{M} \cdot \left[\frac{\sin\left(\frac{M}{2}\gamma(t,\phi)\right)}{\sin\left(\frac{1}{2}\gamma(t,\phi)\right)} \right] \right) \cdot \left(\frac{1}{P} \cdot \left[\frac{\sin\left(\frac{P}{2}\eta(\phi)\right)}{\sin\left(\frac{1}{2}\eta(\phi)\right)} \right] \right), \tag{4.21}$$

where

$$\gamma(t,\phi) = (2\pi d_o / \lambda_o) \cdot \cos\phi + \theta(t), \tag{4.22}$$

and

$$\eta(\phi) = (2\pi D_1 / \lambda_1) \cdot \cos\phi. \tag{4.23}$$

Again, for ease in presentation, we have assumed a mobile located at $\phi_o \approx \pi/2$. In (4.22), $\theta(t)$ refers to the antenna array's phase shift $\theta(t, p, \phi)$, which is well approximated by a function of time alone. With $D_1 = Qd_o > d_o \approx 0.5 \cdot \lambda_o$, if M is sufficiently large (e.g., $M \approx N$), simple mathematical manipulation shows that the total antenna array beam pattern in (4.21) can be approximated by

$$AF_{Total}(t,\phi) \approx AF(t,\phi) = \frac{1}{M} \cdot \left[\frac{\sin\left(\frac{M}{2}\gamma(t,\phi)\right)}{\sin\left(\frac{1}{2}\gamma(t,\phi)\right)} \right] \tag{4.24}$$

where $AF(t,\phi)$ is the beam pattern of a single antenna array (any one of the P antenna arrays).

Moreover, we place Q subcarriers, with frequencies ranging from $f_o + pQ\Delta f$ to $f_o + (pQ + Q - 1)\Delta f$ within the p^{th} antenna array. We must ensure the size of Q is small enough that all frequencies placed into the p^{th} array generate identical patterns. This leads directly to Equation (4.12).

Finally, it is easily shown that the array's time varying phase, $\theta(t, p)$ should be selected according to (4.14) or (4.15), in order to create constant large scale fading and L independent fades over T_S.

4.3 Receiver Design

The k^{th} user's transmitted signal, without an antenna array (using (4.1) and (4.2)), corresponds to

$$s_k(t) = b_k[i] \cdot \left(\sum_{n=0}^{N-1} \cos\left(2\pi(f_o + n\Delta f) \cdot t + \beta_k^n\right) \right) \cdot g(t), \quad t \in [0, T_S], \tag{4.25}$$

For carrier $n = pQ + q$, the q^{th} carrier sent on antenna array p, the transmitted signal can be written in isolation using

$$s_k^{p,q}(t) = b_k[i] \cdot \cos\left(2\pi \left(f_o + (pQ+q)\Delta f\right) \cdot t + \beta_k^{pQ+q}\right) \cdot g(t), \quad t \in [0, T_S], \tag{4.26}$$

where β_k^{pQ+q} is as shown in (4.3) and (4.4). Now, considering the antenna array, the signal in (4.26) enters the p^{th} smart antenna array. The output of the m^{th} element of the p^{th} antenna array, after application of phase offset $\theta(t)$ in (4.15), is simply:

$$s_k^{p,q,m}(t) = b_k[i] \cdot \cos\left(2\pi f_o t + 2\pi (pQ+q)\Delta f \cdot t + \beta_k^{pQ+q} + m\theta(t)\right), \quad t \in [0, T_S], \tag{4.27}$$

The presence of $\theta(t)$ creates a frequency offset; however, with $\theta(t)$ selected according to (4.15) (and considering $0.0005 < \kappa < 0.05$), and assuming typical parameter values for mobile communication transmissions, it is easily shown that the frequency offset induced by $\theta(t)$ is less than 5% of a 1MHz bandwidth. Hence, we ignore this frequency offset in our presentation. The total downlink transmitted signal, considering all antenna elements (all m), all antenna arrays (all p), all carriers (all q) and all users (all k) is (from (4.27))

$$s(t) = \sum_{k=1}^{K} b_k[i] \cdot \sum_{p=0}^{P-1} \sum_{q=0}^{Q-1} \left(\frac{1}{M} \cdot \sum_{m=0}^{M-1} \cos\left(2\pi (f_o + (pQ+q)\Delta f) \cdot t + \beta_k^{pQ+q} + m\theta(t)\right) \right), t \in [0, T_S]. \tag{4.28}$$

where $1/M$ is a normalization factor corresponding to transmission over M array elements. At the receiver side, considering the transmit diversity which leads to an L fold time diversity, the received signal in $[0,T_S]$ can be divided into time slots $[lT_S/L,(l+1)T_S/L]$, where $l \in \{0,1,....,L-1\}$, and each time slot demonstrates independent fade. This signal corresponds to

$$r_l(t) = \sum_{k=1}^{K} b_k[i] \cdot \sum_{p=0}^{P-1} \sum_{q=0}^{Q-1} \left[\alpha_l^{pQ+q} \cdot \left(\frac{1}{M} \cdot \sum_{m=0}^{M-1} \cos\left(2\pi (f_o + (pQ+q)\Delta f) \cdot t + \beta_k^{pQ+q} + m\gamma(t,\phi) + \xi_l^{pQ+q}\right)\right)\right] + n_l(t), \quad t \in [lT_S/L,(l+1)T_S/L] \tag{4.29}$$

Here, $n_l(t)$ is an additive white Gaussian noise, independent for differing time slots (l); α_l^{pQ+q} is the fade on the $(pQ+q)^{th}$ carrier in the l^{th} time slot (due to fading) and ξ_l^{pQ+q} is the phase offset in the $(pQ+q)^{th}$ carrier and l^{th} time slot (due to fading) (hereafter, phase is assumed to be tracked and removed). From [33], the α_l^{pQ+q} fades over the Q subcarriers $q \in \{0,1,....,Q-1\}$ (applied to the p^{th} smart antenna) are correlated Rayleigh random variables with correlation coefficient between the q' subcarrier fade and the q'' subcarrier fade characterized by:

$$\rho_{q',q''} = \frac{1}{1+((q''-q')\cdot(\Delta f/(\Delta f)_C))^2}. \tag{4.30}$$

where $(\Delta f)_C$ is the coherence bandwidth of the channel.

For different groups of carrier frequencies (different p), if the antenna arrays are located a *far apart*, i.e., at a separation $D > 10\lambda$, α_l^{pQ+q} are independent Rayleigh random variables for different p values; and if the antenna arrays are located in *close proximity*, α_l^{pQ+q} are treated as correlated Rayleigh random variables (across index p) with the correlation characterized by (4.30).

Applying the summation over m (the set of antenna array elements), and combining the two summations over p and q for simplicity in presentation, (4.29) can be rewritten as:

$$r_l(t) = \sum_{k=1}^{K} b_k[i] \cdot \sum_{n=0}^{N-1} \left[\alpha_l^n \cdot AF(t,\phi) \cdot \cos\left(2\pi(f_o + n\Delta f)\cdot t + \beta_k^n + \frac{M-1}{2}\gamma(t,\phi) \right) \right] + n_l(t) \qquad (4.31)$$

Assuming a narrow-beamwidth smart antenna (and assuming the mobile is located at $\phi = \pi/2$), (4.22) can be approximated by $\gamma(t,\phi) \cong \gamma(t) = \theta(t)$. Additionally, with the antenna array peak directed toward the intended mobile at time 0, and with small movements of the antenna array pattern over T_S, the array factor experienced at the mobile over $[0, T_S]$ is well approximated by $AF(t,\phi) \cong 1$.

The CI/MC-CDMA receiver for user j, $j \in \{1,2,...,K\}$, is shown in Fig. 4.3. In this figure, a bank of band pass filters separates the MC-CDMA signal into its N multiple carriers. Next, each carrier is multiplied by a local oscillator generating

$$v^n(t) = \sqrt{2/T_S} \cdot \cos\left(2\pi(f_o + n\Delta f)\cdot t + \frac{M-1}{2}\gamma(t)\right). \tag{4.32}$$

Once each of the N MC-CDMA carriers (located in parallel branches) has been returned to baseband, the baseband signal is integrated over each interval over which the fade is constant, i.e., over $t \in [lT_S/L, (l+1)T_S/L]$, $l \in \{0,1,\ldots,L-1\}$. After applying the spreading code of user j to seperate users, the received signal for each subcarrier n, $n \in \{0,1,\ldots,N-1\}$, and time interval l, $l \in \{0,1,\ldots,L-1\}$, corresponds to:

$$r_l^n = \frac{1}{L}\sqrt{E_S}\alpha_l^n \cdot b_j[i] + \frac{1}{L}\sqrt{E_S}\sum_{k=1,k\neq j}^{K}\alpha_l^n b_k[i]\cos(\beta_j^n - \beta_k^n) + n_l^n, \quad n \in \{0,1,\ldots,N-1\},\ l \in \{0,1,\ldots,L-1\} \tag{4.33}$$

where $\sqrt{E_S} = \sqrt{T_S/2}$ and n_l^n is a zero mean Gaussian random variable with variance $N_o/(2\cdot N\cdot L)$. The first term in (4.33) represents the $l^{th} \times n^{th}$ component of the desired signal, the second term is multi-access interference and the third term is noise. It is important to note the factor of $1/L$ in the desired signal is a direct result of the division of the received signal interval into L partitions (to create L-fold time diversity) (i.e., a direct result of the L-fold oversampling strategy).

With $N \times L$ diversity components, N over frequency and L over time, the combiner can be designed using EGC, MRC or MMSEC, applied to the frequency components then the time components (or vice versa). Examples of the combiner follow.

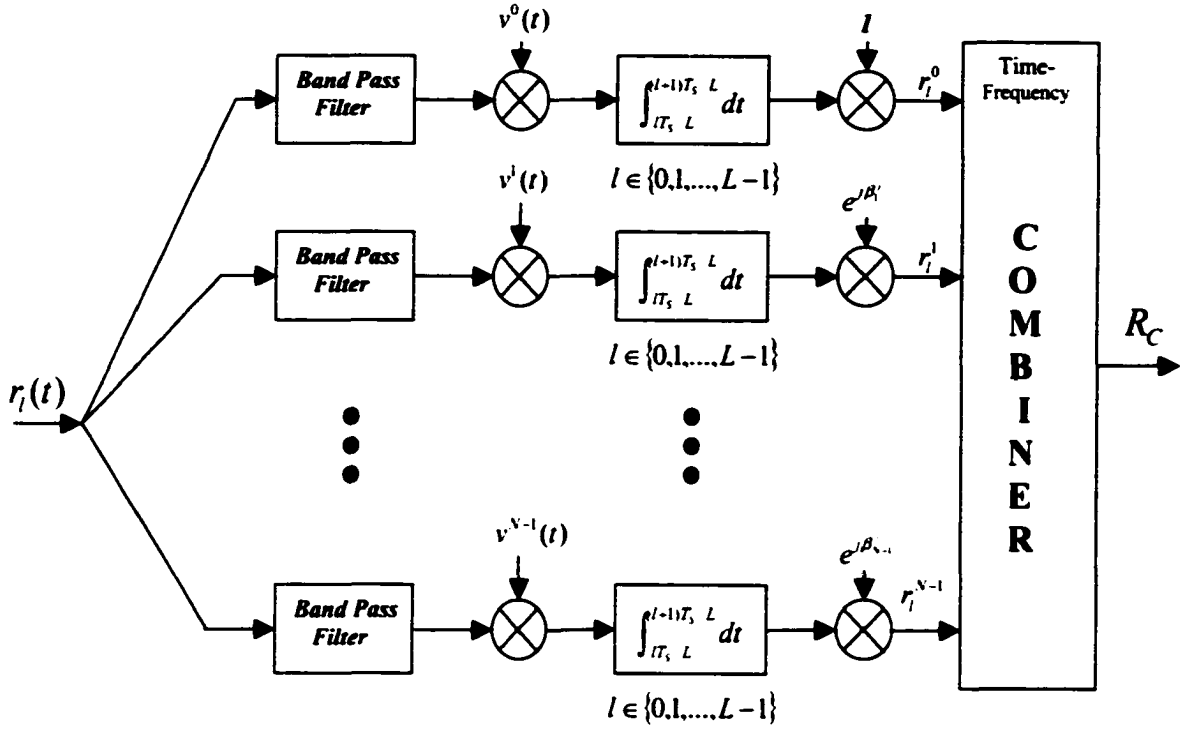

Fig. 4.3 The MS receiver.

a. EGC-EGC scheme: EGC applied in time then in frequency, or equivalently EGC applied to the frequency components then in time, results in

$$R_{C,EGC-EGC} = \sum_{l=0}^{L-1}\sum_{n=0}^{N-1} r_l^n = \sum_{n=0}^{N-1}\sum_{l=0}^{L-1} r_l^n . \tag{4.34}$$

b. MRC-EGC scheme: MRC applied to the frequency components (or time components) followed by EGC in time (or frequency) leads to:

$$R_{C,MRC-EGC} = \sum_{l=0}^{L-1}\sum_{n=0}^{N-1} \alpha_l^n r_l^n = \sum_{n=0}^{N-1}\sum_{l=0}^{L-1} \alpha_l^n r_l^n . \tag{4.35}$$

c. *EGC-MRC scheme:* Applying EGC to the time components, then MRC in frequency results in:

$$R_{C\_EGC_{time}-MRC_{freq}} = \sum_{n=0}^{N-1} \alpha^n r^n \,. \tag{4.36}$$

where

$$r^n = \alpha^n \cdot \frac{1}{L}\sqrt{E_S} \cdot b_j[i] + \frac{1}{L}\sqrt{E_S} \sum_{k=1, k\neq j}^{K} \alpha^n \cdot b_k[i] \cdot \cos\left(\beta_j^n - \beta_k^n\right) + n^n \,, \tag{4.37}$$

and

$$\alpha^n = \sum_{l=0}^{L-1} \alpha_l^n \,. \tag{4.38}$$

$$n^n = \sum_{l=0}^{L-1} n_l^n \,. \tag{4.39}$$

Applying EGC in frequency then MRC in time leads to:

$$R_{C\_EGC_{freq}-MRC_{time}} = \sum_{l=0}^{L-1} \alpha_l r_l \,, \tag{4.40}$$

where

$$r_l = \alpha_l \cdot \frac{1}{L}\sqrt{E_S}\cdot b_j[i] + \frac{1}{L}\sqrt{E_S}\sum_{k=1,k\neq j}^{K}\alpha_{l,k}\cdot b_k[i] + n_l\,, \tag{4.41}$$

and

$$\alpha_l = \sum_{n=0}^{N-1}\alpha_l^n, \tag{4.42}$$

$$\alpha_{l,k} = \sum_{n=0}^{N-1}\alpha_l^n \cdot \cos\left(\beta_j^n - \beta_k^n\right), \tag{4.43}$$

$$n_l = \sum_{n=0}^{N-1} n_l^n. \tag{4.44}$$

d. MMSEC-EGC scheme: Applying the Wiener filter principle [75] to determine the MMSEC across CI/MC-CDMA carriers, and following this with EGC across the time components (index *l*), the decision variable with $K=N$ (i.e., $K=N$ users on N carriers) is (see Appendix 2):

$$R_{C\_MMSEC-EGC} = \sum_{l=0}^{L-1}\sum_{n=0}^{N-1}\frac{\sqrt{E_S}\cdot\alpha_l^n / L}{P\cdot(\alpha_l^n)^2 + N_o^n/2}\cdot r_l^n = \sum_{n=0}^{N-1}\sum_{l=0}^{L-1}\frac{\sqrt{E_S}\cdot\alpha_l^n / L}{P\cdot(\alpha_l^n)^2 + N_o^n/2}\cdot r_l^n \tag{4.45}$$

where

$$P = \frac{E_S}{L^2}\cdot\begin{cases} K & for\ n = 0\ or\ N/2, \\ K/2 & else, \end{cases} \tag{4.46}$$

and $N_o''/2$ is the noise variance of n_l'', i.e., $N_o/(2\cdot N\cdot L)$.

e. EGC-MMSEC scheme: Here, the decision variable corresponds to:

$$R_{C\_EGC_{time}-MMSEC_{freq}} = \sum_{n=0}^{N-1} \frac{\sqrt{E_S}\cdot\alpha^n / L}{P\cdot(\alpha^n)^2 + N_o^{n'}/2}\cdot r^n, \tag{4.47}$$

where r^n, α^n and P are as defined in (4.37), (4.38) and (4.46) respectively and $N_o^{n'}/2$ is the noise variance of n^n in (4.39), i.e., $(N_o/2)/N$. Additionally,

$$R_{C\_EGC_{freq}-MMSEC_{time}} = \sum_{l=0}^{L-1} \frac{\sqrt{E_S}\cdot\alpha_l / L}{\frac{E_S}{L^2}\cdot\left(\alpha_l^2 + \sum_{k=1,k\neq l}^{K}\alpha_{l,k}^2\right) + N_{ol}'/2}\cdot r_l, \tag{4.48}$$

where r_l, α_l and $\alpha_{l,k}$ are defined in (4.41), (4.42) and (4.43) respectively and $N_{ol}'/2$ is the noise variance of n_l in (4.44), i.e., $(N_o/2)/L$.

4.4 Simulated Performance

We simulate the following CI/MC-CDMA system with smart antenna arrays:

1) N=32 subcarriers in the CI/MC-CDMA system;

2) K = 32 orthogonal users on the N = 32 subcarriers;

3) beam pattern movement is assumed to result in $L = 7$ independent fades in the duration T_S;

4) a frequency selective channel creates 4-fold frequency diversity over the entire bandwidth.

a. Four antenna arrays with 8 carriers on each ($P = 4$ and $Q = 8$): Antenna arrays with large separation.

Simulation results for this case are provided in Fig. 4.4(a) for EGC, MRC and MMSEC combining across frequency terms followed by EGC in the time domain. It is seen that the performance results of EGC-EGC exceed those of MMSEC-EGC and MRC-EGC for signal to noise ratios greater than 6dB. A similar conclusion results from the performance curves of Fig. 4.4(b), where EGC, MRC or MMSEC combining schemes are applied in the time domain followed by EGC across the frequency terms.

In Fig. 4.4(c), simulation results are provided for EGC across the time components followed by EGC, MRC or MMSEC in the frequency domain. EGC-EGC curves again demonstrate the best performance among these schemes. Only minor differences are observed between the performance curves of Fig. 4.4(d), where EGC is applied in the frequency domain followed by an EGC, MRC or MMSEC combining in the time domain. Moreover, the overall performance of these combining schemes is better than those in Fig. 4.4(c). Specifically in this figure, EGC-MRC and EGC-MMSEC outperforms EGC-EGC. The performance results across various combining schemes are very close, but the

small deviation in performance show, except in Fig. 4.4(d), EGC-EGC slightly outperforming EGC-MRC, EGC-MMSEC, MRC-EGC, and MMSEC-EGC results. Here, we believe that the EGC-EGC combining scheme represents a closer approximation to the truly optimal 2-D frequency-time combining (required to achieve optimal performance at a cost of high complexity).

The simulation results of Fig. 4.4 (a-d) are compared with a more traditional CI/MC-CDMA/smart antenna system. Here, the smart antenna consists of P arrays of M elements each (as shown in Fig. 4.1(b)), but the smart antennas operate in a conventional manner, supporting directionality gains but no transmit diversity gains (i.e., no pattern movement) [72]. The top line on all figures shows the performance of CI/MC-CDMA with this $P \cdot M$ element antenna array, where MMSEC is applied to the subcarriers of the received CI/MC-CDMA signal. It is observed that the introduction of the beam pattern movement by the BS array introduces an improvement of more than 7dB at a probability of error of 10^{-3} (at the mobile).

Additionally, the bottom line on each curve represents the benchmark AWGN (additive white Gaussian noise) performance curve. We see that while an MC-CDMA system with a conventional antenna array (offering only directionality benefits) loses close to 9dB relative to AWGN performance (at $P(\varepsilon) = 10^{-3}$), the addition of beam pattern movement (creating induced time diversity gains) leads to an MC-CDMA system that is only 2dB away from ideal AWGN performance.

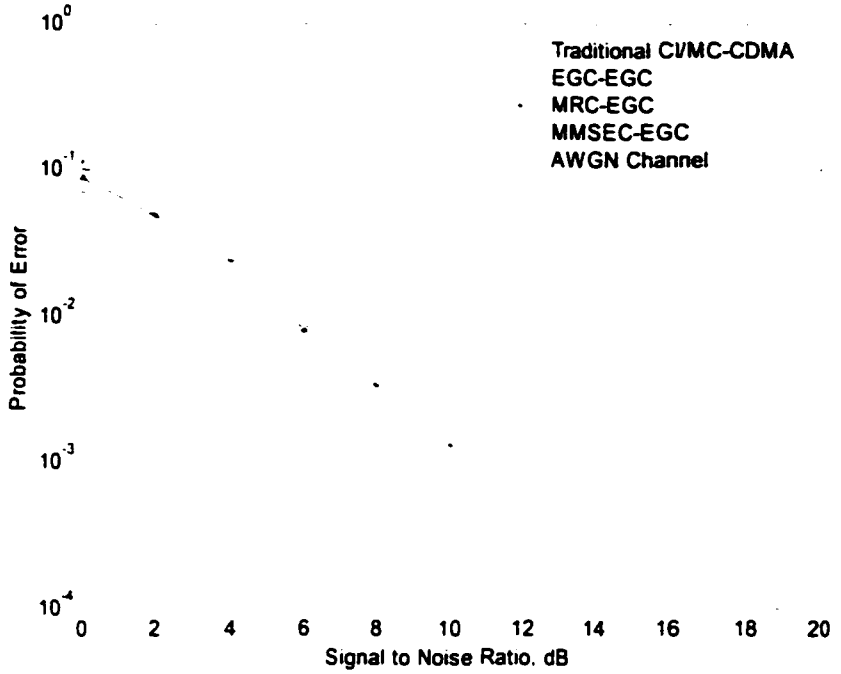

a) MRC, MMSEC and EGC first in frequency, then EGC in time.

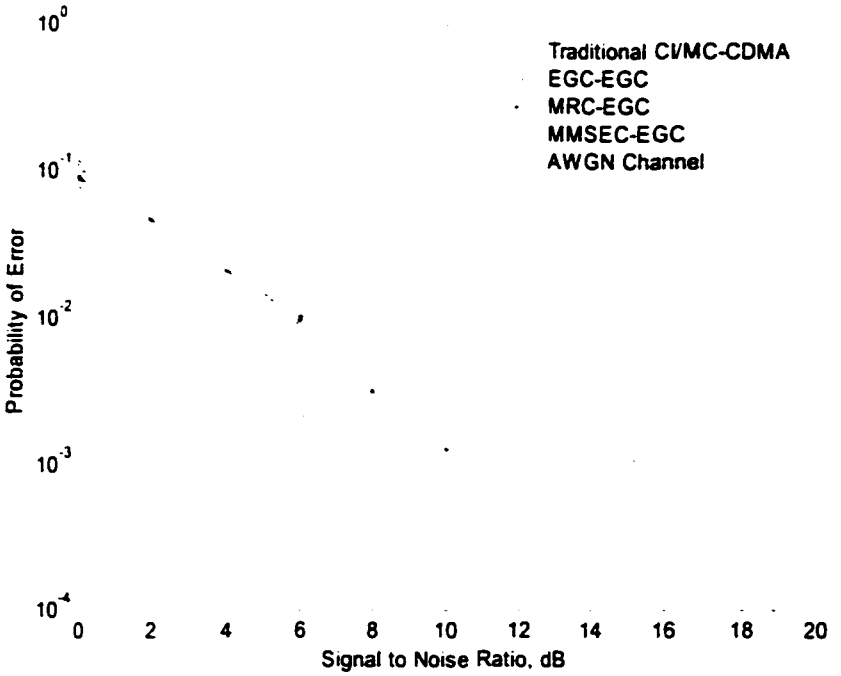

b) MRC, MMSEC and EGC first in time, then EGC in frequency.

Fig. 4.4(a,b) Simulation results for 7 independent fades, 32 users and 32 subcarriers (in each P=4 group of subcarriers there are Q = 8 correlated subcarriers) compared with one dimensional frequency diversity over CI/MC-CDMA carriers.

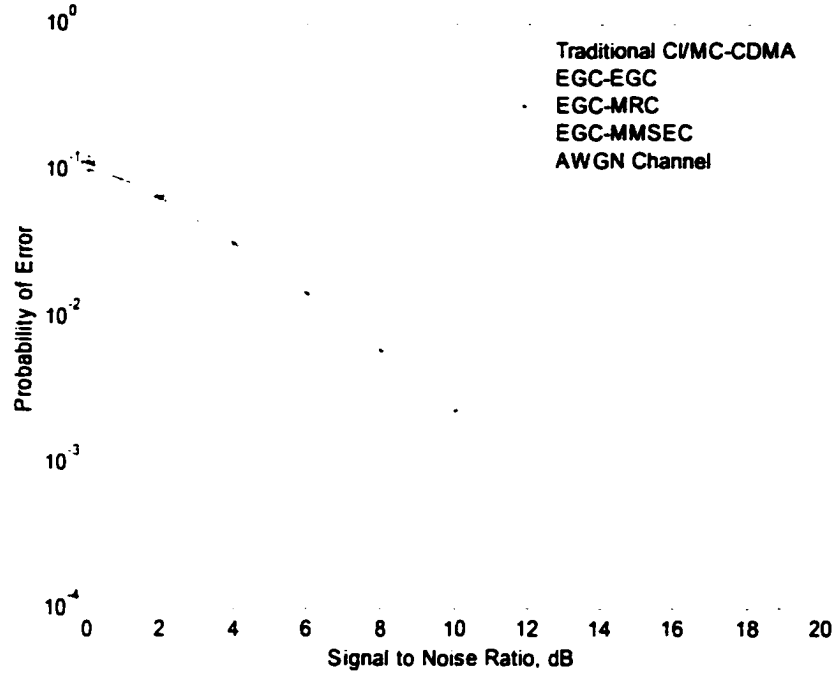

c) EGC first in time, then EGC, MRC and MMSEC in freq.

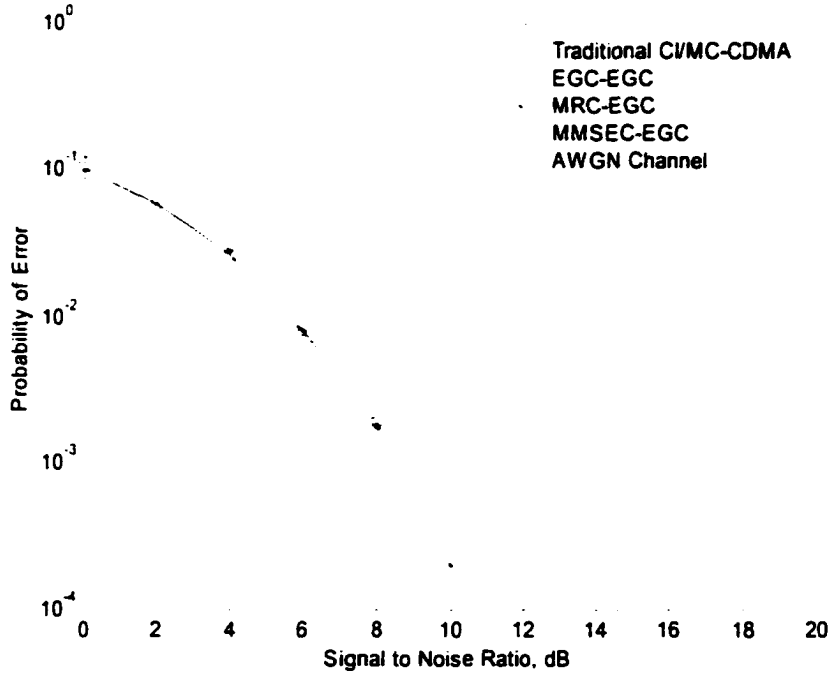

d) EGC first in frequency, then EGC, MRC and MMSEC in time.

Fig. 4.4(c,d) Simulation results for 7 independent fades, 32 users and 32 subcarriers (in each P=4 group of subcarriers there are Q = 8 correlated subcarriers) compared with one dimensional frequency diversity over CI/MC-CDMA carriers.

b. Four located antenna arrays with 8 carriers on each (P = 4 and Q = 8): Antenna arrays in close proximity.

Simulation results are provided in Fig. 4.5(a) for EGC, MRC and MMSEC combining across frequency terms followed by EGC in the time domain. It is seen that the performance results of EGC-EGC exceed those of MMSEC-EGC and MRC-EGC for signal to noise ratios greater than 7dB. A similar conclusion can be reached when considering the performance curves of Fig. 4.5(b), where EGC, MRC or MMSEC combining schemes are applied in the time domain followed by EGC across the frequency terms.

In Fig. 4.5(c), simulation results are provided for EGC across the time domain terms followed by EGC, MRC or MMSEC in the frequency domain. EGC-EGC curves demonstrate the best performance among these schemes. Only minor differences are observed among the many performance curves of Fig. 4.5(d), where EGC is applied in the frequency domain followed by an EGC, MRC or MMSEC combining in the time domain. Moreover, just in this case, we observe EGC-MRC outperforms the other combining schemes.

When compared to the performance of an MC-CDMA/smart antenna merger without the benefit of beam pattern oscillation, we observe that 7dB performance gains are achieved by the beam pattern oscillation at a $P(\varepsilon) = 10^{-3}$.

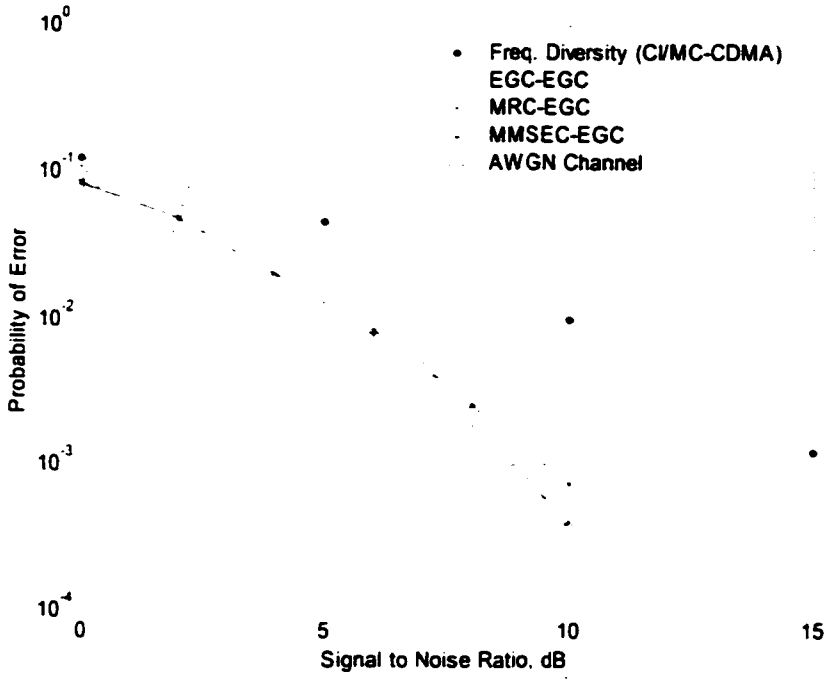

a) MRC, MMSEC and EGC first in freq.,then EGC in time.

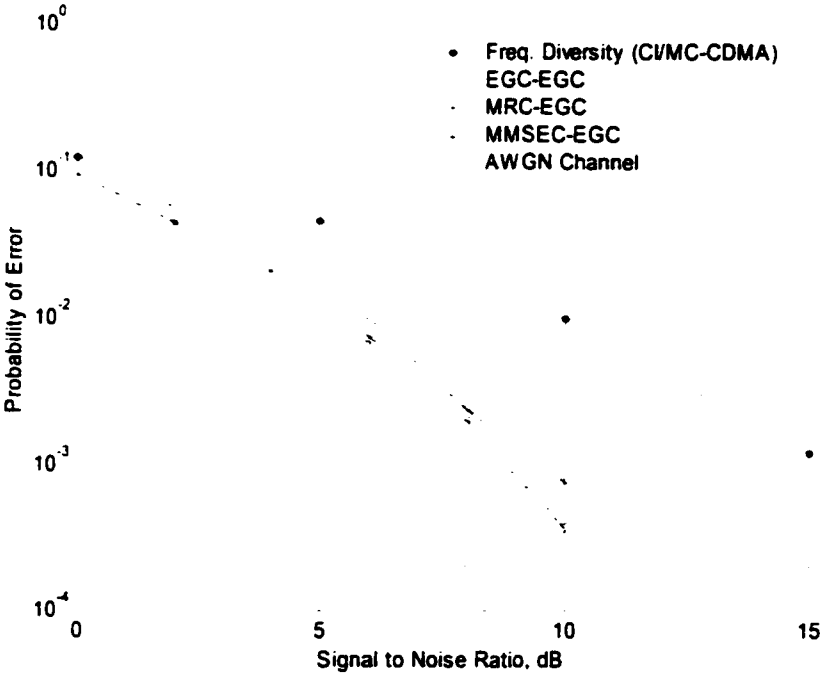

b) MRC, MMSEC and EGC first in time,then EGC in freq.

Fig. 4.5(a,b) Simulation results for 7 independent fades in time domain, and 32 correlated fades in frequency domain, compared with one dimensional frequency diversity over CI/MC-CDMA.

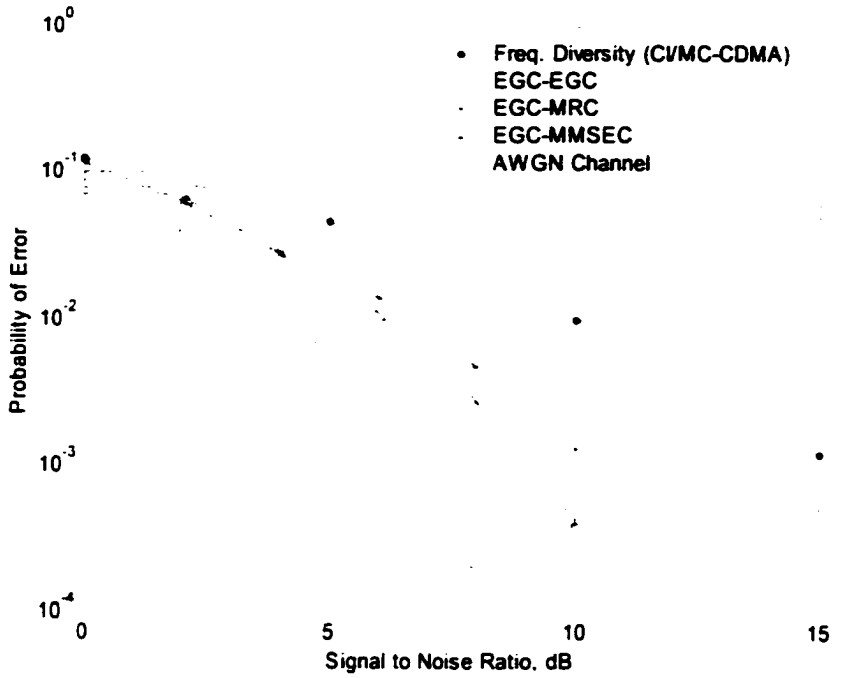

c) EGC first in time, then EGC, MRC and MMSEC in freq.

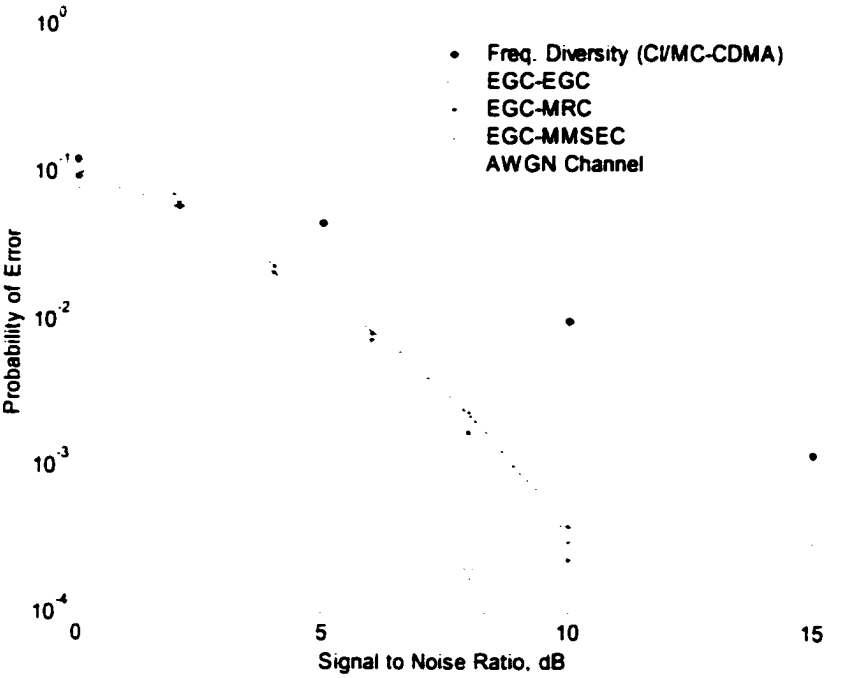

d) EGC first in freq., then EGC, MRC and MMSEC in time.

Fig. 4.5(c,d) Simulation results for 7 independent fades in time domain, and 32 correlated fades in frequency domain, compared with one dimensional frequency diversity over CI/MC-CDMA.

c. One antenna array (P = 1 and Q = 32)

In Fig. 4.6(a) the simulation results are provided for EGC in the time domain followed by EGC, MRC or MMSEC in the frequency domain. Only minor differences are observed between the performance curves of Fig. 4.6(a) and those of Fig. 4.6(b), where EGC is applied in the frequency domain followed by an EGC, MRC or MMSEC in the time domain.

The simulation results in Fig. 4.6(a,b) are compared with a CI/MC-CDMA/smart antenna system, where the arrays does not support beam oscillation. The top line on all figures shows the performance of MC-CDMA without the proposed pattern movement, where MMSEC is applied to the subcarriers of the received MC-CDMA signal. Very similar to the previous cases, it is observed that the introduction of the antenna array at the BS improves performance by more than 7dB at a probability of error of 10^{-3} (at the mobile).

4.5 Conclusions

CI/MC-CDMA signals are sent via P antenna arrays at the BS, and received by a single antenna at the mobile. The phase shifts introduced to the BS antenna array elements are designated to control the antenna pattern movement (oscillation) such that it achieves directionality and transmit diversity. The proposed system achieves (1) high network capacity via the combining of SDMA and CDMA multiple access techniques and (2) high performance via the combined frequency-time diversity gains.

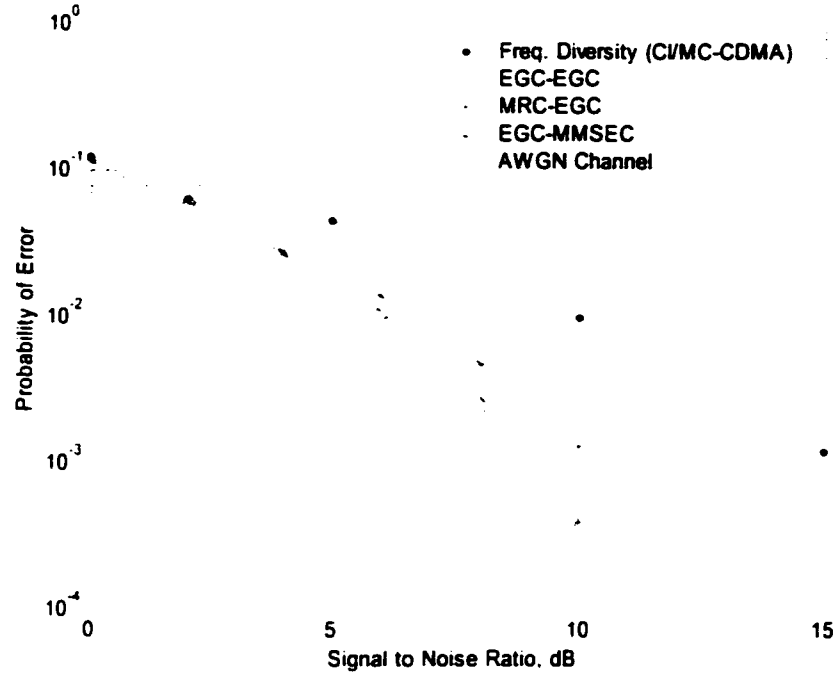

a) EGC first in time, then EGC, MRC and MMSEC in frequency.

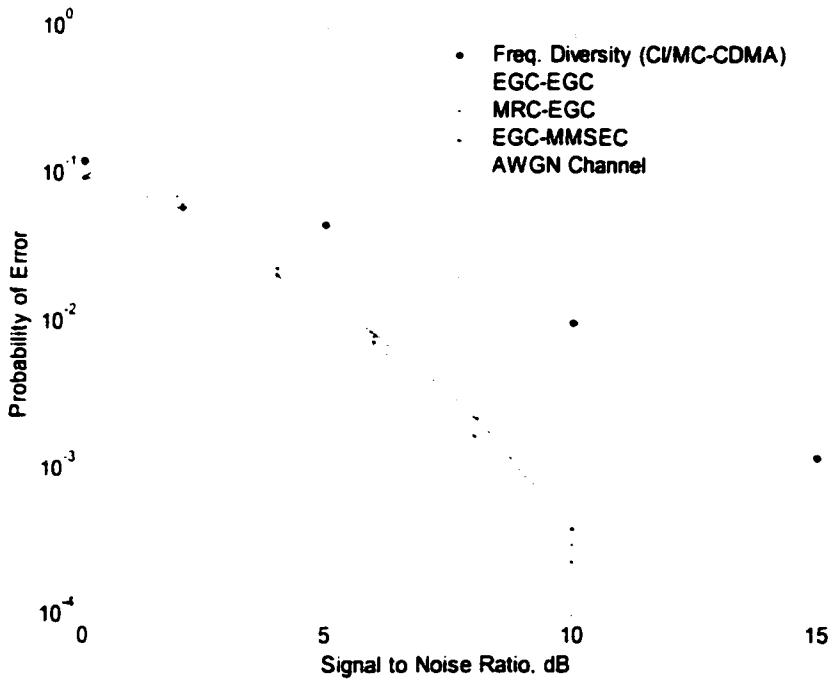

b) EGC first in frequency, then EGC, MRC and MMSEC in time.

Fig. 4.6(a,b) Simulation results for 7 independent fades, 32 users and 32 subcarriers compared with one dimensional frequency diversity over CI/MC-CDMA carriers.

Focusing on the available performance benefits, we construct receivers that employ diversity combining in the frequency and time domains. Different combining strategies, e.g., MMSEC-EGC, MRC-EGC and EGC-EGC, have been simulated and the performance results characterized. Significant performance improvement is demonstrated in a rich scattering environment when compared to the CI/MC-CDMA/smart antenna system without the benefit of beam pattern oscillation.

Chapter 5

High Performance Wireless via the Merger of CI Chip Shaped DS-CDMA and Oscillating-Beam Smart Antenna Arrays

In this chapter, a novel merger of DS-CDMA and smart antenna arrays is introduced. With regard to the DS-CDMA scheme, we employ CI/DS-CDMA, a novel implementation of DS-CDMA where chips are decomposable into N narrowband frequency components. With regard to the antenna array, we deploy the proposed oscillating-beam smart array: Here, applying proper time-varying phases to the array elements, we create small movement (oscillation) in the antenna array's pattern, while steering the antenna pattern main lobe to the position of the intended user. The oscillating antenna pattern creates a time-varying channel with a controllable coherence time as seen in chapter 3. This, in turn, provides transmit diversity in the form of a time diversity gain at the mobile receiver side (Chapter 2).

Direct-sequence code division multiple access (DS-CDMA) [52]-[55] is the world's most popular CDMA architecture. In DS-CDMA, each user's bit is multiplied by a sequence of N chips (short pulses of duration T_c), where each chip has amplitude +1 or −1. By careful selection of +1 and −1 values (spreading sequences), the receiver can separate users one from another. To enhance performance via path diversity (e.g., [54]), most DS-CDMA systems employ RAKE receivers, which attempt to separate and linearly recombine the multiple paths.

Recently, a novel chip shape referred to as the CI (Carrier Interferometery) chip shape was introduced to DS-CDMA [76]-[81]. Here, each chip is decomposable into N orthogonal carrier components. As a result, when applying these chip shapes, the DS-CDMA receiver: 1) achieves a frequency diversity benefit (rather than a path diversity benefit) by decomposing chips into carrier components and frequency combining; and 2) the use of frequency combining in place of path combining (as done in RAKE receivers) leads to a significantly improved performance via the ability to avoid inter-path interference [76]-[81].

In this chapter, we innovatively apply the oscillating-beam antenna arrays of Chapter 2 to DS-CDMA systems with CI chip shapes (CI/DS-CDMA) of [76]-[81]. This enables: 1) very high capacity via the merger of SDMA (directionality of the antenna array) and code division multiple access (inherent in CI/DS-CDMA); and 2) very high performance via the construction of receivers that exploit both transmit diversity and frequency diversity. We focus on the performance benefits of the proposed merger.

In this chapter, we assume carrier frequency (f_c) much larger than system bandwidth (BW) (e.g., $f_c > 100 \cdot (BW)$), a reasonable assumption in today's mobile systems. Hence, the antenna pattern is identical for the entire transmit bandwidth. With this in mind, the CI/DS-CDMA signal is fed into a single M-element smart antenna array. By carefully designing the phase shifts applied to antenna array elements, the resulting beam-pattern corresponds to an oscillating beam pattern similar to that in Chapter 2. This leads to a time-varying channel with a controllable coherence time. The controllable coherence time is used by the mobile to exploit time diversity and enhance performance.

The benchmark for comparison in this chapter is a CI/DS-CDMA system employed in conjunction with a conventional smart antenna array (an antenna array which creates an adaptive beam pattern directed toward the intended user, leading to increased capacity via SDMA, but, unlike the proposed scheme, offers no improvements in performance to the CI/DS-CDMA system). This chapter highlights the performance benefits that can be achieved by small oscillations in the beam pattern of the smart antenna array.

Receivers are constructed to exploit both the transmit diversity, which corresponds to an induced time diversity provided by the antenna array, as well as the diversity inherent in the CI/DS-CDMA system (an exploitable frequency diversity). Thus, at the receiver, three stages of combining are present: 1) a combining of the time components with different fades (to exploit time diversity); 2) a combining across frequency components (to exploit frequency diversity); and 3) a combining across chips (to eliminate users in a traditional DS-CDMA manner). We can apply the combining first on the frequency

components or first on the time components, i.e., the first and the second combining stages can be interchanged.

Simulation results demonstrate the proposed system achieving a 14dB gain over a CI/DS-CDMA system with a conventional smart antenna array at a probability of error of 10^{-3}. Performance gains are even more impressive when the proposed system is compared to a traditional DS-CDMA system with a conventional smart antenna array. (These performance benefits are in addition to the usual network capacity gains provided via SDMA.)

Section 5.1 introduces the merger of the beam-sweeping smart antenna arrays and CI/DS-CDMA. Section 5.2 presents receiver structures employing EGC across frequency components followed by MRC across time domain components. Section 5.3 presents simulated performance results, while Section 5.4 presents a conclusion.

5.1 The Merger of CI/DS-CDMA and Beam-Sweeping Antenna Arrays

A. The CI/DS-CDMA system.

In DS-CDMA, a unique time sequence (N chips each with amplitude +1 or −1) is assigned to each user. Hence, the k^{th} user's data bit, b_k, is sent as:

$$s_k(t) = \mathrm{Re}\left\{b_k \cdot C_k(t) \cdot e^{j2\pi f_c t}\right\}, \tag{5.1}$$

where b_k is +1 or −1, f_o is the center or carrier frequency, and $C_k(t)$ is the k^{th} user spreading code, corresponding to

$$C_k(t) = \sum_{i=0}^{N-1} c_k^i \cdot h(t - iT_C) \cdot g(t). \tag{5.2}$$

Here, $c_k^i \in \{-1,+1\}$ is the i^{th} element of user k's spreading code, and $g(t)$ is a rectangular waveform limiting the chip shape to duration T_S. In the proposed CI/DS-CDMA system of [76]-[81], the chip shape $h(t)$ corresponds to a multi-carrier signal. Specifically, the chip shape $h(t)$ is a superpositioning of N narrowband subcarriers equally spaced in frequency by Δf:

$$h(t) = \sum_{n=0}^{N-1} e^{j2\pi n \Delta f t}. \tag{5.3}$$

Here, $\Delta f \geq 1/T_S$ to ensure orthogonality (separability) between subcarriers of the chip shape. The magnitude of $h(t)$ is shown in the Fig. 5.1(a) assuming $\Delta f = 1/T_S$ and the set $\{h(t - iT_C), i = 0, 1, \ldots, N-1\}$ is shown in Fig. 5.1(b). It is important to note that $h(t - jT_C)$ and $h(t - kT_C)$ ($k \neq j$) are orthogonal to one another, and hence chips are separable. Refering to (5.3) and Fig. 5.1, the CI chip shape corresponds to a frequency sampled version of the sinc(.) shape. The transmitter generating the $s_k(t)$ of Equation (5.1), (5.2) and (5.3) is shown conceptually in Fig. 5.2(a,b).

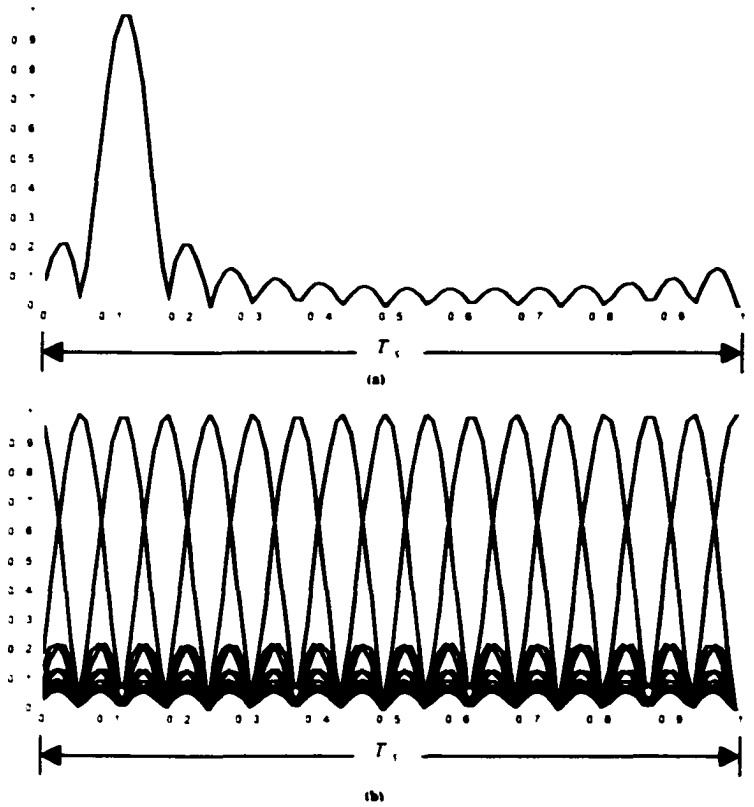

Fig. 5.1 (a) h(t) and (b) $\{h(t-iT_c), i = 0, 1, \ldots, N-1\}$ (N=16).

B. Proposed Antenna Array Structure.

The CI/DS-CDMA signal characterized by Equations (5.1)-(5.3) is fed into a single *M*-element antenna array (see Fig. 5.3). The m^{th} array element applies the phase shift $m\theta(t,\phi)$, $m \in \{0,1,\ldots,M-1\}$.

The beam pattern oscillation is created by careful selection of the antenna element's phase offset, $\theta(t)$. The antenna array's beam pattern movement will be designed to ensure: 1) constant large scale fading, i.e., the mean of the Rayleigh fading is constant over the symbol duration T_S; and 2) L independent fades are generated within each

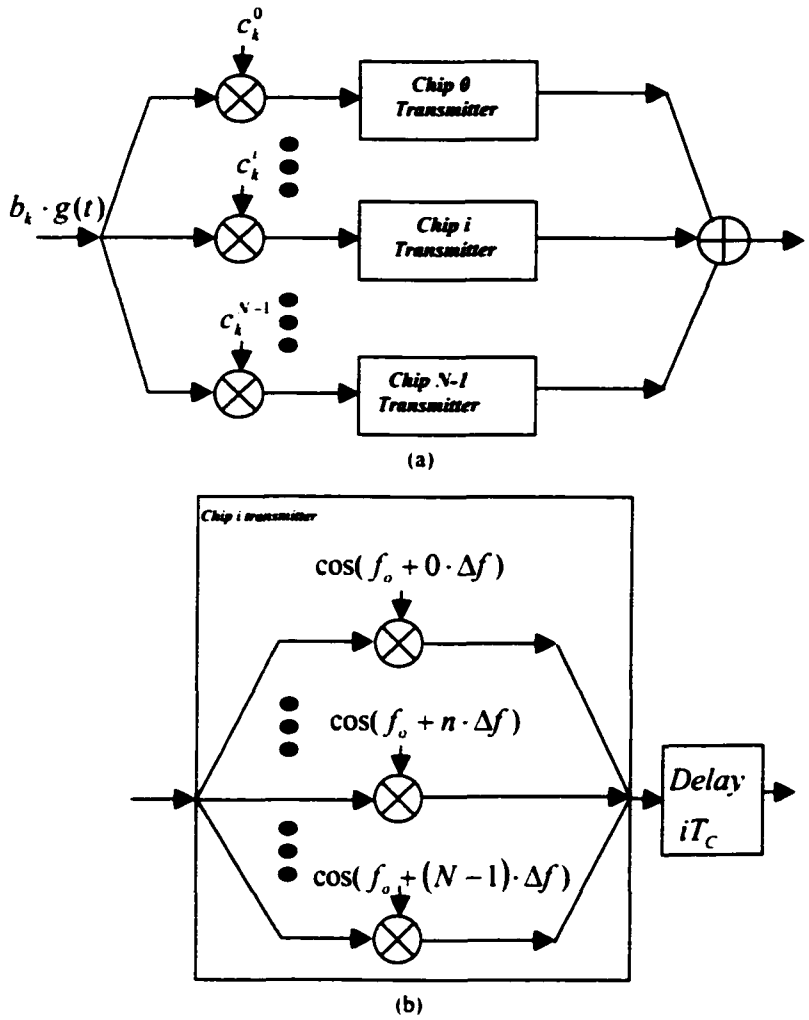

Fig. 5.2 (a) The CI/DS-CDMA transmitter, (b) the Chip i transmitter shown in Fig. 2(a).

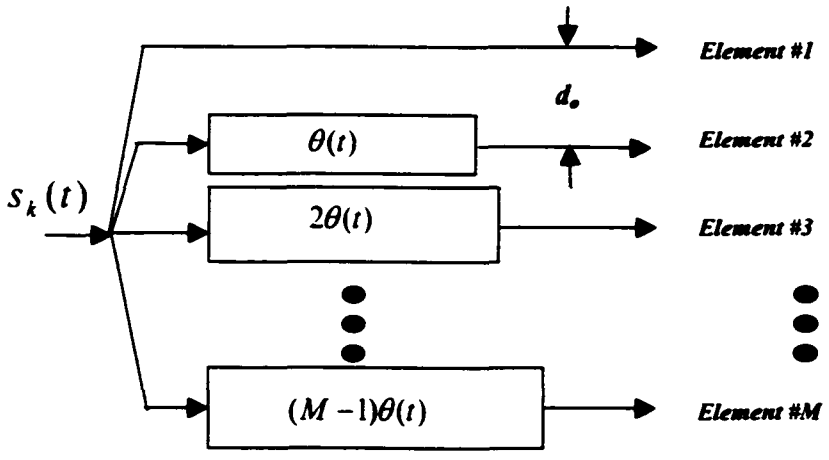

Fig. 5.3 The antenna array structure over which the CI/DS-CDMA signal is sent.

partition T_S. In other words, the antenna array beam pattern is swept in a manner which ensures constant large scale fading over symbol duration T_S while ensuring L independent fades within each T_S. Please see Chapters 2 for details.

5.2 Receiver Design

User k's signal, input to the antenna array of Fig. 5.3, corresponds to (using (5.1) and (5.2))

$$s_k(t) = \mathrm{Re}\left\{ b_k \cdot e^{j2\pi f_o t} \cdot \sum_{i=0}^{N-1} c_k^i \cdot h(t - iT_C) \cdot g(t) \right\}, \tag{5.4}$$

which, using $h(t)$ in (5.3), leads to

$$s_k(t) = \mathrm{Re}\left\{ b_k \cdot e^{j2\pi f_o t} \cdot \sum_{i=0}^{N-1} c_k^i \cdot \sum_{n=0}^{N-1} e^{j2\pi n\Delta f (t - iT_C)} \cdot g(t) \right\}, \tag{5.5}$$

$$s_k(t) = b_k \cdot g(t) \cdot \left(\sum_{i=0}^{N-1} c_k^i \cdot \sum_{n=0}^{N-1} \cos\left(2\pi (f_o + n\Delta f) \cdot t - \beta_n^i\right) \right), \; t \in [0, T_S], \tag{5.6}$$

where $\beta_n^i = 2\pi i \cdot n\Delta f T_C$. The output of the m^{th} element of the antenna array, after application of phase offset $m\theta(t)$, is simply:

$$s_k^m(t) = b_k \cdot g(t) \cdot \left(\sum_{i=0}^{N-1} c_k^i \cdot \sum_{n=0}^{N-1} \cos\left(2\pi (f_o + n\Delta f) \cdot t - \beta_n^i + m\theta(t)\right) \right), \tag{5.7}$$

The presence of $\theta(t)$ creates a frequency offset; however, with $\theta(t)$ selected according to

$$\theta(t) \cong \kappa \cdot \frac{2\pi d_o \cdot HPBW}{\lambda_o T_S} \cdot \left(t - \frac{T_S}{2}\right), t \in [0, T_S] \cdot \tag{5.8}$$

(see Chapter 2 and note that $\theta(t) = 2\pi f_o \tau(t)$) (and considering $\kappa < 0.05$), and assuming typical parameter values for mobile communication transmissions, it is easily shown that the frequency offset induced by $\theta(t)$ is less than 5% of a 1MHz bandwidth. Hence, we ignore this frequency offset in our presentation. The total downlink transmitted signal, considering all antenna elements (all m) and all users (all k) in $t \in [0, T_S]$, is (from (5.7))

$$s(t) = \sum_{k=1}^{K} b_k \cdot g(t) \cdot \left(\sum_{i=0}^{N-1} c_k^i \cdot \sum_{n=0}^{N-1} \frac{1}{M} \cdot \sum_{m=0}^{M-1} \cos\left(2\pi(f_o + n\Delta f) \cdot t - \beta_n^i + m\theta(t)\right) \right) \quad , \quad t \in [0, T_S] \tag{5.9}$$

where $1/M$ is a normalization factor compensating for transmission over M array elements.

At the receiver side, the transmit diversity (due to antenna array movement generated by $\theta(t)$) corresponds to an L fold time diversity. Hence, the received signal in duration $[0, T_S]$ can be divided into time slots $[lT_S/L, (l+1)T_S/L]$, where $l \in \{0,1,...,L-1\}$, and

each time slot contains a signal with an independent frequency-selective fade. The received signal corresponds to

$$r^l(t) = \sum_{k=1}^{K} b_k \cdot g(t) \cdot \left(\sum_{i=0}^{N-1} c_k^i \cdot \sum_{n=0}^{N-1} \alpha_n^l \cdot AF(t,\phi) \cdot \cos\left(2\pi(f_o + n\Delta f) \cdot t - \beta_n^l + \frac{M-1}{2}\gamma(t,\phi) + \xi_n^l \right) \right) + n^l(t),$$
$$t \in [lT_S / L, (l+1)T_S / L], l \in \{0,1,\ldots,L-1\} \quad (5.10)$$

First, we explain the α_n^l and ξ_n^l terms in (5.10). Because each chip shape is a multi-carrier signal, the frequency-selectivity of the fade is resolved by the multi-carrier components of the CI chip shape (as in OFDM [82] and MC-CDMA [50]-[53]). That is, each carrier n, $n \in \{0,1,\ldots,N-1\}$, that makes up the chip shape experiences a unique flat fade: α_n^l is the fade on the n^{th} carrier in the l^{th} time slot (due to fading) and ξ_n^l is the phase offset in the n^{th} carrier and l^{th} time slot (due to fading) (hereafter, this phase is assumed to be tracked and removed). The fades α_n^l over the subcarriers that make up each CI chip, i.e., $\{\alpha_0^l, \alpha_1^l, \ldots, \alpha_{N-1}^l\}$, are correlated Rayleigh random variables with correlation coefficient between the p subcarrier fade and the q subcarrier fade characterized by [33]:

$$\rho_{p,q} = \frac{1}{1 + ((p-q) \cdot (\Delta f / (\Delta f)_C))^2}, \quad (5.11)$$

where $(\Delta f)_C$ is the coherence bandwidth of the channel. In addition, in (5.10), the $n^l(t)$ term represents the white Gaussian noise in the l^{th} time slot, and the antenna array introduces the phase offset $\gamma(t,\phi)$ corresponding to

$$\gamma(t,\phi) = (2\pi d_o / \lambda_o)\cdot\cos\phi + \theta(t). \tag{5.12}$$

Here, $(2\pi d_o / \lambda_o)\cdot\cos\phi$ represents the phase offset due to the difference in distance between antenna array elements and the mobile (assuming the smart antenna array is mounted horizontally). Moreover, in (5.10), the antenna array also introduces the normalized gain $AF(t,\phi)$, corresponding to

$$AF(t,\phi) = \frac{1}{M}\cdot\left[\frac{\sin\left(\frac{M}{2}\gamma(t,\phi)\right)}{\sin\left(\frac{1}{2}\gamma(t,\phi)\right)}\right] \tag{5.13}$$

Assuming the mobile is located on the antenna beam main axis ($\phi_o = \pi/2$), and assuming a small beam pattern movement ($\kappa < 0.05$), (5.10) can be simplified by assuming $\gamma(t,\phi) \cong \gamma(t) = \theta(t)$ and $AF(t,\phi) \cong 1$ at the mobile's position for all $t \in [0, T_S]$.

The CI/DS-CDMA receiver is shown in Fig. 5.4(a,b), where Fig. 5.4(a) shows the overall receiver structure for user h, and Fig. 5.4(b) details the block entitled 'chip j receiver' (in Fig. 5.4(a)). In other words, the receiver operates as follows: first, the received signal is

processed through a total of N chip receivers, where chip j's receiver: a) decomposes its chip into N carrier components, and b) recombines across the carrier components to recreate the chip while achieving a frequency diversity benefit. In addition, because a time diversity benefit is available (via transmit diversity), chip j's receiver also: c) combines across time components to recreate the chip with a frequency-time diversity gain. Next, once each chip is recreated with an enhanced diversity benefit, the receiver of Fig. 5.4(a) performs a combining across chips in a usual DS-CDMA manner to eliminate interfering users' signals.

Mathematically, the receiver operates as follows. First, the received signal enters chip j's receiver. Here, the carrier component is removed from the incoming signal, and the signal is split into N branches (one per carrier component). On the n^{th} branch, the n^{th} carrier is returned to baseband and separated from other carriers by application of a lowpass filter. (To ensure perfect separability of the carriers (that make up the j^{th} chip) via filtering, we select $\Delta f = 2/T_S$.)

Each baseband signal (one per carrier) is integrated over each interval over which the fade is constant, i.e., over $t \in [lT_S/L, (l+1)T_S/L]$, $l \in \{0,1,\ldots,L-1\}$. After applying phase offsets to the N frequency components (phase offsets corresponding to the delay jT_C, separating the j^{th} chip from other chips), the signal in the j^{th} chip's receiver, for each carrier n, $n \in \{0,1,\ldots,N-1\}$, and time interval l, $l \in \{0,1,\ldots,L-1\}$, corresponds to:

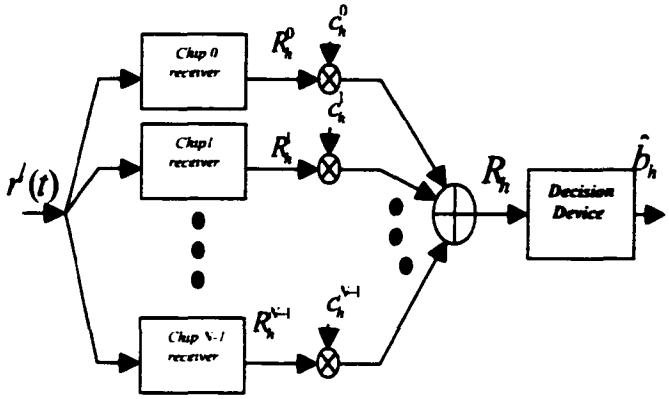

(a)

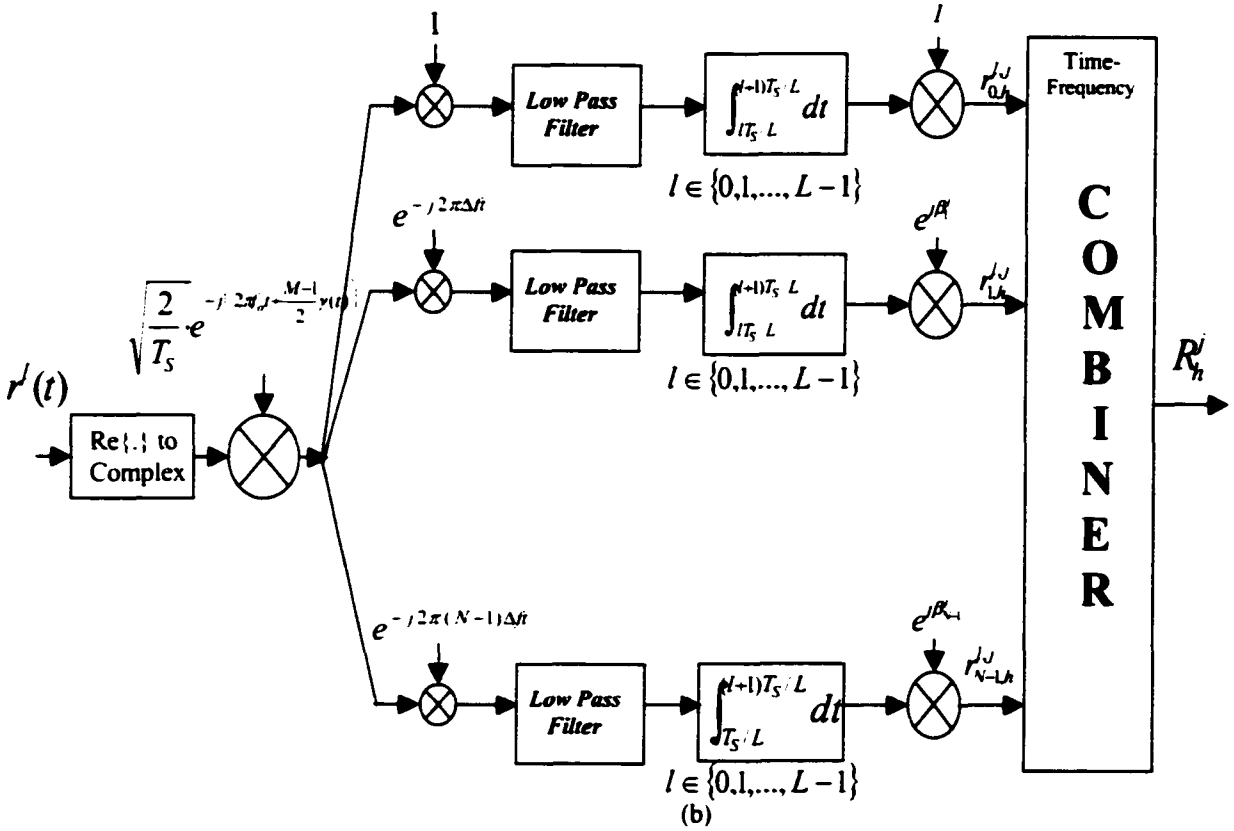

(b)

Fig. 5.4 User h (a) mobile receiver and (b) chip j receiver.

$$r_{n,h}^{l,j} = \frac{1}{L}\sqrt{E_S}\cdot\alpha_n^l\cdot b_h\cdot c_h^j \;+\frac{1}{L}\sqrt{E_S}\cdot\alpha_n^l\cdot b_h\cdot\sum_{\substack{i=0\\ i\neq j}}^{N-1} c_h^i\cdot\rho_{i,j}^n$$
$$+\frac{1}{L}\sqrt{E_S}\cdot\alpha_n^l\cdot\sum_{\substack{k=1\\ k\neq h}}^{K} c_k^j\cdot b_k+\frac{1}{L}\sqrt{E_S}\cdot\alpha_n^l\cdot\left(\sum_{\substack{k=1\\ k\neq h}}^{K} b_k\cdot\sum_{\substack{i=0\\ i\neq j}}^{N-1} c_k^i\cdot\rho_{i,j}^n\right)+n_{n,h}^{l,j}, \tag{5.14}$$

where $\sqrt{E_S}=\sqrt{T_S/2}$. In (5.14), the first term represents the desired n^{th} frequency component and l^{th} time component of chip j for the desired user (user h); the second term is the interchip interference due to other chips from the same user (where $\rho_{i,j}^n=\cos\left(\beta_n^i-\beta_n^j\right)$ is the correlation between the i^{th} chip and the j^{th} chip in carrier n); the third term is the interference due to the same chip from other users, and the fourth term represents the interference from different chips of different users. Moreover, $n_{n,h}^{l,j}$ is a zero mean Gaussian random variable with variance $(N_o/2)/(N^2\cdot L)$, independent across different carriers n and different time slots l, but correlated across chips, with correlation $\rho_{i,j}^n$ between the i^{th} chip noise and the j^{th} chip noise.

It is also important to note the factor of $1/L$ in the first term (desired term) in (5.14), which is a direct result of the division of the received signal interval into L time partitions (to create L-fold time diversity) (a direct result of the L-fold oversampling strategy).

Following the decomposition of the j^{th} chip into its time and frequency components, each with a unique fade, a linear combining strategy is employed to recreate the j^{th} chip with a joint time-frequency diversity benefit. Using the linear combining scheme discussed in

the next paragraph, we combine the $r_{n,h}^{l,j}$ over time components (l) and frequency components (n) (with $L \times N$ diversity components, L over time and N over frequency) to simultaneously reduce the inter-chip interference and the noise and achieve high diversity gains. This leads to the output, R_h^j, which (referring to Fig. 5.4(a)) is combined across the N chips in the usual DS-CDMA manner to eliminate other users interference (term 3 in (5.14)). The chip combiner output for user h corresponds to

$$R_h = \sum_{j=0}^{N-1} c_h^j \cdot R_h^j . \tag{5.15}$$

This R_h term enters a hard decision device which generates the final decision, $\hat{b}_h$.

The time-frequency combiner recreating the j^{th} chip from its time-frequency components (in Fig. 5.4(b)) is designed using EGC (equal gain combining) across L time components followed by MRC (maximal ratio combining) across N frequency components. We selected this scheme after extensive emulation demonstrated EGC-MRC achieving excellent performance relative to other combining options. Applying EGC in time, then the MRC across carriers, the decision variable corresponds to:

$$R_h^j = \sum_{n=0}^{N-1} \alpha_n \cdot r_{n,h}^j, \tag{5.16}$$

where

$$r_{n,h}^{J} = \sum_{l=0}^{L-1} r_{n,h}^{l,J} = \frac{1}{L}\sqrt{E_S}\cdot b_h \cdot c_h^{J} \cdot \alpha_n + \frac{1}{L}\sqrt{E_S}\cdot b_h \cdot \alpha_n \cdot \sum_{\substack{i=0 \\ i\neq J}}^{N-1} c_h^{i} \cdot \rho_{C_{i,J}}^{n}$$

$$+ \frac{1}{L}\sqrt{E_S}\cdot \alpha_n \cdot \sum_{\substack{k=1 \\ k\neq h}}^{K} c_k^{J} \cdot b_k + \frac{1}{L}\sqrt{E_S}\cdot \alpha_n \cdot \left(\sum_{\substack{k=1 \\ k\neq h}}^{K} b_k \cdot \sum_{\substack{i=0 \\ i\neq J}}^{N-1} c_k^{i} \cdot \rho_{C_{i,J}}^{n} \right) + n_{n,h}^{J}. \tag{5.17}$$

$$\alpha_n = \sum_{l=0}^{L-1} \alpha_n^{l}. \tag{5.18}$$

$$n_{n,h}^{J} = \sum_{l=0}^{L-1} n_{n,h}^{l,J}. \tag{5.19}$$

and $N_{on}'/2$ is the noise variance of $n_{n,h}^{J}$ in (5.19), i.e., $(N_o/2)/N^2$.

5.3 Simulated Performance

For simulation purposes, we consider:

(1) CI/DS-CDMA with a processing gain of N=32;

(2) each CI/DS-CDMA chip is composed of N=32 carriers (see Equation (5.3));

(3) the CI/DS-CDMA system is fully loaded with K = 32 orthogonal users employing Hadamard-Walsh codes;

(4) the frequency selectivity of the channel results in 4 fold frequency diversity over the entire bandwidth, i.e., $(\Delta f)_C / BW = 0.25$, and

(5) beam pattern movement results in $L = 7$ independent fades in the duration T_S.

In Fig. 5.5, a typical simulation result is provided for the proposed CI/DS-CDMA – oscillating beam antenna-array merger. The simulation results in Fig. 5.5 are compared with those of CI/DS-CDMA with a conventional smart antenna at the BS: Here, MRC is applied to the subcarriers of the received CI/DS-CDMA signal. It is observed that the introduction of a smart antenna array with beam-pattern-oscillation at the BS introduces an improvement of more than 14 dB at a probability of error of 10^{-3} (at the mobile) compared to CI/DS-CDMA with traditional smart antenna arrays. When compared to traditional DS-CDMA with RAKE reception (e.g, [54][55]) combined with a conventional smart antenna array, even larger performance gains are achieved, as shown in Fig. 5.5.

5.4 Conclusions

CI/DS-CDMA signals are sent via an antenna array at the BS, and received by a single antenna at the MS. The phase shifts introduced to the BS antenna array elements are designated to control the antenna pattern movement (oscillation) such that it achieves directionality and transmit diversity.

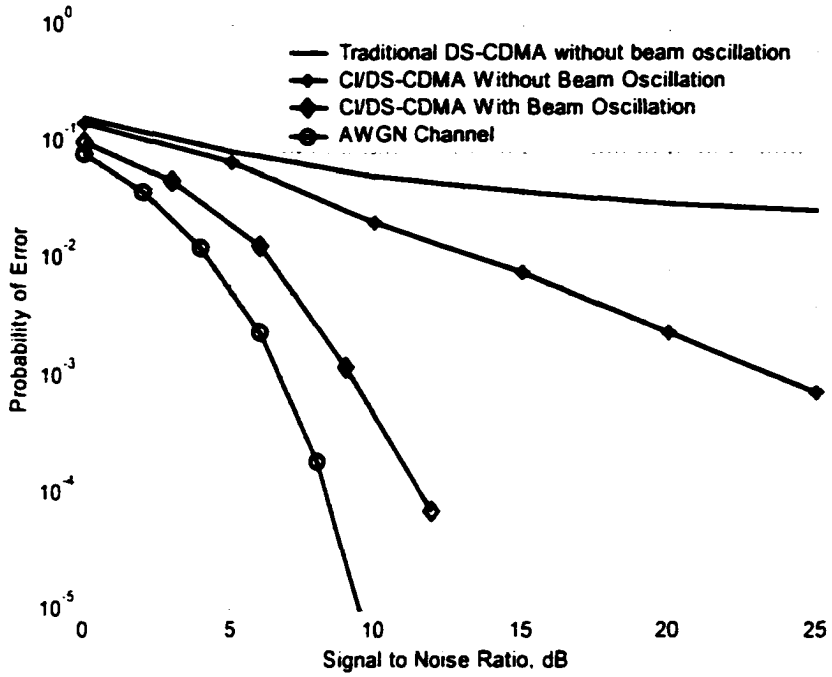

Fig. 5.5 Simulation results.

Receivers employ diversity combining in the frequency and time domains, and significant performance improvement is shown when compared to the CI/DS-CDMA system with a conventional antenna array. This performance gain highlights the significance of small beam pattern movement in smart-antenna-array CDMA systems.

Chapter 6

Achieving High Capacity Wireless by Merging Multi-Carrier CDMA Systems and Oscillating-Beam Smart Antenna Arrays

In this chapter, considering a cellular network with the proposed antenna array/MC-CDMA merger, we characterize the *network capacity*. We study the effect of interference generated by signals in other cells, considering both urban and rural settings. Using computer-based emulation, we demonstrate the dramatic network capacity gains achieved by the small beam pattern oscillation of the antenna array.

Section 6.1 reviews the merger of antenna pattern oscillation and CI/MC-CDMA. Section 6.2 studies the received signal and channel interference modeling. Sections 6.3 and 6.4 present the receiver structure and the simulation results, respectively. Section 6.5 concludes this chapter.

6.1 The Merger of Antenna Pattern Oscillation and CI/MC-CDMA

In this chapter, we will assume carrier frequency (f_o) much larger than system bandwidth (BW) (e.g., $f_o \geq 100 \cdot (BW)$), a reasonable assumption in most mobile systems. As a result, the antenna pattern from an antenna array is identical for all transmit frequencies of a CI/MC-CDMA system.

We apply the output of a CI/MC-CDMA transmitter, i.e., the signal

$$s(t) = \sum_{k=1}^{K} s_k(t), \tag{6.1}$$

to the BS antenna array of Fig. 6.1. Here $s_k(t)$ is the CI/MC-CDMA signal of (4.1) and K is the number of users in the multi-access system.

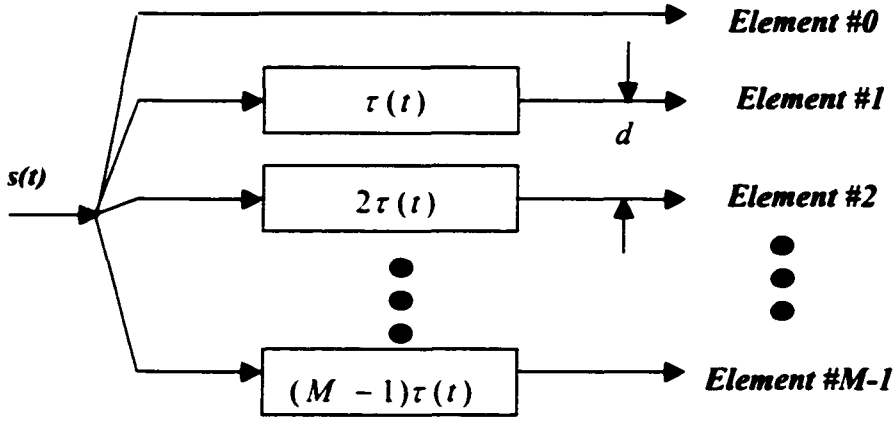

Fig. 6.1 BS antenna array structure.

6.2 The Received Signal and Channel Interference Modeling

Considering the antenna array at the BS and a single antenna at the mobile, we model the received signal at the intended mobile (shown in Fig. 6.2). In modeling the mobile's received signal, we include interference due to transmitted signals from neighboring base stations, i.e., the cells 1-6 of Fig. 6.2. We only consider the effect of the so-called one-tier cells, neglecting the effect of interference from higher tier cells (a typical modeling because of the well-known relationships between signal power and distance [86][87]).

In cell c ($c \in [0,6]$), the signal input to the base station antenna array for user k (using (4.1) and (4.2)) corresponds to

$$s_k^c(t) = b_k^c[i] \cdot \left(\sum_{n=0}^{N-1} c^{n,c} \cdot \cos\left(2\pi(f_o + n\Delta f) \cdot t + \beta_k^n\right) \right) \cdot g(t), \quad t \in [0, T_S], \tag{6.2}$$

Here, $c^{n,c} \in \{-1,+1\}$ represents the n^{th} element in the pseudo-random code (long code) applied to each user in the c^{th} cell (to minimize inter-cell interference). The signal in (6.2) enters the smart antenna array, where the output of the m^{th} element, after application of offset $m\tau(t)$, is simply:

$$s_k^{c,m}(t) = b_k^c[i] \cdot \sum_{n=0}^{N-1} c^{n,c} \cdot \cos\left(2\pi f_o t + 2\pi n\Delta f \cdot t + \beta_k^n + m\theta(t)\right), \quad t \in [0, T_S], \tag{6.3}$$

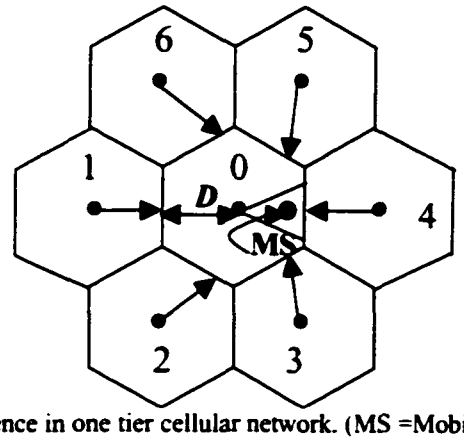

Fig. 6.2 Interference in one tier cellular network. (MS =Mobile Station.)

where $\theta(t) = 2\pi f_o \tau(t)$. The total downlink transmitted signal from the c^{th} cell, considering all antenna elements (all m), and all users in the cell (all $k \in \{1,2,....,K_c\}$) is (from (6.3))

$$s^{c}(t) = \sum_{k=1}^{K} b_k^c[i] \cdot \sum_{n=0}^{N-1} c^{n,c} \cdot \frac{1}{M} \sum_{m=0}^{M-1} \cos\left(2\pi(f_o + n\Delta f)\cdot t + \beta_k^n + m\theta(t)\right), t \in [0, T_S], \tag{6.4}$$

where $\frac{1}{M}$ is a normalization factor compensating for transmission over M array elements.

At the receiver side, considering the beam pattern movement which leads to an L fold time diversity, the received signal in $[0,T_S]$, $r(t)$, can be divided into time slots $[lT_S/L,(l+1)T_S/L]$, where $l \in \{0,1,...,L-1\}$. Each time slot demonstrates an independent fade. The signal received in $[lT_S/L,(l+1)T_S/L]$, denoted

$r_l(t)$, corresponds to

$$r_l(t) = \sum_{c=0}^{6} \sum_{k=1}^{K} AF(t,\phi_k^c) \cdot b_k^c[i] \cdot \sum_{n=0}^{N-1} [\alpha_l^{n,c} \cdot c^{n,c} \cdot \cos\left(2\pi(f_o + n\Delta f) \cdot t + \beta_k^n + \frac{M-1}{2}\gamma(t,\phi) + \theta_l^{n,c}\right)] + n_l(t),$$
$$t \in [lT_S / L, (l+1)T_S / L], \tag{6.5}$$

Here, $n_l(t)$ is an additive white Gaussian noise; $\alpha_l^{n,c}$ is the gain on the n^{th} carrier in the l^{th} time slot and c^{th} cell (due to fading) and $\theta_l^{n,c}$ is the phase offset in the n^{th} carrier, l^{th} time slot, and c^{th} cell (due to fading) (hereafter, this phase is assumed to be tracked and removed). In addition, $AF(t,\phi_k^c)$ is the normalized array factor of the smart antenna array (characterized in (2.1)).

With K_c users in the c^{th} cell, and assuming an antenna array on each base station, only a small fraction of the K_c users, $c \in \{0,1,\ldots,6\}$, interferes with the mobile at cell *0* (Fig. 6.2). Specifically, only the users in cell *c* located in the sector of space consistent with the direction of the arrow (see Fig. 6.2) impact the intended user. If a user in cell *c* has any part of its HPBW in the direction of the arrow (Fig. 6.2), we assume $AF(t,\phi_k^c) \cong 1$; otherwise, we assume $AF(t,\phi_k^c) \cong 0$. Of the K_c users in cell c, we assume K_c' of these users demonstrate $AF(t,\phi_k^c) \cong 1$, where

$$\frac{E[K_c']}{K_c} = \frac{HPBW}{2\pi}. \tag{6.6}$$

In (6.6), $E[\cdot]$ denotes expected value.

It is important to note that the term $\alpha_l^{n,c}$, representing the fading gain, contains both a short term and a long term fading component:

$$\alpha_l^{n,c} = \frac{v_l^{n,c}}{(R^c)^a}. \tag{6.7}$$

where $v_l^{n,c}$ representes the short-term fade and $1/(R^c)^a$ characterizes the long-term fade (path loss). The set of values $\{v_l^{n,c},\ n = 0,1,\ldots,N-1\}$ are correlated Rayleigh fades over the N subcarriers with correlation coefficient between the n' subcarrier fade and the n^* subcarrier fade determined by [33]:

$$\rho_{n^*,n'} = \frac{1}{1+((n^*-n')\cdot(\Delta f/(\Delta f)_C))^2}. \tag{6.8}$$

Here, $(\Delta f)_C$ is the coherence bandwidth of the channel.

In the long-term fade component of (6.7), R^c represents the distance between the c^{th} cell BS and the intended mobile in the 0^{th} cell. We will assume the intended mobile is located at the distance of $D/\sqrt{2}$ from the 0^{th} cell's BS (where D is the cell radius) (Fig. 6.2). (Note: assuming a uniform distribution of users within each cell, $D/\sqrt{2}$ represents the approximate center of mass of users in the antenna pattern coverage area, when

approximating this coverage area with a triangle.) For the geometry of Fig. 6.2, the vector that represents R^c for $c \in \{0,1,...,6\}$ corresponds to

$$\boldsymbol{R}=[1.00\ 3.83\ 3.44\ 1.975\ 1.83\ 1.975\ 3.44]. \tag{6.9}$$

where R^0 is normalized to 1.00 and all other values are defined with respect to this normalization.

In (6.9), the power a in $\left(R^c\right)^a$ is a function of user location, BS antenna height, and environment. Here, for simplicity in presentation, we consider two environments, urban and rural, and we approximate a for these two areas as follows (based on [86][87]). *In urban areas*, the parameter a depends on the carrier frequency and the BS antenna height: $a = 1$ if $R^c < D_{\max}$, and $a = 2$ if $R^c > D_{\max}$, where $D_{\max} = D_{\max}(f_o, h_a)$, i.e., $D_{\max}$ is a function of carrier frequency f_o and BS antenna height, h_a. For urban areas with $f_o = 900MHz$ and a BS antenna height larger than 25m, $D_{\max} \approx 1000m$ (see [87]), assuming a cell dimension of, e.g., $D \approx 500m$, referring to (6.9), $a = 2$ for cells 1,2 and 6, and $a = 1$ for other cells. Thus, we can ignore the effect of interference due to cells 1,2 and 6 and consider only interference due to cells 3, 4 and 5, with little loss in accuracy. *In rural areas* with $f_o = 900MHz$ and a typical antenna height of, e.g., 10m, $a = 1$ for, e.g., $R^c < D_{\max} \cong 200m$, and $a = 2$ otherwise (the majority of cells). (Note that $a = 1$ ($a = 2$) in the amplitude attenuation model of Equation (6.7) corresponds to power loss as a function of $1/(R^c)^2$ ($1/(R^c)^4$).), otherwise (the majority of cells).

6.3 The CI/MC-CDMA Receiver

The CI/MC-CDMA receiver for user j, $j \in \{1,2,...,K_C\}$, is shown in Fig. 6.3 (an alternative representation of the receiver in Fig. 4.3). In this figure, the center frequency is removed from the incoming signal, and the resulting signal is split into N branches, one per subcarrier. On branch n, the n^{th} subcarrier is returned to baseband and seperated from other carriers by application of a lowpass filter. The isolated n^{th} subcarrier term is integrated over each interval over which the fade is constant, i.e., over $t \in [lT_S / L, (l+1)T_S / L]$, $l \in \{0,1,...,L-1\}$. The n^{th} element of the long code for cell 0 (i.e., $c^{n,0}$) is applied to minimize interference from neighboring cells, and the spreading code for user j seperates the intended user from interfering users in the same cell. The received signal, after the above processing, for each subcarrier n, $n \in \{0,1,...,N-1\}$, and time interval l, $l \in \{0,1,...,L-1\}$, corresponds to:

$$\begin{aligned} r_l^n = & \frac{1}{L}\sqrt{E_S}\alpha_l^{n,0} \cdot b_l^0[i] \\ & + \frac{1}{L}\sqrt{E_S}\sum_{k=1,k\neq j}^{K_0} \alpha_l^{n,0} \cdot b_k^0[i] \cdot e^{-j(\beta_l^n - \beta_k^n)} \\ & + \frac{1}{L}\sqrt{E_S}\sum_{c=1}^{6}\sum_{k=1}^{K_c} \alpha_l^{n,c} \cdot b_k^c[i] \cdot c^{n,c} \cdot c^{n,0} \cdot e^{-j(\beta_l^n - \beta_k^n)} + n_l^n, \end{aligned} \tag{6.10}$$

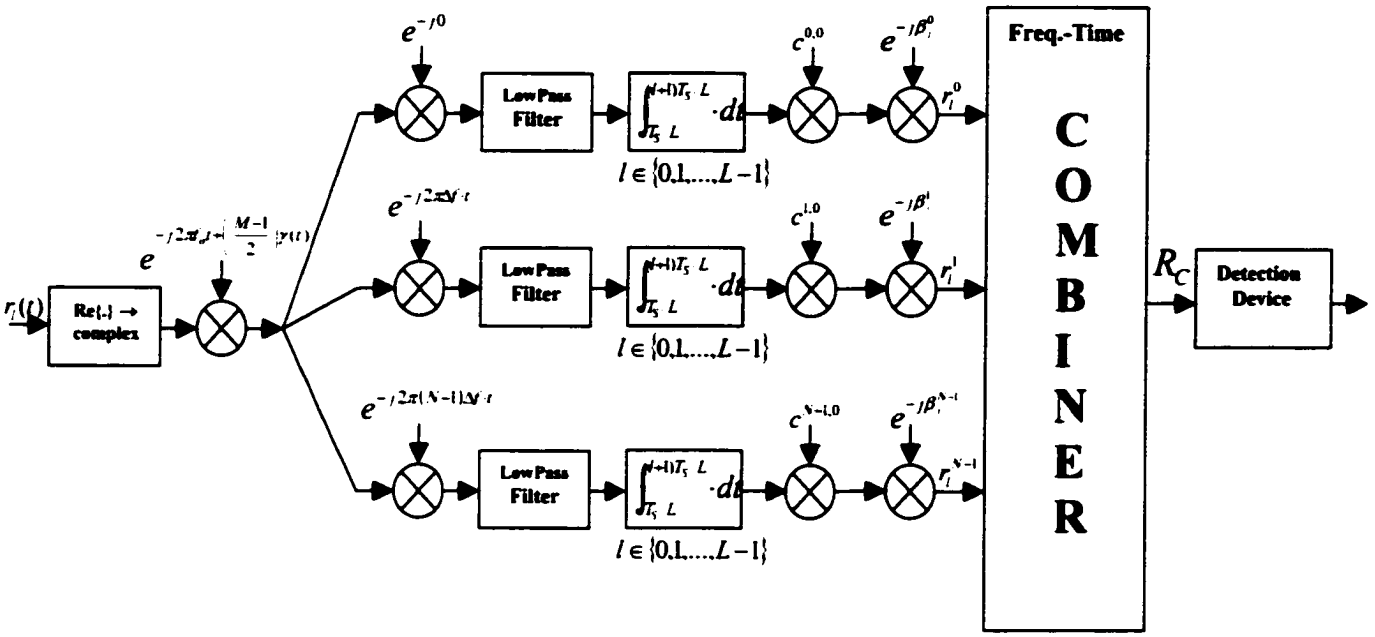

Fig. 6.3 The MS receiver structure of MC-CDMA.

where $\sqrt{E_S} = \sqrt{T_S / 2}$ and n_l^n is a zero mean Gaussian random variable with variance $N_0/(2 \cdot N \cdot L)$. The first term in (6.10) represents the desired signal (in the cell *0*), the second term represents the interference from other users in the cell 0, the third term represents the interference from users in neighboring cells, and the final term denotes the noise.

In the case of BPSK, i.e., $b_k[i] \in \{-1,+1\}$, the received signal r_l^n can be replaced by its real component, in which case we can express

$$
\begin{aligned}
r_l^n &= \frac{1}{L}\sqrt{E_S}\alpha_l^{n,0}\cdot b_l^0[i] \\
&+ \frac{1}{L}\sqrt{E_S}\sum_{k=1,k\neq l}^{K_0}\alpha_l^{n,0}\cdot b_k^0[i]\cdot\cos\left(\beta_l^n-\beta_k^n\right) \\
&+ \frac{1}{L}\sqrt{E_S}\sum_{c=1}^{6}\sum_{k=1}^{K^c}\alpha_l^{n,c}\cdot b_k^c[i]\cdot c^{n,c}\cdot c^{n,0}\cdot\cos\left(\beta_l^n-\beta_k^n\right)+n_l^n,
\end{aligned}
\tag{6.11}
$$

With $N\times L$ diversity components, N over frequency ($n\in\{0,1,\ldots,N-1\}$) and L over time $l\in\{0,1,\ldots,L-1\}$, we perform EGC (equal gain combining) in the frequency domain followed by MRC (maximal ratio combining) in time. We propose this combining because emulations indicate that, relative to other sequential combinings, EGC-MRC offers a very high performance. This combining strategy leads to

$$
R_C=\sum_{l=0}^{L-1}\zeta_l^0\cdot r_l\,. \tag{6.12}
$$

where

$$
r_l=\frac{1}{L}\sqrt{E_S}\zeta_l^0\cdot b_l^0[i]+\frac{1}{L}\sqrt{E_S}\sum_{k=1,k\neq l}^{K_0}\zeta_{l,k}^0\cdot b_k^0[i]+\frac{1}{L}\sqrt{E_S}\sum_{c=1}^{6}\sum_{k=1}^{K^c}\zeta_{l,k}^c\cdot b_k^c[i]+n_l\,, \tag{6.13}
$$

and

$$
\zeta_l^0=\sum_{n=0}^{N-1}\alpha_l^{n,0}, \tag{6.14}
$$

$$\zeta_{l,k}^{c} = \sum_{n=0}^{N-1} \alpha_l^{n,c} \cdot c^{n,c} \cdot c^{n,0} \cdot \cos\left(\beta_j^n - \beta_k^n\right), \tag{6.15}$$

$$n_l = \sum_{n=0}^{N-1} n_l^n. \tag{6.16}$$

The R_C value of (6.12) enters a hard decision device to create the final decision $\hat{b}_j^0[i]$.

6.4 Simulation Results

For simulation purposes, we consider:

1) an N=32 carrier CI/MC-CDMA system;
2) a 4-element ($HPBW \approx 25^\circ$) and a 6-element ($HPBW \approx 17^\circ$) antenna array (per base station);
3) a frequency selectivity resulting in 2-fold frequency diversity over the entire bandwidth, i.e. $(\Delta f)_C / BW = 0.5$;
4) beam pattern movement resulting in L = 7 independent fades in the duration T_S in urban areas (a rich scattering environment) and L = 3 independent fades in rural areas (a poor scattering environment)[40].
5) an SNR = 8.3dB in urban areas, and 9.9dB in rural areas ; and
6) assignment of codes to users performed via a random sampling from the code set.

Simulation results plotting bit error rate versus number of users per cell are generated by processing the received signal (of Equation (6.11)) through the receiver of Fig. 6.3, as characterized in Section 6.3. Fig. 6.4(a) presents emulation results assuming a 4-element antenna in an urban environment, whereas Fig. 6.4(b) introduces the 6-element urban environment results.

In each figure, two curves are provided. The upper curve is the performance when a traditional antenna array is applied, i.e., an antenna array providing directionality but no time diversity (no beam pattern movement) is applied (as in, e.g., [88]-[89]); and the lower curve is the performance of the proposed system with beam pattern oscillation.

We observe large network capacity gains achievable in urban areas by small oscillations in beam pattern movement. Assuming a cell with a 4-element antenna array mounted on the BS, antenna array beam-pattern-oscillation enables 160 users to be supported with the same performance as a 40-user system without pattern oscillation. Network capacity gains are more impressive when a 6-element array is applied (Fig. 6.4(b)).

Fig. 6.5(a),(b) presents BER versus number-of-user plots for rural areas. Again, notable network capacity gains are observed when using beam pattern oscillation. For example, assuming a referenced BER of 10^{-2} prior to FEC (forward error correction), a system where the antenna array provides beam pattern movement supports approximately 160 users, whereas a system without the pattern movement only supports in the vicinity of 50 users. Dramatic network capacity gains are achievable via small pattern oscillations.

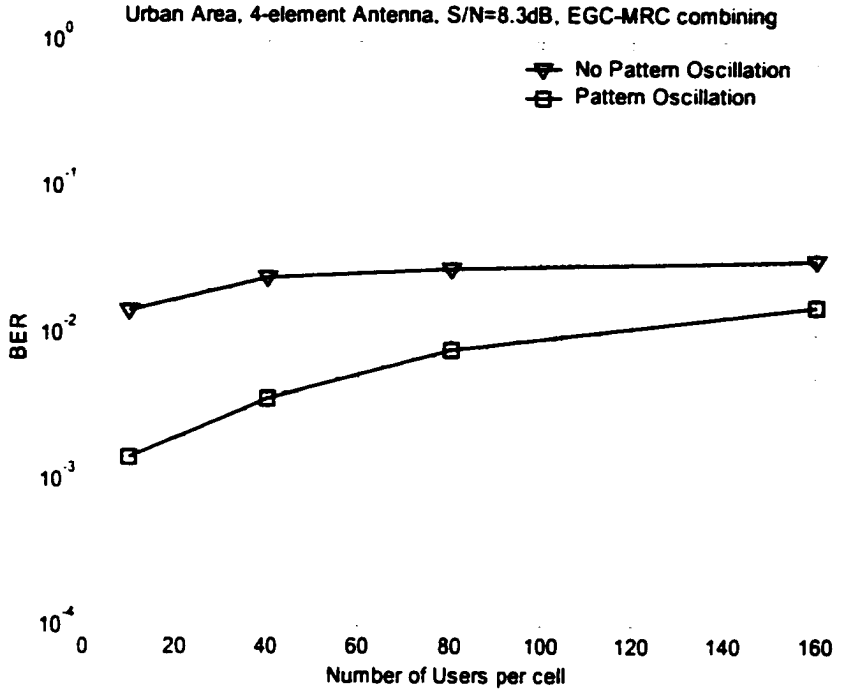

(a)

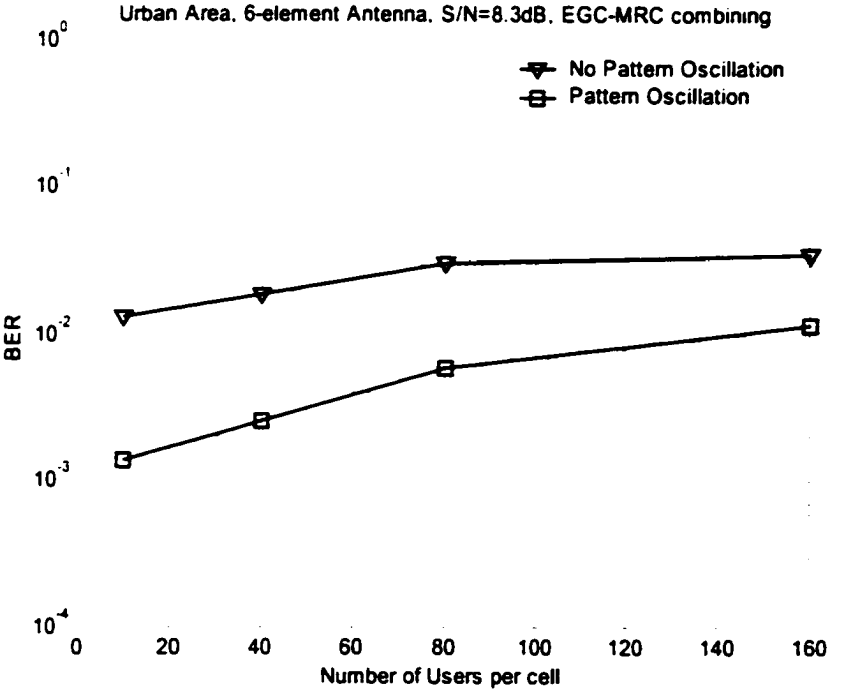

(b)

Fig. 6.4(a,b) Capacity simulation results for urban areas.

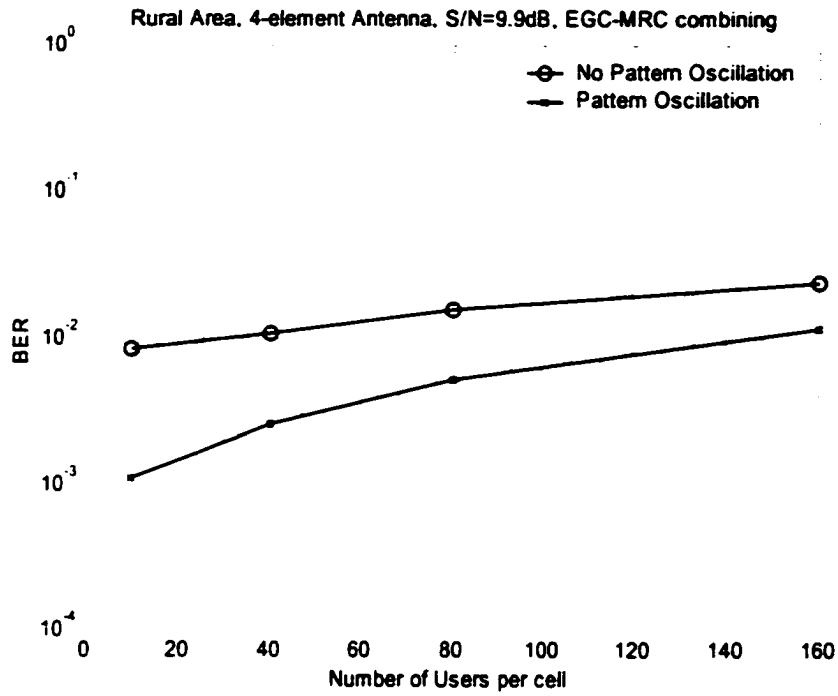

(a)

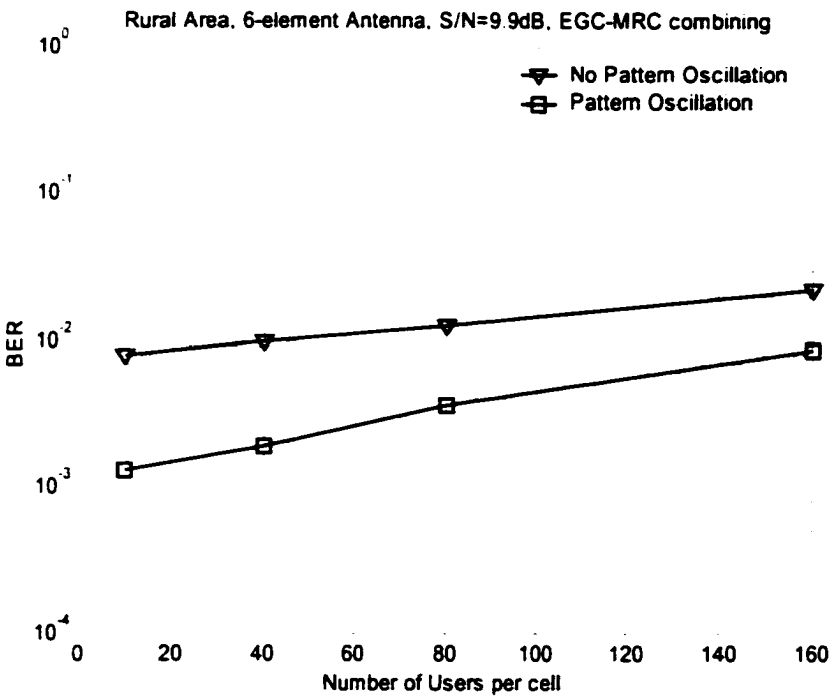

(b)

Fig. 6.5(a.b) Capacity simulation results for rural areas.

6.5 Conclusions

At each base station, an oscillating bean antenna array is used to transmit CI/MC-CDMA signals, while at the mobile a single antenna is used for reception. Capacity curves for these receivers show the significant improvement available when comparing CI/MC-CDMA systems with the benefit of oscillation in the antenna patterns to CI/MC-CDMA systems without the oscillation in the antenna pattern. This capacity improvement is in the order of three-fold for typical urban areas and rural settings.

Chapter 7

Conclusions

This chapter highlights the contributions of this dissertation (Section 7.1), introduces a plan for continuation of this work (Section 7.2) and summarizes the dissertation (Section 7.3).

7.1 Contribution

A novel transmit diversity technique has been introduced, in which we enhance both the network capacity and the receiver performance. Specifically, time-varying time-delays (phase shifts) are introduced to the base station antenna array elements that control the antenna pattern movement. This leads to movement (oscillation) that creates directionality and transmit diversity.

The coherence time created by the oscillating beam pattern was determined by using a comprehensive geometric-based stochastic channel model with both circular and semi-

elliptic coverage. Simulation results show that a coherence time can be established by beam pattern oscillation which leads to about $L = 7$ fold time diversity at the mobile (when small beam pattern movement is present). Hence, beam pattern motion can create a very significant increase in performance at the mobile.

Receivers which take advantage of the induced time diversity have been studied based on equal gain combining (EGC) and maximal ratio combining (MRC). For BPSK transmission, about a 15dB improvement in performance was observed (when comparing the proposed system to one without the benefit of antenna pattern oscillation). A key feature in receiver design is that time separation between each diversity component allows for a low complexity receiver even in cases of larger degrees of diversity. The cost of this scheme is low because complexity is focused on the base station.

Carrier interferometery multi-carrier code division multiple access (CI/MC-CDMA) signals are sent via oscillating beam antenna arrays at the BS, and received by a single antenna at the mobile. The proposed system achieves (1) very high network capacity via the combining of spatial division multiple access (SDMA) and CDMA multiple access techniques and (2) very high performance via the combined frequency-time diversity gains.

Focusing on the available performance benefits, we construct receivers that employ diversity combining in the frequency and time domains. Different combining strategies, e.g., MMSEC-EGC (minimum mean square error combining-equal gain combining),

MRC-EGC (maximal ratio combining-equal gain combining) and EGC-EGC, have been simulated and the performance results characterized. More than 7dB improvement in performance is demonstrated when compared to the CI/MC-CDMA/smart antenna system without the benefit of beam pattern oscillation.

Capacity curves for these receivers show the significant improvement available when comparing CI/MC-CDMA systems with the benefit of oscillation in the antenna patterns to CI/MC-CDMA systems without the oscillation in the antenna pattern. Here, we considered the effect of interference generated by signals in other cells for both urban and rural settings. Computer-based emulation demonstrates a 3-fold network capacity gains achieved by the small beam pattern oscillation of the antenna array for typical urban areas and rural settings.

Finally, we merged CI direct sequence code division multiple access (CI/DS-CDMA) signals and oscillating-beam smart antenna arrays. We observed more than 14dB improvement in performance over a CI/DS-CDMA/smart antenna system without the benefit of beam pattern oscillation.

7.2 Future works

In the following, we provide suggestions for future research.

7.2.1 Coherence beamwidth

The introduction of oscillating beam patterns in antenna array systems can be characterized in terms of a new parameter: Coherence beamwidth. For a given environment, coherence beamwidth refers to the sweep of space (as a percent of beamwidth) required to achieve an independent fade. We intend to parametrize environment based on this term, which characterizes the diversity benefits of pattern oscillation.

7.2.2 A merger of orthogonal frequency multiple access (OFDM) and oscillating beam smart antennas

Orthogonal frequency division multiplexing (OFDM) [82]-[85] is a multicarrier modulation scheme that enables transmitters to send high data rates over channels at a low complexity while avoiding multipath fading. In this scheme, high rate symbol streams serial to parallel converted to N low rate stream, and low rate streams are transmitted in parallel using orthogonal subcarriers. OFDM has been selected as part of IEEE 802.11a and IEEE 802.11g WLAN (wireless local area network) standards [74].

Chapter 4 demonstrated the potential benefits when merging multicarrier signals and the proposed antenna array. With this in mind, we anticipate large performance gains for merging the proposed future work of OFDM systems and oscillating-beam antenna arrays.

7.2.3 Indoor channel modeling for oscillating-beam antenna arrays

In Chapter 3 we presented channel models and channel emulations for outdoor environments (e.g., mid-size city center). We intend to apply the oscillating-beam antenna array to indoor applications (e.g., for WLANS). This will require an appropriate model to emulate indoor wireless channel. Simulation of indoor environment will lead to a characterization of the available diversity in the presence of beam pattern movement, through which we establish probability-of-error performance curves and determine the available performance gain.

7.2.4 Multiple-input multiple-output (MIMO) systems

In Multiple-input multiple-output (MIMO) systems [90]-[94], antenna arrays (usually smart antenna arrays) are mounted on both the base station and the mobile. They are capable of enhancing the capacity of wireless systems beyond the gains of conventional smart antenna systems (smart antennas only at the base station).

In the future, we will merge MIMO systems and oscillating-beam antenna pattern systems. Here, we may oscillate the antenna pattern at the transmitter side, receiver side or at the both sides. We will propose various schemes for pattern oscillation, model the channel to establish the available diversity and determine the performance gain for various signaling schemes.

7.2.5 Code reassignment schemes

In most CDMA-based cellular standards, long codes are introduced to minimize interference among users in nearby cells. In addition to long codes, code reuse (reassignment) strategies [95][96] can further reduce the inteference. Code reuse strategies refer to a methodology for inter-cell and intra-cell code selection, such that interference is reduced.

In Chapter 6, we presented the capacity gains available via a merger of CI/MC-CDMA systems and oscillating-beam antenna arrays, assuming a random selection of spreading codes within each cell and between the neighboring cells. Improved code reassignment techniques will be designed, and the resulting capacity and performance benefits will be presented.

7.3 Summary

We live in an era of incrasing demand for wireless systems. Specifically, we are requiring wireless systems providing both a high-quality-of-service and a high capacity. In this dissertation, a novel antenna array technique is introduced, investigated and developed, that allow wireless systems to achieve their objectives interms of quality and capacity, all the while maintaining a low cost. It is our hope that this technology has a positive impact on future generation systems.

Appendix 1

Calculation of Semi-elliptic Coverge Area $A(\phi_n')$

In this appendix, we calculate $A(\phi_n')$, the portion of the coverage area contained within the angular spread $2\phi_n'$ in Chapter 3 (Fig. 3.7). This area corresponds to twice the area of the triangle specified by the BS-MS-C points, $A_1(\phi_n')$, and twice the area of the C-MS-D region, $A_2(\phi_n')$ (see Fig A1.1). That is $A(\phi_n')$ corresponds to

$$A(\phi_n') = 2\left(A_1(\phi_n') + A_2(\phi_n')\right). \tag{A1.1}$$

Here,

$$A_1(\phi_n') = \tfrac{1}{2} h \cdot x_{n,\max}, \tag{A1.2}$$

$$h = x_o \cdot \sin(\phi_n'), \tag{A1.3}$$

$$x_{n,\max} = x_o \cdot \cos(\phi_n') + R \cdot \cos(\varphi), \tag{A1.4}$$

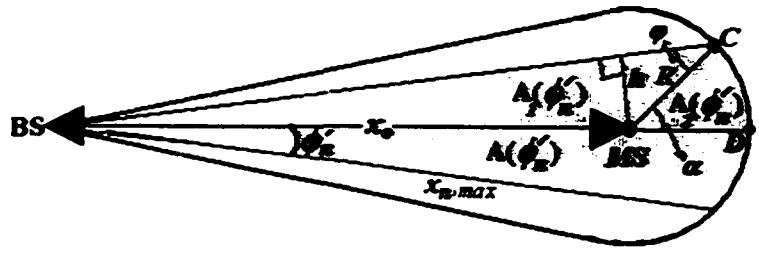

Fig. A1.1 Calculation of the CDF of AOA.

where $x_{n,\max}$ is the maximum possible distance between the n^{th} scatterer in the antenna coverage area and the base station; $R = x_o \cdot \sin(\beta/2)$ and φ is the angle $\angle(BS-C-MS)$. Now, using (A1.3),

$$\sin(\varphi) = \frac{h}{R} = \frac{\sin(\phi_n')}{\sin(\beta/2)}. \tag{A1.5}$$

Substituting (A1.3) and (A1.4) in (A1.2), and applying (A1.5), $A_1(\phi_n')$ corresponds to

$$A_1(\phi_n') = \tfrac{1}{2} x_o^2 \cdot \left(\sin(|\phi_n'|)\cos(|\phi_n'|) + \sin(|\phi_n'|) \cdot \sin(\beta/2)\sqrt{1 - \left(\frac{\sin(|\phi_n'|)}{\sin(\beta/2)}\right)^2} \right) \tag{A1.6}$$

Moreover,

$$A_2(\phi_n') = \tfrac{1}{2}\alpha \cdot R^2 \tag{A1.7}$$

$$\alpha = \varphi + \phi_n', \ \phi_n' \geq 0. \tag{A1.8}$$

Here, α is the angle $\angle(C-MS-D)$ shown in Fig. 3.7. Substituting (A1.8) in (A1.7) and using (A1.5), $A_2(\phi_n')$ corresponds to

$$A_2(\phi_n') = \tfrac{1}{2} x_0^2 \cdot \left(\sin^{-1}\left(\frac{\sin(|\phi_n'|)}{\sin(\beta/2)} \right) + |\phi_n'| \right) \cdot \sin^2(\beta/2) \qquad \text{(A1.9)}$$

Now, substituting (A1.9) and (A1.6) in (A1.1), Equation (3.30) results.

Appendix 2

MMSE Receiver Equation

In this appendix we calculate the MMSE receiver equation presented in Chapter 4, Equation (4.45). The received signal corresponds to:

$$r_{n,l} = \frac{1}{L}\sqrt{E_S}\cdot\alpha_{n,l}b_l[m] + \frac{1}{L}\sqrt{E_S}\cdot\sum_{k=1,k\neq l}^{K}\alpha_{n,l}b_k[m]\cos\left(\beta_l^n - \beta_k^n\right) + n_{n,l}, \quad l\in\{0,1,\ldots,L-1\},\ n\in\{0,1,\ldots,N-1\} \tag{A2.1}$$

where

$$\beta_k^n = \frac{2\pi}{N}\cdot n\cdot k\ . \tag{A2.2}$$

Refering to Wienner filter principle [75], the optimal combining weights are selected according to:

$$W_{opt} = R_{r_{n,l}}^{-1}\cdot\Delta\ . \tag{A2.3}$$

Here $R_{r_{n,j}}$ is the expectation of $r_{n,j}^2$ given $\alpha_{n,j}$, i.e., $R_{r_{n,j}} = E[r_{n,j}^2 \mid \alpha_{n,j}]$, and $\Delta = E(r_{n,j} b_j[m] \mid \alpha_{n,j})$.

Using (A2.1), $R_{r_{n,j}}$ corresponds to

$$\begin{aligned} R_{r_{n,j}} &= E\left[r_{n,j}^2 \mid \alpha_{n,j}\right] = \alpha_{n,j}^2 \cdot (E_S / L^2) + (E_S / L^2) \cdot \sum_{k=1, k \neq j}^{K} \alpha_{n,j}^2 \cdot \cos^2\left(\beta_j^n - \beta_k^n\right) + N_o'' / 2 \\ &= (E_S / L^2) \cdot \alpha_{n,j}^2 \cdot \sum_{k=1}^{K} \cos^2\left(\beta_j^n - \beta_k^n\right) + N_o'' / 2. \end{aligned} \tag{A2.4}$$

Substituting the β_k^n of (A2.2):

$$R_{r_{n,j}} = \frac{E_S}{L^2} \cdot \alpha_{n,j}^2 \cdot \frac{K}{2} \cdot \left(1 + \frac{\sin\left(\frac{2\pi n}{N} K\right)}{K \cdot \sin\left(\frac{2\pi n}{N}\right)} \cdot \cos\left(\frac{2\pi n}{N}(K + 1 - 2j)\right) \right) + \frac{N_o''}{2}. \tag{A2.5}$$

Moreover,

$$\Delta = E\left[r_{n,j} b_j[m] \mid \alpha_{n,j}\right] = \alpha_{n,j} \cdot \sqrt{E_S} / L. \tag{A2.6}$$

Substituting (A2.5) and (A2.6) in (A2.3), and assuming K=N, i.e., assuming a fully loaded system, the optimum filter corresponds to

$$W_{opt} = \begin{cases} \dfrac{\alpha_{n,J} \cdot \sqrt{E_S / L}}{\dfrac{E_S}{L^2} \cdot \dfrac{K}{2} \cdot \alpha_{n,J}^2 + \dfrac{N_o}{2}} & \text{If } n \neq 0, \dfrac{N}{2} \\ \dfrac{\alpha_{n,J} \cdot \sqrt{E_S / L}}{\dfrac{E_S}{L^2} \cdot K \cdot \alpha_{n,J}^2 + \dfrac{N_o}{2}} & \text{If } n = 0, \dfrac{N}{2} \end{cases} \qquad \text{(A2.7)}$$

Appendix 3

Power-Azimuth-Spectrum Modeling for Antenna Array Systems: A Geometric-Based Approach

In this appendix, which contains related research conducted in the course of this dissertation, an analytical method for power azimuth spectrum (PAS) modeling is presented. This analytical method is based on the principles of geometric-based channel modeling. We show that, when assuming a geometry (consistent with the TSUNAMI II project environment), the new PAS model we generate fits to the project measurements and the empirical-based Laplacian model.

A3.1 Introduction

In a wireless communication system employing a base station (BS) antenna array, the power azimuth spectrum (PAS) characterizes the amount of power arriving at the mobile as a function of angle of arrival (azimuth angle) [97]-[99]. This PAS is an important measure, as it helps characterize: (1) the network capacity of a wireless system

employing an antenna array; (2) optimal selection of antenna array parameters; and (3) the performance of the mobile's receiver [97].

Measurement data from the TSUNAMI II project [100] was used in [98] to establish an empirical model for PAS. These measurements were performed in an area with 1) irregular street shapes, 2) an eight-element antenna array mounted at the base station (BS), 3) an omnidirectional antenna at the mobile station (MS), 4) the BS antenna mounted on a rooftop (20-32 m in height), and 5) nearby building heights ranging from 4 to 7 floors.

Using the measurement data and a goodness-of-fit measure, the empirically-based Laplacian function was introduced as the best candidate to model PAS [98][99]. However, this model is not based on the geometry of the antenna array coverage area, and as a result demonstrates a number of shortcomings. For example, this function's validity is limited to the parameter range of the original set of measurements, and it offers no physical (analytical) insight to understanding PAS.

In this appendix, assuming an antenna array at the BS and an omnidirectional antenna at the mobile, we demonstrate how a semi-elliptic geometry [40] can be used to establish the PAS. A key advantage of this PAS derivation is: Because the PAS is established analytically (based on channel geometry), PAS models can now be extended to any area of interest (assuming only that the region's configuration is known).

In this appendix, we assume semi-elliptic geometry consistent with the TSUNAMI II scenario, and show how our new PAS model is a better fit to the experimental data than the empirically-based Laplacian model. This indeed confirms the validity of geometric-based model.

The analytical model for PAS is presented and discussed in detail in Section A3.2. In Section A3.3, analytical results are compared with the experimental data and the Laplacian model, and the advantages of our model over the Laplacian model are highlighted. Conclusions follow in Section A3.4.

A3.2 The Power Azimuth Theoretical Model

Consider an antenna array mounted at the base station (BS), and a single-element omnidirectional antenna at the mobile station (MS). Based on the TSUNAMI II geometry, we assume:

1) the channel angular dispersion (α) is much less than the half power beam width (HPBW) due to the low antenna height and geometry of typical city streets [101],
2) scatterers are uniformly distributed in the so-called semi-elliptic area shown in Fig. A3.1. That is, we assume the height of the BS antenna array is low, e.g., on the roof top of a building of average height, leading to a coverage area approximated by regions located in a semi-elliptic geometry, and

3) the signal received at the MS is the sum of horizontally propagated plane waves, where each plane wave represents the reflection of the incident wave from one point scatterer.

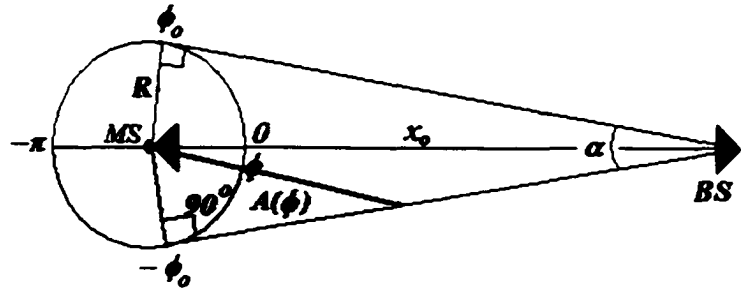

Fig. A3.1 The semi-elliptic scenario.

The total power received by the MS within the angle $-\pi$ to ϕ ($\phi \in [-\pi, \pi)$), normalized by the total transmit power from the BS, is (using $\alpha <<$ HPBW)

$$P_{Total,MS}(\phi) = \Pr(\Phi < \phi) \tag{A3.1}$$

where $\Pr(\Phi < \phi)$ is the probability of a reception within the angle $-\pi$ to ϕ assuming uniformly distributed scatterers,

$$\Pr(\Phi < \phi) = F(\phi) = \frac{A(\phi)}{A_{Total}}. \tag{A3.2}$$

Here, A_{Total} is the entire area in the semi-elliptic region covered by the BS, and $A(\phi)$ is the portion of A_{Total} covered when the angle of arrival is limited to the range $[-\pi, \phi]$. That

is, $\Pr(\Phi < \phi)$, which can be viewed as the cumulative distribution function (CDF) of ϕ (the angle of arrival (AOA)), is the ratio of the shaded region in Fig. A3.1, $A(\phi)$, to the total area of the semi-elliptic region, A_{Total}.

Alternatively, the total normalized power received by the MS in the angle $-\pi$ to ϕ, shown in (A3.1), can be expressed as

$$P_{Total\_MS}(\phi) = \int_{-\pi}^{\phi} p(\Phi)d\Phi, \tag{A3.3}$$

where $p(\Phi)$ represents the probability density function (PDF) of power as a function of angle of arrival, i.e., *power azimuth spectrum (PAS)*. From (A3.3),

$$p(\phi) = \frac{dP_{Total\_MS}(\phi)}{d\phi}, \tag{A3.4}$$

and, from (A3.2),

$$p(\phi) = \frac{dF(\phi)}{d\phi} = \frac{dA(\phi)}{d\phi} \cdot \frac{1}{A_{Total}} \tag{A3.5}$$

Now, assuming the TSUNAMI II geometry of Fig. A3.1, the area $A(\phi)$ corresponds to

$$A(\phi)=\begin{cases}\frac{1}{2}x_o^2\cdot(\pi+\phi)\cdot\cos^2(\phi_o) & \text{if } -\pi\le\phi<-\phi_o,\\ \frac{1}{2}x_o^2\cdot\left((\pi-\phi_o)\cdot\cos^2(\phi_o)+\cos^2(\phi_o)\cdot\tan(\phi_o+\phi)\right) & \text{if } -\phi_o\le\phi\le 0,\\ x_o^2\cdot\left(\sin(\phi_o)\cdot\cos(\phi_o)+\frac{1}{2}\cos^2(\phi_o)\cdot(\pi-\phi_o)-\frac{1}{2}\cos^2(\phi_o)\cdot\tan(\phi_o-\phi)\right) & \text{if } 0\le\phi\le\phi_o,\\ x_o^2\cdot\left(\sin(\phi_o)\cdot\cos(\phi_o)+\frac{1}{2}\cos^2(\phi_o)\cdot(\pi-\phi_o)+\frac{1}{2}\cos^2(\phi_o)\cdot(\phi-\phi_o)\right) & \text{if } \phi_o<\phi\le\pi,\end{cases} \tag{A3.6}$$

where $\phi_o=\frac{1}{2}(\pi-\alpha)$, and the total coverage area corresponds to

$$A_{Total}=x_o^2\cdot\left(\sin(\phi_o)\cos(\phi_o)+(\pi-\phi_o)\cos^2(\phi_o)\right). \tag{A3.7}$$

Using (A3.6) and (A3.7) in (A3.5) leads to (after mathematical manipulation):

$$p(\phi)=\frac{0.5}{(\pi-\phi_o)+\tan\phi_o}\cdot\begin{cases}\dfrac{1}{\cos^2(\phi_o-|\phi|)} & \text{if } |\phi|\le\phi_o,\\ 1 & \text{if } |\phi|>\phi_o.\end{cases} \tag{A3.8}$$

where $\phi\in[-\pi,\pi)$. Hereafter, we refer to the analytically-derived PAS of (A3.8) as the secant-square PAS model.

A3.3 Comparison between proposed PAS, Laplacian PAS, and the experimental results

In [98][99], the Laplacian model is proposed as the model with the best fit to the TSUNAMI II project data, i.e.,

$$p(\phi) = \frac{C}{\sqrt{2}\sigma}\exp\left[-\sqrt{2}|\phi|/\sigma\right], \quad \phi \in [-\pi, +\pi) \ , \tag{A3.9}$$

where, C is a constant selected such that the integral of $p(\phi)$ is unity over $[-\pi, \pi)$, and σ represents the angular spread.

We apply the least square error technique as our criteria for the goodness of fit of the measurement data with both our analytical secant-square model and the empirical Laplacian model. Using this measure, and the TSUNAMI II measurement data, the squared error for the Laplacian model is 0.0041 while the error value for the secant-square model is 0.0033, indicating the secant-square PAS model is a better fit. Fig. A3.2 plots the measurement data, the Laplacian PAS model [98] and the secant-square PAS model assuming $\alpha \approx 2°$ ($\phi_0 = 89°$).

The advantage of the secant-square PAS model, when compared to the Laplacian PAS model, are as follows: 1) secant square considers the effect of the received power from all directions, i.e., -180° to 180°, which is not the case for the Laplacian PAS (presented in [98][99]); 2) secant square has a better fit to the measured data; and 3) most importantly, the secant-square model confirms that very accurate analytical PAS models can be generated using geometric based channel representations.

A3.4 Conclusions

In this appendix we proposed a novel analytical method for the creation of power azimuth spectrum (PAS) models. Based on semi-elliptic geometric-based channel modeling, our method was tested in the TSUNAMI II environment.

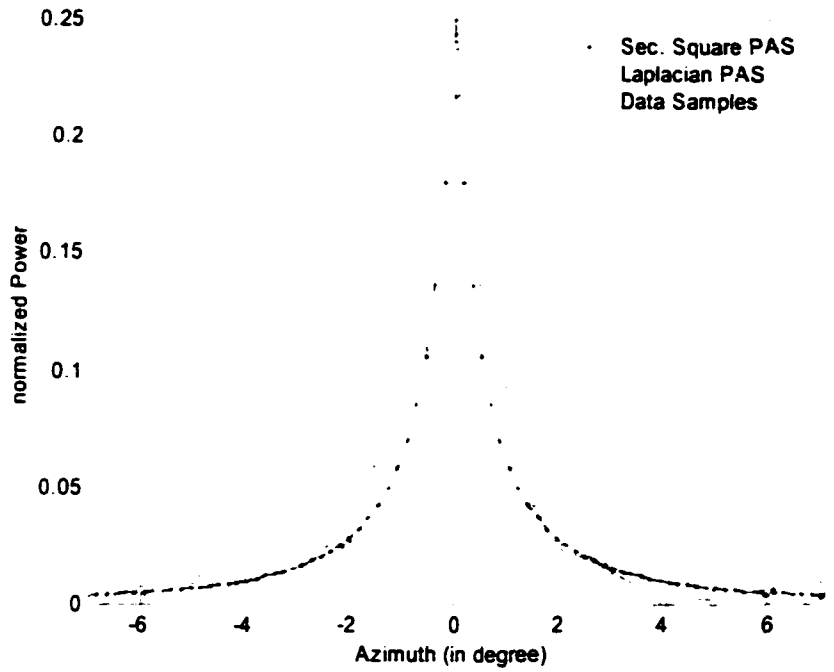

Fig. A3.2 The normalized Secant Square, Laplacian and data samples PAS for $\alpha \approx 2°$.

References

[1] T. S. Rappaport, *Wireless communications: Principles and practice.* Prentice Hall, Upper Saddle River, NJ, 1996.

[2] S. R. Saunders, *Antennas and propagation for wireless communication systems*, John Wiley and Sons, New York, NY, 1999.

[3] P. Mohana Shankar, *Introduction to wireless systems*, John Wiley & Sons, New York, NY, 2002.

[4] S. Onoe, and S. Yasuda, "Flexible re-use for dynamic channel assignment in mobile radio systems, " proceedings of *IEEE International Conference on Communications*, ICC'89, Vol. 1, pp. 472-476, 1989.

[5] R.C. Bernhardt, "Time-slot management in frequency reuse digital portable radio systems, " proceedings of *IEEE Vehicular Technology Conference, VTC'90*, pp. 282-286.

[6] R.C. Bernhardt, "Call performance in a frequency reuse digital portable radio system, " *IEEE Transactions on Vehicular Technology*, Vol. 40, N0. 4, pp. 777-785, Nov. 1991.

[7] Q. T. Zhang, "Bridging the gap between dynamic and static methods for cell planning, " *IEEE Transactions on Vehicular Technology*, Vol. 50, No. 5, pp.1224-1230, Sept. 2001.

[8] M. Kuwahara, and N. Doi, " Code reassignment scheme on CDMA smart antenna system, " proceeding of *IEEE Vehicular Technology Conference, VTC'2000*, pp. 21372141.

[9] T. Minn and Kai-Yeung Siu, " Dynamic assignment of orthogonal variable-spreading-factor codes in W-CDMA, " *IEEE Journal on Selected Areas in Communications*, Vol. 18, No. 8, pp. 1429-1440, August 2000.

[10] C. A. Balanis, *Antenna theory*, John Wiley & Sons, New York, NY, 1997.

[11] J.C. Liberti, Jr. and T.S. Rappaport, *Smart antennas for wireless communications: IS-95 and third generation CDMA applications*, Prentice Hall, Upper Saddle River, NJ, 1999.

[12] C. Fasakh and J.A. Nossek, "On the mobile radio capacity using through SDMA, " proceedings of *IEEE International Zurich seminar on Broadband communications: accessing, transmission, networking*, pp. 293-298, Zurich, Switzerland, 1998.

[13] F. Piolini and A. Rolando, "Smart channel algorithm for SDMA systems, " proceedings of *IEEE Radio and Wireless Conference, RAWcon'98*, Colorado Springs, 1998.

[14] F. Shad, T.D. Todd, V. Kezys, J. Litva, "Indoor SDMA Capacity using a smart antenna base station," proceedings *of IEEE International Conference on Universal Personal Communications*, pp. 868-872, San Diego, CA, 1997.

[15] M. Cooper and R. Roy, "SDMA technology: Overview and development status, " *46th National Engineering Consortium on Annual review of communications*, NEC, 1992.

[16] M. Goldburg and R. H. Roy, " The impacts of SDMA on PCS system design, " proceedings of *IEEE 3rd Annual International Conference on Universal Personal Communications*, pp. 242-246, San Diego, CA, 1994.

[17] N. Seshadri and J. H. Winters, "Two signaling schemes for improving the error performance of frequency division-duplex transmission system using transmitter antenna diversity," *International Journal on Wireless Information Networks*, Vol. 1, No. 1, pp. 49-60, Jan. 1994.

[18] S.M. Alamouti, "A simple transmit diversity technique for wireless communications," *IEEE Journal on Selected areas in Communications*, Vol. 16, No. 8, pp. 1451-1458, 1998.

[19] K. Kuchi, R. Pirhonen, R. Srinivasan, "Hopped delay diversity for EDGE, " proceedings *IEEE Vehicular Technology Conference*, VTC'01, pp.152-156, May, 2001.

[20] H. Olofsson, M. Almgren, and M. Hookin., "Transmitter diversity with antenna hopping for wireless communication systems," proceedings of *IEEE Vehicular Technology Conference, VTC'97*, Vol. 3, pp. 1743-1747, May 1997.

[21] Robert W. Heath Jr. and Arogyaswami Paulraj, "Transmit diversity using decision-directed antenna hopping, " proceedings of *IEEE Communications Mini-Conference*, pp. 141-145, June, 1999.

[22] A. Hiroike, F. Adachi, and N. Nakajima, "Combined effects of phase sweeping transmitter diversity and channel coding," *IEEE Transactions On Vehicular Technology*, Vol. 41, No.2, pp. 170-176, May 1992.

[23] Bing D. Su and Stephen G. Wilson, "Phase sweeping transmitter diversity in mobile communications, " proceedings of *Vehicular Technology Conference, VTC'96*, Vol. 1, pp. 131-135, 1996.

[24] V. Tarokh, N. Seshadri, and A.R. Calderbank, "Space-time codes for high data rate construction," *IEEE Transactions on Information Theory*, Vol. 44, No. 2, pp. 744-765, March 1998.

[25] N. Seshadri, V. Tarokh and A.R. Calderbank, "Space-time codes for wireless communiaction: Code construction, " proceedings of *IEEE Vehicular Technology Conference*, VTC'97, pp. 637-641, Phoenix, AZ, May 1997.

[26] S. A. Alamouti, V. Tarokh, P. Poon, "Trellis-coded modulation and transmit diversity: Design criteria and performance evaluation," proceedings of *IEEE 1998 International Conference on Universal Personal Communications*, pp. 703-707, Florence, Italy, Oct. 1998.

[27] O. Norklit, and J.B. Andersen, "Mobile radio environments and adaptive arrays," proceedings of *5th IEEE International Symposium on Personal, Indoor and Mobile Radio Communications, PIMRC'94*, Vol. 2, pp. 725-728, 1994.

[28] O. Norklit, P.C.F. Eggers and J.B. Andersen, "Jitter diversity in multipath environments," proceedings of *Vehicular Technology Conference*, VTC'95, Vol. 2, pp. 853 -857, 1995.

[29] P. A. Bello, "Characteristics of randomly time-variant linear channels, " *IEEE Transactions on Communication Systems*, Vol. CS-11, pp. 360-393, 1963.

[30] T. Zwick, C. Fischer, D. Didascalou and W. Wiesbeck, "A stochastic spatial model based on wave-propagation modeling," *IEEE Journal on Selected Areas Communications*, Vol. 18, No. 1, pp. 6-15, Jan 2000.

[31] H. Hashemi, "The indoor radio propagation channel, " *IEEE Proceedings*, Vol. 81, No. 7, pp. 943-968, July 1993.

[32] H. Suzuki, "A statistical model for urban radio propagation, " *IEEE Transactions on Communications*, Vol. COM-25. pp. 673-680, July, 1977.

[33] J. W. C. Jakes, ed., *Microwave mobile communications*, New York, NY, John Wiley & Sons, 1974.

[34] R. B. Ertel, P. Cardieri, K. W. Sowerby, T. S. Rappaport and J. H. Reed, "Overview of spatial channel models for antenna array communication systems, " *IEEE Personal Communications*, Vol. 5, No. 1, pp. 10-22, Feb. 1998.

[35] A. F. Molisch, A. Kucher, J. Laurila, K. Hugl and E. Bonek, "Efficient implementation of a geometry-based directional model for mobile radio channels, " proceedings of *IEEE Vehicular Technology Conference, VTC'99*, pp. 1449-1453, 1999.

[36] R. B. Ertel, "Angle and time of arrival statistics for circular and elliptical scattering models, " *IEEE Journal on Selected Areas Communications*, Vol. 17, No. 11, pp.1829-1840, 1999.

[37] P. Petrus, J. H. Reed and T. S. Rappaport, "Geometrically based statistical channel model for macro cellular mobile environments, " *proceedings of IEEE Globecom '96*, pp. 1197-1201, 1996.

[38] J.C. Liberti and T. S. Rappaport, "A geometric based model for line-of-sight multipath radio channels, " proceedings of *IEEE Vehicular Technology Conference. VTC '96*, pp. 844-848, 1996.

[39] Y. Oda, K. Tsunekawa and M Hata, "Geometrically based directional channel model for urban mobile communication systems, " proceedings of *2000 IEEE-APS Conference on Antennas and Propagation for Wireless Communications*, pp. 87-90, 2000.

[40] S. A. Zekavat and C. R. Nassar, "Smart antenna arrays with oscillating beam patterns: characterization of transmit diversity using semi-elliptic-coverage geometric-based stochastic channel modeling," accepted in *IEEE Transactions on Communications*.

[41] S. A. Zekavat and C. R. Nassar, "Semi-elliptic-coverage geometric-based stochastic channel modeling for smart antenna arrays with oscillating beam patterns, " proceedings of *IEEE Globcom '01*, pp. 3237-3241, San Antonio, Nov. 25-26, 2001.

[42] S. A. Zekavat, C. R. Nassar, "Fading channel characterization for oscillating-beam-pattern smart antennas using geometric-based stochastic channel modeling, with circular coverage scenario, " proceedings of *IEEE Vehicular Technology Conference, VTC fall 2001*, pp. 1452-1456, Atlantic City, Oct. 7-11, 2001.

[43] S. A. Zekavat, C. R. Nassar, "Geometric-based stochastic channel modeling for adaptive antennas with oscillating beam patterns, " proceedings of *IEEE*

International Symposium on Personal, Indoor and Mobile Radio Communications, PIMRC'01, pp. 130-134, San Diego, Sep., 2001.

[44] S. A. Zekavat, C. R. Nassar, "Diversity gains in wireless systems with oscillating beam smart antennas: An evaluation via geometric-based stochastic channel models, with point scatterers, " proceedings of *SPIE's International Symposium on the Convergence of Information Technologies and Communication, ITCOM'01*, pp.118-124 Denver, Aug. 20-24, 2001.

[45] S. A. Zekavat and C. R. Nassar, "Transmit diversity and directionality via oscillating beam pattern adaptive antennas: An evaluation using geometric-based stochastic circular-scenario channel modeling, " submitted to *IEEE Transactions on Wireless Communications*.

[46] S. A. Zekavat, C. R. Nassar, "Adaptive antennas power-azimuth spectrum using a geometric-based channel model with a semi-elliptic scenario, " proceedings of *Antenna Measurement and Technologies Associated, AMTA'01*, pp. 346-348, Denver, Oct. 2001.

[47] S. A. Zekavat, C. R. Nassar, "Power-azimuth-spectrum modeling for antenna array systems: A geometric-based approach, " submitted to *IEE Electronic Letters*.

[48] S. A. Zekavat, C.R. Nassar and S. Shattil, "Combined directionality and transmit diversity via smart antenna spatial sweeping, " proceedings of *38th Annual Allerton Conference on Communication, Control, and Computing, University of Illinois in Urbana-Champaign*, pp. 203-211, Urbana-Champaign, Oct. 2000.

[49] S. A. Zekavat, C.R. Nassar and S. Shattil, "Smart antenna spatial sweeping for combined directionality and transmit diversity," *Journal of Communications and*

Networks (JCN), Special issue on Adaptive Antennas for Wireless Communications, Vol. 2, No. 4, pp. 325-330, Dec. 2000.

[50] M. Akhtar, and J. Asenstorfer, "Iterative detection for MC-CDMA system with base station antenna array for fading channels, " proceedings of *IEEE Globecom '98*, pp. 241-246, 1998.

[51] C. K. Kim and Y. S. Cho, "Performance of a wireless MC-CDMA with an antenna array in a fading channel: revers link, " *IEEE Transactions on Communications*, Vol. 48, No. 8, pp. 1257-1261, Aug. 2000.

[52] S.Hara and R.Prasad, " Overview of multi-carrier CDMA," *IEEE Communications Magazine*, " Vol. 35, No. 12, pp. 126-133, Dec. 1997.

[53] A. J. Viterbi, *CDMA. principles of spread spectrum*, Addison-Wesley, Reading, MS, 1995.

[54] U.S. Goni and A. M. D. Turkmani, "BER performance of a direct-sequence CDMA system in multipath fading mobile radio channels with rake reception, " proceedings of *IEEE 44th Vehicular Technology Conference*, pp. 747-751, 1994.

[55] Y. Amezawa and S. Sato, "Performance analysis of optimum RAKE receiver for fast Fading in DS/CDMA mobile radio communication system, " proceedings of *IEEE Vehicular Technology Conference, VTC'96*, pp. 647-651, 1996.

[56] S. A. Zekavat, C. R. Nassar and S. Shattil, "Oscillating beam adaptive antennas and multi-carrier systems: Achieving transmit diversity, frequency diversity and directionality, " accepted in *IEEE Transactions on Vehicular Technology*.

[57] S. A. Zekavat, C. R. Nassar and S. Shattil, "Merging oscillating-beam smart antenna arrays and wideband multi-carrier CDMA: Exploiting transmit diversity, frequency diversity and directionality, " accepted in *IEEE 3Gwireless'02*, 2002.

[58] S. A. Zekavat, C. R. Nassar and S. Shattil, "Merging carrier interferometery DS-CDMA and oscillating-beam smart antenna arrays: Exploiting transmit diversity, frequency diversity and directionality, " accepted in *IEEE ICC'02*, New York, 2002.

[59] S. A. Zekavat, C. R. Nassar and S. Shattil, "Transmit diversity, frequency diversity and directionality via oscillating beam adaptive antennas and multi-carrier systems, " accepted in *IEEE Spring VTC'02*, 2002.

[60] S. A. Zekavat, C. R. Nassar and S. Shattil, "The merger of a single oscillating-beam smart antenna and MC-CDMA: Transmit diversity, frequency diversity and directionality, " proceedings of *IEEE Emerging Technologies Symposium on Broad Band Communications For Internet Era*, pp. 107-112, Dallas, Sep. 2001.

[61] S. A. Zekavat, C. R. Nassar and S. Shattil, "Merging CI chip shaped DS-CDMA and oscillating-beam smart antenna arrays: Exploiting transmit diversity, frequency diversity and directionality, " submitted to *IEEE Transactions on Wireless communications.*

[62] S. A. Zekavat, C. R. Nassar and S. Shattil, "Merging multi-carrier CDMA and oscillating-beam smart antenna arrays: Exploiting directionality, transmit diversity and frequency diversity, " submitted to *IEEE Transactions on communications.*

[63] S. A. Zekavat and C. R. Nassar, " Achieving high capacity wireless by merging multi-carrier CDMA systems and oscillating-beam smart antenna arrays, " submitted to *IEEE Transactions on Vehicular Technology.*

[64] S. A. Zekavat and C. R. Nassar, " High capacity wireless via MC-CDMA/oscillating-beam smart antenna array systems, " submitted to *IEEE International Symposium on Wireless Personal Multimedia Communications, WPMC'02*, Hawaii, 2002.

[65] J. G. Proakis, *Digital Communications*, 3th Edition, McGraw-Hill, New York, NY, 1995.

[66] A. Papulis, *Probability, random variables, and stochastic processes*, 3rd Edition, Mc Graw Hill, New York, NY, 1991.

[67] B. B. Mohebbi, A. H. Aghvami and W. G. Chambers, "Broad-band propagation channel analysis for DS and hybrid CDMA system design, " proceedings of *5th IEEE International Symposium on Personal, Indoor and Mobile Radio Communications, PIMRC'94*, Vol. 2, pp.700-704, 1994.

[68] D. C. Cox, "Correlation bandwidth and delay spread multipath propagation statistics for 910-MHz urban mobile radio channels," *IEEE Transactions on Communications*, Vol. COM-23, No. 11, pp. 1271-1280, Nov. 1975.

[69] P. J. Brockwell and R. A. Davis, *Introduction to time series and forecasting*, Springer-Verlag, New York, NY, 1996.

[70] B. Natarajan, C.R. Nassar, S. Shattil, Z. Wu, and M. Michelini, "High performance MC-CDMA via carrier interferometry codes," *IEEE Transaction on Vehicular Technology*, Vol. 50, No. 6, pp. 1344-1353, Nov. 2001.

[71] C.R. Nassar, M. Michelini, B. Natarajan, and S. Shattil, "Introduction of carrier interference to spread spectrum multiple access," *Symposium on Emerging Technologies in Wireless Communications Systems*, Richardson, TX, pp. 4.1-4.5, April 12-13, 1999.

[72] Z. Wu, B. Natarajan, C.R. Nassar, S. Shattil, " High performance, high capacity MC-CDMA via carrier interferometry, " *IEEE International Symposium on Personal, Indoor and Mobile Radio Communications, PIMRC'01*, Vol. 2, pp. 11-16, San Diego, Sep/Oct 2001.

[73] William Webb, *The Future of wireless communications*, Artech House, Boston, MA, 2001.

[74] ISO/IEC 8802.11:1999 (ANSI/IEEE Std 802.11, 1999 Edition), information technology—telecommunications and information exchange between systems—local and metropolitan area networks—specific requirements, part 11: wireless LAN medium access control (MAC) and physical layer (PHY) specifications, August 1999.

[75] S. Haykin, *Adaptive filter theory*, 2nd Edition, Prentice Hall, Englewood Cliffs, NJ, 1991.

[76] Carl R. Nassar, B. Natarajan, and Z. Wu, "Multi-carrier technology platform for wireless communications: Part 1: High-performance, high-throughput TDMA and DS-CDMA via multi-carrier implementations," accepted for publication in *Wireless Communications and Mobile Computing*.

[77] Z. Wu, Carl R. Nassar and S. Shattil, " High-performance high-capacity DS-CDMA via carrier interformetry, " submitted to *IEEE Transaction on Communications*.

[78] Z. Wu, Carl R. Nassar, and S. Shattil, "High performance DS-CDMA via carrier interferometry," proceedings *Wireless 2001*, pp. 564-569, Calgary, Alberta, July 2001.

[79] Z. Wu, Carl R. Nassar, and S. Shattil, "Chip shaping advances for high capacity DS-CDMA," *IEEE 2001 International Conference on Third Generation Wireless and Beyond*, pp. 404-409, May 30-June 2, 2001.

[80] Z. Wu and C.R. Nassar, "MMSE frequency combining for CI/DS-CDMA," *IEEE Radio and Wireless Conference*, pp. 103-106, Denver, CO, Sept. 10-13, 2000.

[81] C.R. Nassar and Z. Wu, "High performance broadband DS-CDMA via carrier interferometery chip shaping," proceedings of *2000 International Symposium on Advanced Radio Technologies*, Boulder, CO, Sept. 6-8, 2000.

[82] Ramjee P., and R. van Nee, *OFDM for Wireless Multimedia Communications*, Artech House Publishers, Boston, 2000.

[83] R.W. Chang, "Orthogonal frequency division multiplexing, " *U.S. Patent 3,488,445*, filed 1966, issued Jan. 6, 1970.

[84] S. B. Weinstein and P. M. Ebert, "Data transmission by frequency-division multiplexing using the discrete fourier transform," *IEEE Transactions on Communications Technology*, Vol. COM--19, No.5, pp.628--634, Oct. 1971.

[85] L. J. Cimini, Jr., "Analysis and simulation of a digital mobile channel using orthogonal frequency division multiplexing, " *IEEE Transactions on Communications*, Vol. COM-33, No.7, pp.665--675, July 1985.

[86] Howard H. Xia, Henry L. Bertoni, L. R. Maciel, Andrew Lindsay-Stewart, and Robert Rowe, "Radio propagation characteristics for line-of-sight microcellular and personal communications, " *IEEE Transactions on Antennas and Propagation*, Vol. 41, No. 10, pp. 1439-1446, Oct 1993.

[87] A. J. Rustako, Jr., N. Amitay, G. J. Owens, and R. S. Roman ," Radio propagation at microwave frequencies for line-of-sight microcellular mobile and personal

communications, " *IEEE Transactions on Vehicular Technology*, Vol. 40, No. 1, pp.203-210, Feb 1991.

[88] A. Kavak, "Adaptive antenna arrays for downlink capacity increase in third generation wireless CDMA," proceedings of *IEEE Radio and Wireless Conference, RAWCON'01*, pp. 77-80, Boston, August 2001.

[89] A. F. Naguib, A. Paulraj, and T. Kailath, "Capacity improvement with base-station antenna arrays in cellular CDMA, " *IEEE Transactions on Vehicular Technology*, Vol. 43, No. 3, pp. 691-698, August 1994.

[90] M. A. Beach, D. P. McNamara, P. N. Fletcher and P. Karlsson, " MIMO – a solution for advanced wireless access?, " *proceedings Eleventh International Conference on Antennas and Propagation, 2001*, Vol. 1, pp. 231-235, 2001.

[91] A. M. Sayeed, "Modeling and capacity of realistic spatial MIMO channels, " proceedings of *IEEE International Conference on Acoustics, Speech and Signal Processing, 2001*, Vol. 4, pp. 2489-2492, 2001.

[92] P. F. Driessen and G. J. Foschini, "On the capacity formula for multiple input-multiple output wireless channels: a geometric interpretation, " proceedings of *IEEE International Conference on Communications, ICC'99*, Vol. 3, pp. 1603-1607, 1999.

[93] A. Paulraj, "MIMO wireless for fixed broadband service, " proceedings of *Symposium on Communications and Vehicular Technology, SCVT-2000*, pp. 263-297, 2000.

[94] I. E. Teltar, "Capacity of multi-antenna Gaussian channels, " *European Transactions on Telecommunications*, Vol. 10, No. 6, pp. 585-595, 1999.

[95] M. Thit and Siu Kai-Yeung, "Dynamic assignment of orthogonal variable-spreading-factor codes in W-CDMA, " *IEEE Journal on Selected Areas in Communications*, Vol. 18, No. 8, pp.1429-1440, Aug. 2000.

[96] M. Kuwahara, N. Doi, "Code reassignment scheme on CDMA smart antenna systems, " *proceedings IEEE Vehicular Technology Conference, VTC'00*, Vol. 3, pp. 2137-2141, Tokyo, 2000.

[97] P. C. F. Eggers, "Angular propagation descriptions relevant for base station adaptive antenna operations, " *Wireless Personal Communications*, Vol. 11, pp. 3-29, 1999, Kluwer Academic Publishers.

[98] K. I. Pedersen, P. E. Mogensen and B. Fleury, "Power azimuth spectrum in outdoor environments, " *Electronics Letters*, Vol. 33, No. 18, pp. 1583-4, Aug. 1997.

[99] K. I. Pedersen, P. E. Mogensen and B. Fleury, "A stochastic model of the temporal and azimuthal dispersion seen at the base station in outdoor propagation environments, " *IEEE Transactions on Vehicular Technology*, Vol. 49, No. 2, March 2000.

[100] P. E. Mogensen, F. Frederiksen, H. Dam, K. Olesen, and S. L. Larsen "TSUNAMI (II) stand alone testbed, " Proceedings of *ACTS Mobile Telecommunications, Summit'96*, pp. 517-527, Granada, Spain, Nov. 1996.

[101] J. Fuhl, A. F. Molisch and E. Bonek, "Unified channel model for mobile radio systems with smart antennas, " *IEE Proceedings on Radar, Sonar and Navigation*, Vol. 145, No. 1, pp. 32-41, 1998.